Fall 2003

Studies on improved integrated membrane-based chromatographic process for bioseparation

Yanke Xu
New Jersey Institute of Technology

ABSTRACT

STUDIES ON IMPROVED INTEGRATED MEMBRANE-BASED CHROMATOGRAPHIC PROCESS FOR BIOSEPARATION

by

Yanke Xu

To improve protein separation and purification directly from a fermentation broth, a novel membrane filtration-cum-chromatography device configuration having a relatively impermeable coated zone near the hollow fiber module outlet has been developed. The integrated membrane filtration-cum-chromatography unit packed with chromatographic beads on the shell side of the hollow fiber unit enjoys the advantages of both membrane filtration and chromatography; it allows one to load the chromatographic media directly from the fermentation broth or lysate and separate the adsorbed proteins through the subsequent elution step in a cyclic process.

Interfacial polymerization was carried out to coat the bottom section of the hollow fiber membrane while leaving the rest of the hollow fiber membrane unaffected. Myoglobin (Mb), bovine serum albumin (BSA) and α-lactalbumin (α-LA) were used as model proteins in binary mixtures. Separation behaviors of binary protein mixtures were studied in devices using either an ultrafiltration (UF) membrane or a microfiltration (MF) membrane. Experimental results show that the breakthrough time and the protein loading capacities were dramatically improved after coating in both UF and MF modules. For a synthetic yeast fermentation broth feed, the Mb and α-LA elution profiles for the four consecutive cyclic runs were almost superimposable. Due to the lower transmembrane

flux in this device plus the periodical washing-elution during the chromatographic separation, fouling was not a problem as it is in conventional microfiltration.

A mathematical model describing the hydrodynamic and protein loading behaviors of the integrated device using UF membrane with a coated zone was developed. The simulation results for the breakthrough agree well with the experimental breakthrough curves. The optimal length of the coated zone was obtained from the simulation.

A theoretical analysis of the protein mass transfer was performed using a diffusion-convection model considering the feed-side concentration polarization and the permeate-side concentration gradient formed by the adsorption. The permeate-side adsorption can enhance the observed protein transmission through the membrane considerably at low permeate flux. But the enhancement effect can be neglected at higher permeate flux when convection dominates the total mass transfer process or the proteins are very highly rejected by the membrane.

STUDIES ON IMPROVED INTEGRATED MEMBRANE-BASED CHROMATOGRAPHIC PROCESS FOR BIOSEPARATION

by
Yanke Xu

A Dissertation
Submitted to the Faculty of
New Jersey Institute of Technology
In Partial Fulfillment of the Requirements for the Degree of
Doctor of Philosophy

Otto H. York Department of Chemical Engineering

January 2004

APPROVAL PAGE

STUDIES ON IMPROVED INTEGRATED MEMBRANE-BASED CHROMATOGRAPHIC PROCESS FOR BIOSEPARATION

Yanke Xu

Dr. Kamalesh K. Sirkar, Advisor — Date
Distinguished Professor of Chemical Engineering, NJIT
Foundation Professor, Membrane Separations

Dr. Gordon A. Lewandowski, Committee Member — Date
Distinguished Professor of Chemical Engineering, NJIT

Dr. Dana E. Knox, Committee Member — Date
Associate Professor of Chemical Engineering, NJIT

Dr. Michael C. Y. Huang, Committee Member — Date
Assistant Professor of Chemical Engineering, NJIT

Dr. Barbara Kebbekus, Committee member — Date
Professor of Chemistry, NJIT

BIOGRAPHICAL SKETCH

Author: Yanke Xu

Degree: Doctor of Philosophy

Date: January 2004

Undergraduate and Graduate Education:

- Doctor of Philosophy in Chemical Engineering
  New Jersey Institute of Technology, Newark, NJ 2004
- Master of Science in Chemical Engineering
  Dalian University of Technology, Dalian, China, 1993
- Bachelor of Science in Chemical Engineering
  Dalian University of Technology, Dalian, China, 1990

Major: Chemical Engineering

Presentations and Publications:

Yanke Xu, K.K. Sirkar, 2003, Protein Mass Transfer Enhancement in the Membrane Filtration-cum-Adsorption Process." *Journal of Membrane Science*, 221: 79-87.

Yanke Xu, X.P. Dai, R.G. Luo, and K.K. Sirkar, 2003, "A New Integrated Membrane Filtration-cum-Chromatography Device". Submitted.

C.B. Ching, P. Fu, S.C. Ng and Y. K. Xu, 2000, "Effect of the Mobile Phase Composition on the Separation of Propranonal Enantiomers Using a Perphenylcarbomate β-Cyclodextrin Bonded Chiral Stationary Phase." *Journal of Chromatography A*. 898:53-61.

C.Y. Yu, Y.K. Xu and X.Z. Wang, 1999, "Study of Spray Fluidized Bed Granulation', *Drying Technology*. 17:1893-1904

Yanke Xu, Caiyuan Yu, Xizhong Wang and Zaiqi Lin, 1995, "Model of Maximum Liquid Feed Rate of Fluidized Spray Granulator.", *Journal of Dalian University of Technology*, 35:155-159.

Yanke Xu, X.P. Dai, R. G. Luo and K.K. Sirkar, 2003 Performance Studies of an Integrated Membrane Filtration-cum-Chromatography Device, 14th NAMS meeting, Jackson Hole, WY.

Yanke Xu, X.P. Dai, R. G. Luo and K.K. Sirkar, 2002 Analysis of the Filtration-cum-Adsorption Process and the Mass Transfer Enhancement Due to the Permeate Side Protein Adsorption, AIChE annual meeting, Indianapolis, IN.

Yanke Xu, X.P. Dai, R.G. Luo and K.K. Sirkar, 2002 Study of an Integrated Membrane-cum-Chromatography Unit, ICOM (The International Congress on Membranes and Membrane Prosesses) , 11 July, Toulouse, France.

Yanke Xu, X.P. Dai, R.G. Luo and K.K. Sirkar, 2002 A New Integrated Membrane Filtration-cum-Chromatographic Device, 13th NAMS meeting, Long Beach, CA.

Yanke Xu, X.P. Dai, R.G. Luo and K.K. Sirkar, 2001 Modeling and Optimization of an Integrated Membrane-cum-Chromatography Unit, AIChE Annual meeting, , Reno, NV.

Yanke Xu, X.P. Dai, R.G. Luo and K.K. Sirkar, 2001 Optimization of the Membrane Chromatography Integrated Unit, 12th NAMS meeting, Lexington, KY.

Yanke Xu, Caiyuan Yu, Xizhong Wang and Zaiqi Lin, 1994 Study of Particles Movement and Drying Rate in The Spray Fluidized Bed Granulator, Proceedings of the 7th National Conference on Chemical Engineering, NCCE'94 Beijing, p405-408.

Yanke Xu, Caiyuan Yu, Xizhong Wang and Zaiqi Lin,1994 Study of the Particle Growth Mechanism in the Spray Fluidized Bed Granulation, Proceedings of the 7th National Conference on Chemical Engineering, NCCE'94 Beijing, p910-913

Patents

Yanke Xu, M. Ma, G. Zhang and Q. Liu, 1998. A Small Membrane Oxygen-Enriched Air Generator for Health and Medical Use, China Patent: CN 2281184Y

Yanke Xu and M. Ma, 1998. A Soft-Shell Flexible Hollow Fiber Membrane Module, China Patent: CN 2280550Y

R.G. Luo, K.K. Sirkar, Yanke Xu and X.P. Dai, 2002. A New Chromatographic Device for Biomolecule Purification using Hollow Fiber Membrane Module. Filed in May, 2002.

To my beloved mom, dad, wife, and daughter-to-be

ACKNOWLEDGMENTS

I would like to express my deepest appreciation to Dr. Kamalesh K. Sirkar, who has been a dedicated advisor, and a judicious mentor. During the four and half year's Ph.D. study, he provided invaluable guidance to my academic work. This dissertation work would not be in the current form without his insightful input and constructive criticism. I extend my sincerest appreciation to Dr. Robert G. Luo, my co-advisor during the first two years, who gave earnest suggestions on my research and helped me in my Ph.D. program.

I am very grateful to Dr. Michael C. Y. Huang, Dr. Barbara Kebbekus, Dr. Dana E. Knox, and Dr. Gordon A. Lewandowski, who served on my dissertation committee. I am thankful for their useful advice and comments on the proposal and the dissertation.

I thank Union Chemical Laboratories, Industrial Technology Research Institute, Taiwan for their financial support through the Center for Membrane Technologies at NJIT, and Otto H. York Department of Chemical Engineering for financial support on my first year Ph.D. study.

I want to thank all of our group members for their help and giving me joyful time here. I want to give Dr. Xiao-Ping Dai special thanks for her help in the earlier work and a lot of constructive discussion, as well as her personal help. Dr. A. Sarma Kovvali's help on interfacial polymerization reaction is also acknowledged herewith.

TABLE OF CONTENTS

Chapter	Page
1 BACKGROUND	1
1.1 Introduction	1
1.2 New Device Concept	12
2 EXPERIMENTAL MATERIALS AND METHODS	16
2.1 Materials	16
2.1.1 Hollow Fiber Membranes and Modules	16
2.1.2 Chromatographic Media	18
2.1.3 Proteins, Adsorbent, and Process Chemicals	19
2.1.4 Cells and Synthetic Fermentation Broth Preparation	20
2.2 Device Fabrication	20
2.2.1 Packing the Beads into the Shell Side of the Hollow Fiber Module	20
2.2.2 Interfacially Polymerized Coating on the Hollow Fiber Inner Skin Near the Outlet Zone	21
2.3 Experimental Setup	25
2.4 Membrane Characterizations and Protein Transmissions	26
2.5 Filtration-cum-Chromatography Operation: Single Cycle Run	27
2.5.1 Cleaning, Loading and Washing Setup and Operations	27
2.5.2 Elution	27
2.6 Cyclic Filtration-cum-Chromatography Operation: Multiple Cycles	29
2.7 Protein Concentration and Cell Density Assay	30
3 RESULTS AND DISCUSSION ON SEPARATION IN THE MODIFIED INTEGRATED DEVICE	34
3.1 Membrane Water Permeance	34

TABLE OF CONTENTS
(Continued)

Chapter **Page**

3.2 Testing of the Partially Coated Fiber Module 35

3.3 Protein Separations in the Device using an UF Hollow Fiber Membrane..... 36

3.3.1 Effect of the Coated Zone on Mb Breakthrough 36

3.3.2 Protein Separation Behavior of the Device with or w/o a Coated Zone.. 38

3.3.3 Comparison of Different Elution Conditions..... 44

3.3.4 Effect of the Feed Ionic Strength 47

3.4 Protein Separations in the Device Using a MF Hollow Fiber Membrane 50

3.4.1 Effect of the Coated Zone on Mb Breakthrough 50

3.4.2 Comparison of Protein Separations in the Device with or w/o a Coated Zone 51

3.5 Adsorption Capacity Utilization 55

3.6 Effect of Yeast Cells in the Feed 56

4 MODELING AND SIMULATION OF THE PARTIALLY COATED DEVICE PERFORMANCE..... 59

4.1 Hydrodynamics of the Coated Device 59

4.1.1 Basic Governing Equations..... 59

4.1.2 Permeable Zone ($0 \le z \le l_p$) 61

4.1.3 Coated Zone ($l_p \le z \le l_t$) 63

4.1.4 Determination of A_1 and A_2..... 64

4.1.5 Estimation of the Parameters A and B..... 67

4.2 Protein Loading Behaviors in the Device with a Coated Zone..... 69

4.2.1 Lumen-Side Material Balance 69

4.2.2 Shell-Side Material Balance 70

4.2.3 Boundary Conditions and Initial Conditions 72

TABLE OF CONTENTS
(Continued)

Chapter **Page**

4.3 Adsorption Isotherm and Protein Transmission Parameters 73

4.4 Numerical Solution Procedure 74

4.5 Results and Discussion 75

4.5.1 Protein Loading in the Non-Coated Module 75

4.5.2 Loading of the Module with a Coated Zone 77

4.5.3 Simulation of the Breakthrough Behavior of the Integrated Device, with and without a Coated Zone 83

4.5.4 Optimal Length of the Coated Zone 84

5 MASS TRANSFER ENHANCEMENT ANALYSIS 86

5.1 Introduction 86

5.2 Theoretical development 86

5.3 Simulation Results and Discussion 92

5.3.2 Effects of the Enhanced Transport on the Permeate Side 93

5.3.3 Effect of Membrane Pore Size 95

5.3.4 Effect of the Permeate Side Mass Transfer Coefficient 97

5.3.5 Effect of Membrane Skin Layer Thickness 98

5.3.6 Protein Transmissions for a BSA and IgG Mixture 99

5.3.7 Protein Transmission Enhancement Observed in the Integrated Device Using UF Membrane 102

5.4 Concluding Remarks 105

6 CONCLUSIONS AND RECOMMENDATIONS FOR FUTURE STUDIES 107

APPENDIX A FORTRAN 77 CODE FOR SIMULATION OF THE INTEGRATED DEVICE WITHOUT COATING 112

TABLE OF CONTENTS
(Continued)

Chapter **Page**

APPENDIX B FORTRAN 77 CODE FOR SIMULATION OF THE INTEGRATED DEVICE WITH A COATED ZONE 116

REFERENCES 121

LIST OF TABLES

Table		Page
2.1	Parameters for Hollow Fiber Membrane Modules	17
2.2	Characteristics of DEAE Sepharose Fast Flow Anion Exchange Beads	19
2.3	Standard Curves for Protein Solutions	32
3.1	Water Permeance of Hollow Fiber Membranes	35
3.2	Water Permeation Results from Hollow Fiber Membrane modules	35
3.3	Experimental Conditions and Protein Loading Results for the UF Modules	41
3.4	Experimental Conditions and Protein Loading Results for the MF Modules	55
4.1	Hydrodynamic Experimental Data and Estimated Parameters for Module #1	68
4.2	Isotherm and Protein Transmission Parameters	74
5.1	Membrane Properties and the Corresponding BSA Transport Parameters	93

LIST OF FIGURES

Figure **Page**

1.1 Simplified downstream processing schematic based on membrane filtration-cum-chromatography. 2

1.2 Schematic presentation of the steps of EBA. (Amersham Biosciences 2000) 5

1.3 Configuration of the device containing membrane and adsorbent beads under different operating conditions. 10

1.4 New device concept: an integrated device with a coated zone near the outlet. 13

2.1 Hollow fiber module from A/G Technology. 16

2.2 Two sets of hollow fiber-based crossflow module. 18

2.3 Structure of DEAE Sepharose Fast Flow beads. 18

2.4 Packing the beads into the shell side of the membrane module. 21

2.5 Interfacial polymerization reaction. 23

2.6 Device for partial coating of the hollow fiber membranes by interfacial polymerization. 24

2.7 Setup for membrane filtration and loading of the integrated device. 25

2.8 System for step-wise and gradient elution. 28

2.9 Cyclic operation. 30

2.10 Standard curve for Mb at 280 nm. 31

2.11 Standard curve for Mb at 410 nm. 31

2.12 Standard curve for α-LA solution. 32

3.1 Mb breakthrough results from the conventional UF module and the module with a coated zone. (Feed: C_{Mb} 0.25 mg/ml, flow rate 200 ml/min, pressure 34.5 kPag) ... 37

LIST OF FIGURES
(Continued)

Figure **Page**

3.2 Comparison of Mb/α-LA separation behaviors at similar loading conditions for an UF module. (Loading time: 15 min. Elution: 0-50 min 0.05 M NaCl, 50-100 min 0.5M NaCl in Tris buffer.) 39

3.3 Loading capacity enhancement in the UF module having a coated zone for Mb-α-LA separation. (Elution: 0-50 min 0.05 M NaCl, 50-90 min 0.5M NaCl in Tris buffer.) 40

3.4 High loading capacity of Mb-α-LA for module 1 with a coated zone. (Feed: 0.505 mg/ml Mb, 0.467 mg/ml α-LA; Loading time: 35 min; Tube-side step-wise elution. Total protein loaded: Mb 51.34 mg, α-LA 14.13 mg) 42

3.5 Effect of coating on Mb/BSA separation for an UF module. (Loading time: a: 15 min; b: 55 min. Elution: 0-50 min 0.05 M NaCl , 50-90 min 0.5M NaCl in Tris buffer.) 43

3.6 Shell-side gradient elution for mixture of Mb and α-LA using module 1 with a coated zone. (Loading time: 15 min.) 45

3.7 Tube-side gradient elution for Mb-α-LA separation. (0.02 M to 0.2 M NaCl in 20 min, followed 0.2 M to 0.5 M NaCl in 30 min, and then 0.5 M NaCl for another 30 min.) 46

3.8 Tube-side step-wise elution for Mb-α-LA separation. (0-50 min 0.05 M NaCl , 50-80 min 0.5M NaCl in Tris buffer) 46

3.9 Loading at different NaCl concentration in the feed for Mb-α-LA system. (Loading time: 15 min, pressure 5 psig, Q_f = 200 ml/min. Shell-side gradient elution.) 48

3.10 Mb breakthrough curves for a device using MF membrane. (Feed: Mb 0.25 mg/ml; Loading condition: pressure 34.5kPag, Q_f = 200 ml/min.). 51

3.11 Effect of coating on Mb/α-LA separation for a MF module. (Feed: 0.0587 mg/ml Mb and 0.0524 mg/ml α-LA before coating; 0.0545 mg/ml Mb and 0.052 mg/ml α-LA after coating. Loading time: 4 min before coating; 29 min after coating. Elution: 0-50 min 0.05 M NaCl, 50-90 min 0.5M NaCl in Tris buffer. Protein loaded amount: before coating, Mb 2.29 mg, α-LA 2.17 mg ; after coating, Mb 10.88 mg, α-LA 9.44 mg.) 52

3.12 Effect of coating on Mb/BSA separation for a MF module. (Feed: 0.0535 mg/ml Mb and 0.0475 mg/ml BSA before coating; 0.0533 mg/ml Mb and 0.049 mg/ml BSA after coating. Loading time: 4 min before coating; 25 min after coating. Elution: 0-50 min 0.05 M NaCl , 50-90 min 0.5M NaCl in Tris buffer. Protein loaded amount: before coating, Mb 1.93 mg, BSA 2.14 mg ; after coating, Mb 8.74 mg, BSA 9.59 mg.) 53

LIST OF FIGURES
(Continued)

Figure **Page**

3.13 High loading capacity for Mb/α-LA separation for a MF module with coated zone.(Feed: 0.499 mg/ml of Mb and 0.461 mg/ml of α-LA. Loading time: 16 min. Elution: 0-50 min: 0.05 M NaCl , 50-90 min: 0.5 M NaCl in Tris buffer. Protein loaded amount: Mb 50.68mg, α-LA 46.84 mg.) 54

3.14 Cyclic runs for Mb/α-LA separation from synthetic yeast broths of different cell densities using the coated MF module. (Feed: 0.0515 mg/ml of Mb and 0.0466 mg/ml of α-LA with yeast cell suspension. Loading time: 29 min. Elution: 0-50 min: 0.05 M NaCl , 50-100 min: 0.5 M NaCl in Tris buffer.) 57

4.1 Fluid flow in the integrated device with a coated zone. 59

4.2 Mass transport in and out of a differential control volume in the shell side..... 70

4.3 Pressure, solvent flux and flow rate profiles during loading in module #1 without coating. (Tube-side feed: flow rate 200 ml/min, pressure 35.4 kPag.) 76

4.4 Protein concentration profiles along module #1 without coating at the end of loading. (Feed concentration: Mb 0.0509 mg/ml, α-LA 0.0495 mg/ml. Loading condition, tube-side feed flow rate 200 ml/min, pressure 35.4 kPag. Loading time 15 min.) 77

4.5 Pressure, solvent flux and flow rate profiles during loading in a module having a coated zone. (Tube-side feed: flow rate 200 ml/min, pressure 35.4 kPag.)..... 79

4.6 Protein concentration profiles along the module #1 with a coated zone. (Feed concentration: Mb 0.0509 mg/ml, α-LA 0.0495 mg/ml. Loading condition, tube-side feed flow rate 200 ml/min, pressure 35.4 kPag.) 80

4.7 Protein concentration profiles at the end of loading, for the high feed concentration, high loading capacity run. (Feed concentration: Mb 0.505 mg/ml, α-LA 0.467 mg/ml. Loading condition, tube-side feed flow rate 200 ml/min, pressure 35.4 kPag. Loading time 35 min.)..... 82

4.8 Comparison of the simulation results with the experimental breakthrough curves. (Loading conditions described in Figure 3.1). 83

4.9 Optimal length of the coated zone. 85

5.1 Crossflow membrane filtration with adsorbent at the permeate side..... 87

5.2 Pseudo-steady state protein transport mechanism: concentration profiles. 88

LIST OF FIGURES
(Continued)

Figure **Page**

5.3 Observed transmission vs. permeate flux at different bulk permeate concentrations. 100K membrane, (C_{bf}=5 kg/m^3, $k_f = k_p$ = 5.2×10^{-6} m/s.) 94

5.4 Observed transmission vs. permeate flux for different pore size membranes. 96

5.5 Effect of the mass transfer coefficient in the permeate side boundary layer on the observed transmission. (100K membrane, C_{bf} = 5 kg/m^3, C_{bp}=0 kg/m^3) 98

5.6 Effect of membrane skin layer thickness on τ_{ob}. (100 K membrane, $k_f = k_p$ = 5.2×10^{-6} m/s, δ_m = 5 μm, C_{bf}=5 kg/m^3, C_{bp} = 0 kg/m^3.) 99

5.7 Observed transmission enhancement for BSA and IgG. (100 K membrane, k_f = 5.2×10^{-6} m/s, k_p = 1×10^{-5} m/s, δ_m = 5 μm, C_{bf}=5 kg/m^3, C_{bp} = 0 kg/m^3. Solid line: UF-cum-adsorption; Dotted line: UF.) 100

5.8 Mb observed transmission for a UF module w. or w/o adsorbent at the permeate side. 102

5.9 Salt effect on pure water permeance. 104

NOMENCLATURE

a	Membrane surface area over the corresponding unit shell-side space volume (m^2/m^3)
A	Water permeation parameter (m/Pa/s)
A_1	Integration constant
A_2	Integration constant
B	Parameter defined by Eq. 4.7f
C	Protein concentration in the liquid (kg/m^3)
C_D	Constant for the axial dispersion coefficient.
J_v	Permeate flux (m/s)
D_0	Protein diffusivity in free solution (m^2/s)
D_S	Module housing internal diameter (m)
D_{eff}	Effective protein diffusivity in the pore (m^2/s)
D_{ieff}	Effective axial dispersion coefficient for species i (m^2/s)
d_i	Hollow fiber inner diameter (m)
d_o	Hollow fiber outer diameter (m)
d_p	Diameter of beads (m)
E_f	Defined as $\exp(J_v/k_f)$, Eq. (1c)
E_m	Exponential of the membrane Peclet number, $\exp(Pe_m)$
E_p	Defined as $\exp(J_v/k_p)$, Eq. (3c)
J_{vz}	Local permeate flux through the membrane (m/s)
k	Mass transfer coefficient (m/s)
K_i	Linear equilibrium constant for species i (mg/ml beads)

K_c	Convective hindrance factor
K_d	Diffusive hindrance factor
l_p	Permeable hollow fiber membrane length after coating(m)
l_t	Total effective hollow fiber membrane length (m)
M	Molecular weight (Da)
M_1	Parameter defined by Eq. 4.6b
M_2	Parameter defined by Eq. 4.6b
M_3	Parameter defined by Eq. 4.7g
N_0	Total number of hollow fibers packed in the module
N_s	Protein flux (kg/m^2-s)
P	Pressure (kPag)
Pe_m	Peclet number for the membrane, $\tau_\infty J_v \delta_m / D_{eff}$
q	Equilibrium protein concentation in the stationary phase (mg/ml)
Q	Flow rate (m^3/s)
Re	Reynolds number ($\rho u d_i/\mu$)
Sc	Schmidt number, ($\mu/\rho D_0$)
Sh	Sherwood number (kd_i/D_0)
S_S	Shell-side cross-sectional area (m^2)
T	Temperature (K)
u	Superficial fluid velocity
v	Interstitial fluid velocity

Greek letters

β	Parameter defined by Eq 4.9b
δ	Thickness (m)
ε	Membrane skin layer porosity or void fraction of the packed bed
μ	Viscosity (Pa-s)
τ_i	Intrinsic membrane transmission
τ_{ob}	Observed protein transmission
τ_∞	Asymptotic intrinsic membrane transmission
ϕ	Protein partition coefficient between the solution and the membrane

Subscripts

0	At the module inlet
b	Bulk solution
i	Species i
I	Membrane-liquid interface
f	Feed side
L	Lumen side of the hollow fiber
m	Membrane
p	Permeate side
S	Shell side of the hollow fiber module
z	At any point from the module inlet

CHAPTER 1

BACKGROUND

1.1 Introduction

Bioproducts produced by cells are either intracellular or extracellular. For an intracellular product, cells are first harvested from the fermentation broth or cell culture, and then lysed to release the bioproducts. For an extracelullar product, the product is excreted by the producing organisms into the surrounding medium. The products are subsequently isolated from the cells or cell debris and purified through a sequence of clarification, concentration, adsorption and chromatography steps. Due to the potential denaturation or contamination of the biomolecules, the bioprodcuts need to be isolated from the complex lysate/medium and purified as soon as possible.

Direct bioproduct recovery and purification from a fermentation broth or a lysate is complicated by the large number of dissolved substances and suspended particles. Most of the biomolecules are sensitive to heat and harsh chemical conditions; adsorption and chromatography under mild conditions are the most widely used methods for separation and purification. Conventional adsorption and chromatography processes are undertaken in the packed bed, which can not process unclarified feed streams containing particulate matter which will lead to column plugging. Traditionally, a number of pretreatment steps have to be employed to eliminate the cellular or colloidal suspended material and concentrate the feed prior to bioproduct purification via adsorption/ chromatography. These processes include centrifugation, flocculation, liquid-liquid extraction and various forms of microfiltration (Russotti and Göklen, 2001). It is common

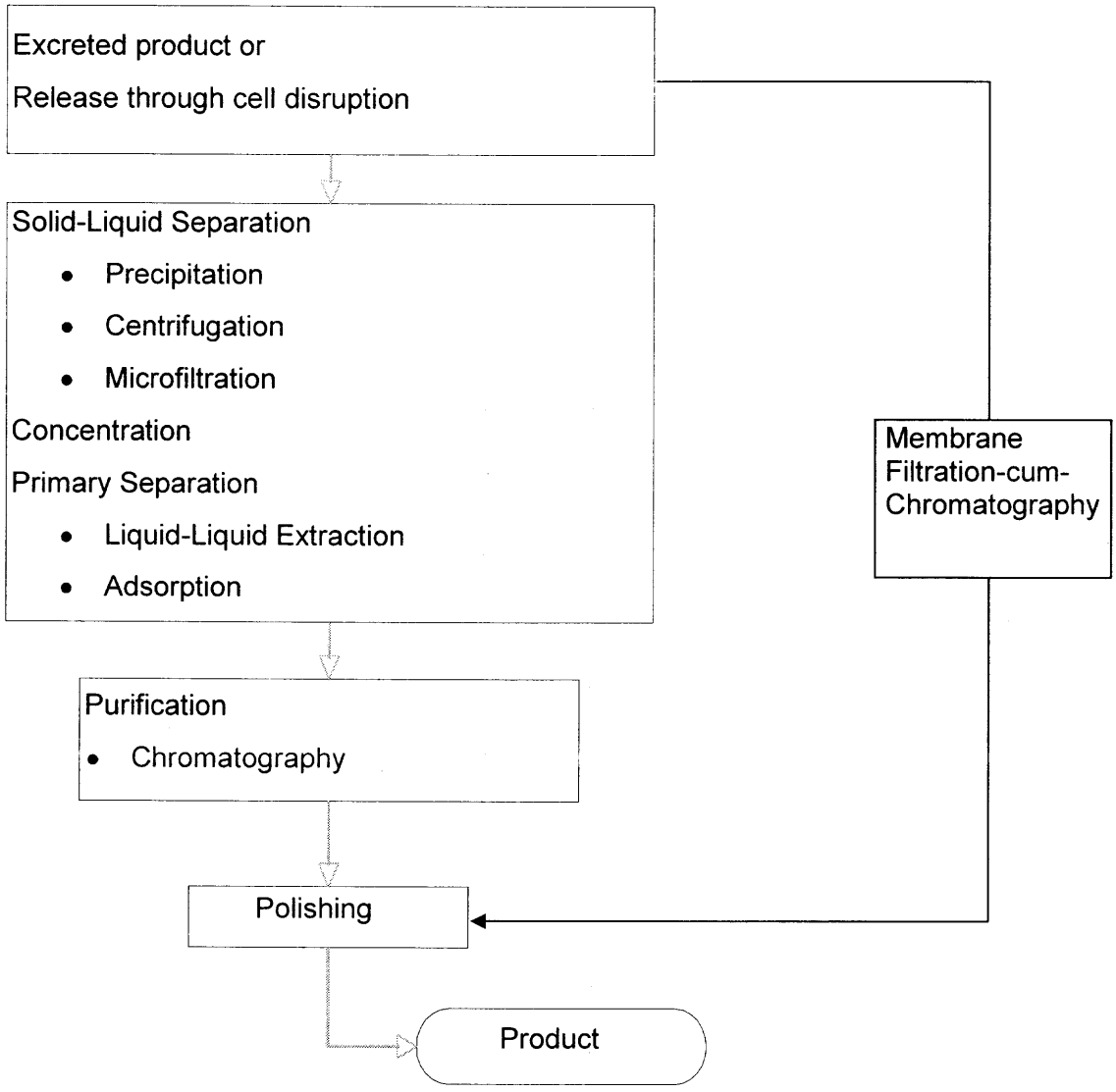

Figure 1.1 Simplified downstream processing schematic based on membrane filtration-cum-chromatography.

to take dozens of steps for product recovery and purification in a biopharmaceutical manufacturing process. For example, in the process of Eli Lilly's human insulin produced from *E. coli* fermentation, 27 out of the 31 total processing steps were associated with product recovery and purification (Prouty 1991; Ladisch 2001). Typically, 50-90% of the total production costs is for downstream recovery and purification (Committe on Bioprocess Engineering 1992; Harrison 1994). Furthermore, there are significant losses of product and risks of contamination in each such complex step. A process/device that could combine clarification along with recovery and purification of the product biomolecule/protein as shown in Figure 1.1 would be highly desirable and crucial to low cost bioproduct manufacturing.

One strategy that has been suggested previously for direct bioproduct capture and separation from the unclarified feed is suspending adsorbent beads in the unclarified feed in a stirred tank; the beads can adsorb the target species in the suspension. Once the beads have been loaded, they can be recovered from the suspension by various filtration techniques. Byers et al. (Byers, Jsacoff and Naples 1991) used hollow fiber membrane filtration to recover such loaded beads and another membrane filtration process to separate the product with the adsorbent beads. Davis (1990) proposed a technique to circulate the affinity bead-containing stream through one side of a membrane while feed containing the bioproduct flowing through the other side of the membrane. The target bioproduct and some impurities bind to the adsorbent upon passing through the membrane. The bound molecules are recovered from the affinity beads in a separate elution process. Bucak et al. (2003) recently developed a magnetic nanoparticle separation technique. The magnetic nanoparticles in the suspension system loaded with

target proteins are easily retained on the steel wire mesh under high-gradient magnetic filtration. The proteins are eluted from the retained nanoparticles by passing eluent with an appropriate pH and ionic strength. The retained nanoparticles are then released by turning off the magnet, and recycled.

Another strategy is using fluidized or expanded bed to capture the bioproduct directly from the fermentation broth or cell culture (Thommes, Halfar, Lenz and Kula 1995; Finette, Baharin, Mao and Hearn 1998). While the bed is fluidized or expanded by the feed stream, void fraction of the bed will be increased enough for cells and cell debris to pass through. The fluidized beads loaded with the target proteins are then washed with buffer to remove the cells in the void volume and settled down for elution. The proteins are eluted from the sedimented bed using suitable buffers. Capture of immunomycin from a *streptomyces* culture in large scale using a fluidized bed has been reported (Gailliot, Gleason, Wilson and Zwarick1990). Common chromatography beads have a low density and narrow size distribution. Thus the fluidized beads experience high degree of axial mixing in the bed, causing early breakthrough during loading and poor purification result during elution. The low density beads having low settling velocity also limit the fluid flow velocity. The bed will be expanded too much and beads will be entrained from the bed at high flow velocity.

Expanded bed adsorption (EBA) technology was developed to alleviate the extent of axial mixing in the fluidized bed so that its breakthrough and elution behaviors resemble those of the packed bed (Chase 1994; Ohashi, Otero, Chwistek, Yamato and Hamel 2002; Bai and Glatz 2003). The adsorbent beads used in EBA are tailored with broader size and density distributions. STREAMLINE adsorbents manufactured by

Amersham Biosciences (Uppsala, Sweden and Piscataway, NJ) are typical media for EBA. Inert crystalline quartz particles are incorporated into the cross-linked agarose matrix to increase the density of the beads. The beads exhibit Gaussian like size and density distribution with a mean particle size of 200 μm (Amersham Biosciences 2000). Second generation EBA sorbent based on gel-permeate porous zirconium oxide beads was developed recently by Ciphergen (Fremont, CA). The new material with a density of 3.2 g/ml, has a higher surface area and can be used at higher flow rates (Tunon 2002). When the bed filled with these beads is fluidized, beads with similar size and density will stay in their local fluidization layers. Larger and heavier beads will stay at the bottom of the bed while smaller and lighter beads will stay at the top of the bed. While an expanded bed is settled down, the mutilayer structure will be kept in the sedimented bed. The operation of the EBA is illustrated in Figure 1.2.

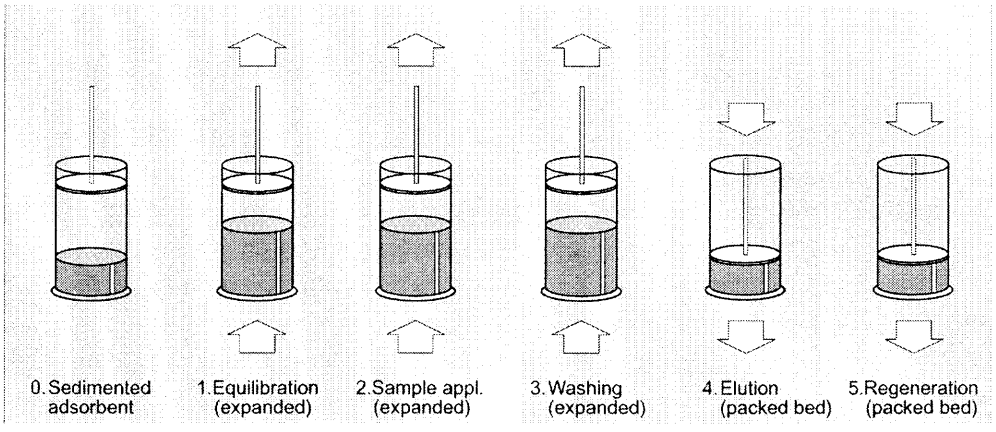

Figure 1.2 Schematic presentation of the steps of EBA. (Amersham Biosciences 2000)

However, in the fluidized or expanded bed process, the cells or cell debris interact with the adsorbent beads, affecting protein adsorption (Fernandez-Lahore, Geilenkirchen, Boldt, Nage, Kula and Thommes 2000) and causing adhesion and agglomeration of the cells and fluidized beads. Draeger and Chase (Draeger and Chase 1991) found that the BSA binding capacity on a quaternary anion-exchange resin dropped about 75% after addition of 2% of *Alkaligenes eutrophus* cells in the feed. The formation of the particle agglomerations will breakdown the stability of the fluidization (Johansson, Jagerstern et al. 1996; Lin, Kula et al. 2003). Cell aggregates can also clog the screen or the flow distributor at the lower column adapter, causing nonhomogeneous fluidization. Furthermore, the cells adhered on the adsorbents are difficult to wash out completely. Adsorbed cells of bakers' yeast on the surface of a DEAE anion-exchange resin were still observed after extensive washing with an elution buffer (Anspach, Curbelo et al. 1999). In purifying G6PDH from unclarified yeast cell homogenates using EBA with ion exchange resin, the eluate was found to have viable cells to the extent of 0.01% of that of the feedstock (Chang and Chase 1996). Due to these limitations, although EBA technology has been promoted heavily for over ten years, adoption of the technique has been slow in spite of its promises of faster processing of crude feedstocks (Tunon 2002).

Microfiltration and ultrafiltration have been widely used in bioprocessing for solid-liquid separation and product concentration (Sirkar and Prasad 1986; Zeman and Zydney 1996; Kalyanpur 2000; Wang 2001). The ultrafiltration membrane can also be used to fractionate proteins of different sizes (Ghosh and Cui 2000). Conventionally, the two proteins have to be five to ten times different in their molecular weights to be separated by ultrafiltration. Zydney and van Reis's group developed high-performance

tangential-flow filtration which can be used to separate two proteins with similar molecular weight by carefully operating in the pressure-dependent regime and controlling the buffer pH and ionic strength (van Reis, Goodrich et al. 1997; Zydney and van Reis 2001). Saksena and Zydney (1994) showed that 20-fold selectivity increase for the filtration of BSA and IgG could be achieved by lowering the pH from 7 to 4.8 and the ionic strength. Cheang and Zydney (2003) also found that the selectivity of α-LA and β-LG could reach over 55 by adjusting pH and ionic strength. These high selectivities are usually achieved at low ionic strength and the buffer pH close to the pI of one protein. The protein near the neutrally charged state will permeate through the membrane easily. While the other protein, carrying a strong charge under the same conditions, is excluded by the membrane pores with the same kind of charge. However the membrane process alone can hardly yield pure product. It should be considered still as a separation and fractionation step, not a purification step. Also, in the real bioseparation processes, the complex fermentation broth contains large amount of different biomolecules and impurities, limiting the extent to which one can play with protein charges to get a high selectivity.

Molinari et al. (1990) explored direct carboxylesterase capture from the fermentation broth and partial purification using a hollow fiber membrane device with affinity or ion exchange beads in the shell side. They circulated the feed broth through the hollow fiber lumen with two shell-side ports totally closed, i.e., Starling flow operation mode (Starling 1896). Due to the higher pressure drop along the module at the lumen side caused by feed flow, the lumen-side pressure was higher than the shell-side pressure in upstream locations, but the pressure difference was reversed in downstream

locations. As a result, a small amount of liquid permeated through the membrane to the shell side in upstream locations, proteins transported along with the liquid were adsorbed on the beads in the shell side, and liquid permeated back to the lumen side at downstream location. The loading was continued for five to seven hours. Then the carboxylesterase was recovered using shell-side elution. The beads at the shell-side acted like a adsorbent bed. No chromatography separation was involved. The purity of the carboxylesterase in the eluate was only 2.3 fold of that in the feed solution.

Among the techniques that have been suggested to improve this situation, the technique proposed by Dai et al. (1999) is especially attractive. In this technique, chromatographic resin beads are used to fill the shell-side space of a hollow fiber membrane module. The hollow fiber membrane may be designed for microfiltration (MF) or ultrafiltration (UF) of the protein solution containing suspended cellular material. The technique is implemented in a cyclic fashion.

First, the device goes through the loading step in which the feed solution containing the suspended cellular material is brought to the tube-side of the fibers at a pressure higher than that in the shell side (Figure 1.3a). Larger entities like cells and cell debris are rejected by the membrane and flow out with the retentate. Small molecules in the buffer solution as well as the proteins can permeate through the membrane to the shell side, where the target proteins will be captured by the beads; the buffer solution and other non-adsorbable impurities flow out through the permeate outlet. The permeate solution going through the membrane containing the protein mixture will flow over the shell-side beads leading to the adsorption of the proteins. After about 5-30 minutes of such protein

loading, the input of the feed solution to the fiber tube side is stopped. The loading is stopped prior to significant protein leakage through the shell-side permeate outlet.

In the next step of the cycle, an eluent solution is supplied to the device either through the tube-side inlet (tube-side outlet remaining closed along with the shell-side inlet) or the shell-side inlet (tube-side ends closed). The eluate leaves the device through the shell-side outlet (Figure 1.3b). After the respective bioproduct peaks emerge from the shell-side outlet, the eluent flow is stopped. The shell-side resin bed is regenerated next by passing the starting buffer for a certain period of time. Once the bed is regenerated, the loading-elution-regeneration cycle is repeated.

As the results in Dai et al. (1999) show, the cyclic process works well. It can separate protein mixtures from a fermentation broth via the hollow fiber membrane and the chromatographic resin beads. Two distinct protein peaks emerge in the eluent solution corresponding to the two different proteins present in the feed fermentation broth. As Figure 10 of Dai et al. (1999) shows, the cyclic process is repeated many times successfully and continuously to separate a mixture of myoglobin and α-lactalbumin from a clean feed. Figure 11 of Dai et al. (1999) demonstrates that the same two proteins can be purified via the cyclic process with two distinct peaks emerging in the eluate if the feed is a synthetic fermentation broth.

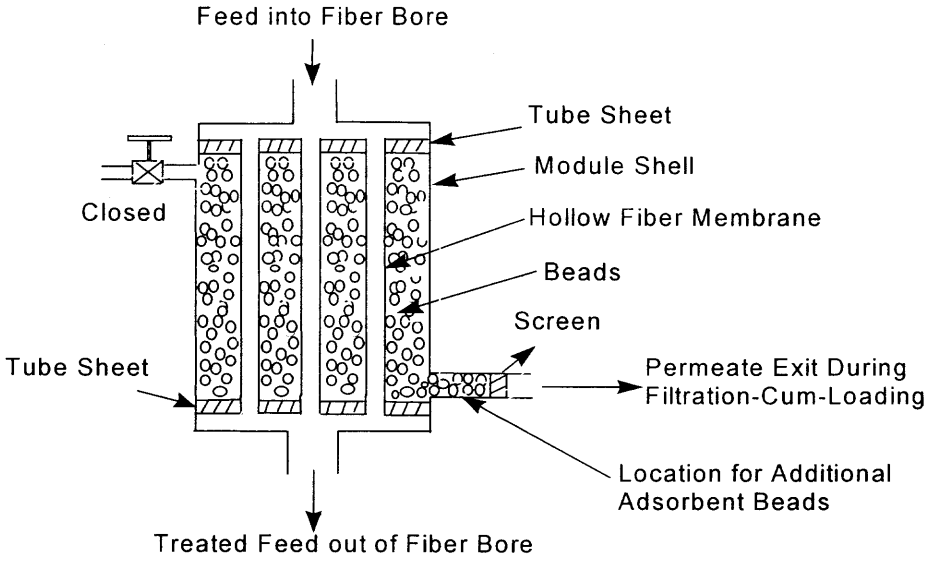

(a) Loading

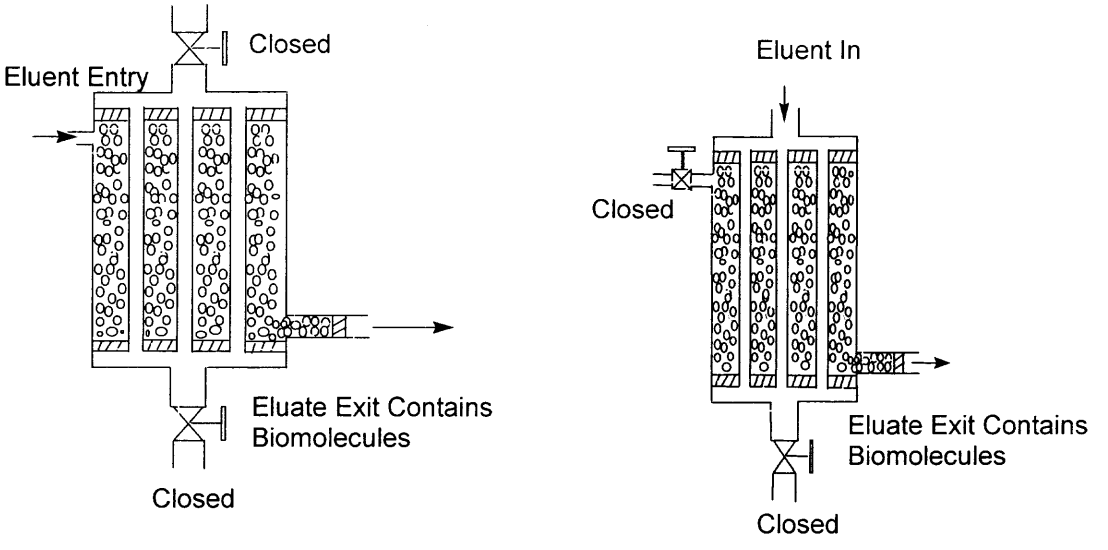

(b) Elutions

Figure 1.3 Configuration of the device containing membrane and adsorbent beads under different operating conditions.

A large variety of membranes and chromatographic media are commercially available. They are the two workhorses in bioprocessing. Based on a specific property of the target protein, broad choice and flexible combination of the membrane and chromatographic beads for the integrated device will save process development time. Integrating the advantages of these two separate processes in one device will save many transitional steps thus simplify the bioprocessing.

The device and process proposed in Dai et al. (1999), however, have an important characteristic. The proteins in the permeate appearing in the shell-side near the tube-side outlet/shell-side outlet can be adsorbed by only a thin layer of chromatographic resin beads in the shell side as it radially flows out to the shell-side permeate outlet. If the loading process is allowed for a longer period, significant amount of proteins will escape adsorption over the shell-side beads requiring recycle of the shell-side outlet fluid. This will reduce the loading capacity of the device.

One strategy therefore used in Dai et al. (1999) is to use an extended section (ES) containing additional chromatographic resin beads at the permeate outlet on the shell side (Figures1.3a and1.3b). This provides additional significant adsorption capacity for proteins coming from permeation at the outlet section of the hollow fiber device and escaping the beads at the bottom of the shell-side column. Such an extended section can accommodate, however, only a limited amount of resin beads; it also imposes a significant amount of pressure drop reducing the permeate flow rate (Dai, Luo, and Sirkar 2000). If the capacity of the shell-side adsorbent bed has to be increased considerably, an

altogether different solution is needed. A new type of integrated membrane-cum-chromatographic device has to be developed.

1.2 New Device Concept

To increase the bed utilization factor and reduce the protein leakage without increasing the permeate outlet back pressure, it is necessary to move the point of the maximum permeate flux upward away from the permeate outlet (Dai, Majumdar, Luo and Sirkar, 2003). This can be achieved by blocking the membrane pores near the module outlet zone thus shutting down the liquid and protein permeation at that zone. Coating the inner skin of the hollow fiber near the outlet zone through interfacial polymerization can be used to realize this idea. This new device employs chromatographic resin beads on the shell side of a UF/MF hollow fiber membrane device as in Dai et al. (1999) and Dai et al. (2003). However, there are two major differences. First, there is no extended section (ES) of resin beads at the permeate outlet. Thus the significant amount of additional pressure drop in the permeate flow due to an ES is eliminated. Second, the bottom section of the hollow fiber membranes in the device, i.e., the section close to the shell-side permeate outlet is radically restructured. Interfacial polymerization (Cadotte 1981; Cadotte, King Majerle and Petersen 1981) will be carried out to form an essentially impermeable thin layer of polyamide membrane on top of the skin surface of the hollow fiber membrane on the tube side near the shell-side permeate exit (Figure 1.4).

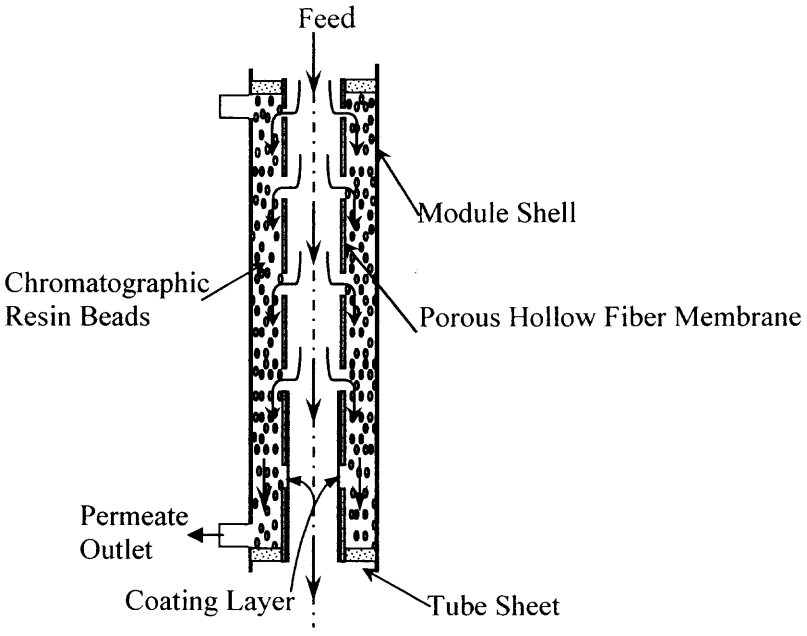

Figure 1.4 New device concept: an integrated device with a coated zone near the outlet.

The coating essentially makes the bottom section of the hollow fiber impermeable to water flow due to the pressure drop applied in UF/MF since the coating conditions create a membrane suitable for reverse osmosis which requires a much higher ΔP for water permeation. As a result, during the protein loading step, there is almost no permeate emerging onto the shell side from the tube side near the shell-side permeate outlet. Therefore, no fresh protein is introduced into the shell side near the shell-side permeate outlet from the tube-side feed solution. Consequently, the protein leakage into the permeate solution observed in Dai et al. (1999) should be drastically reduced. Correspondingly, the overall protein loading capacity of the shell-side bed should be increased dramatically in the new device.

This change introduces a radically new membrane filtration-cum-chromatography device: a hollow fiber device which for most of its length functions as it should in UF/MF while the rest of the fiber length is essentially shut off from a filtration point of view. Correspondingly, the beads on the shell side for this latter section of the device can act as a conventional resin bed which has considerable adsorption/fractionation capacity whereas the rest of the resin bed on the shell side performs as in Dai et al. (1999) and Dai et al. (2003).

The separation performance of this new device will be investigated in this study. The separations of the following protein mixtures will be studied: Mb and α-LA; Mb and BSA. Most of the studies will be carried out with a clear feed solution in devices which either have an UF or a MF membrane. However, a Mb/α-LA solution in an yeast cell-based fermentation broth will also be employed as a feed for four consecutive cycles in a MF-based module. The performance of this device will also be compared with that of the earlier device without the membrane coating for both UF and MF membranes.

A mathematic model describing the hydrodynamic and protein loading behavior of the integrated device with a coated zone will also be presented in this work. Comparison of the simulated pressure, flow rate, permeate flux and protein loading profiles for the module with a coated zone and the module without any coating will allow insight into the mechanism of loading capacity improvement after a coated zone is introduced. Optimal length of the coated zone will be found out through simulation of the model.

Protein mass transfer enhancement was observed earlier in the integrated membrane filtration-cum-chromatography device (Dai, Luo and Sirkar 1999, Dai 2000).

A theoretical analysis of the protein transport through the membrane with adsorbent present at the permeate side will be developed using a diffusion-convection model in this work. The extent of the mass transfer enhancement using different systems and under different operation conditions will be explored.

CHAPTER 2

EXPERIMENTAL MATERIALS AND METHODS

2.1 Materials

2.1.1 Hollow Fiber Membranes and Modules

2.1.1.1 Hollow Fiber Modules from A/G Technology. The hollow fiber modules used were two UFP-100-E-4A ultrafiltration modules (MWCO 100 K) and a CFP-1-E-4A microfiltration module (pore size 0.1 μm) from A/G Technology (Needham, MA). Each module (ϕ1.52×36 cm) contained 50 polysulfone hollow fibers. The hollow fibers were 1 mm in internal diameter (ID) and 1.6 mm in outer diameter (OD). The effective hollow fiber length and the corresponding shell space volume for each module used in the experiments are listed in Table 2.1. Figure 2.1 illustrates the general configuration of the hollow fiber modules.

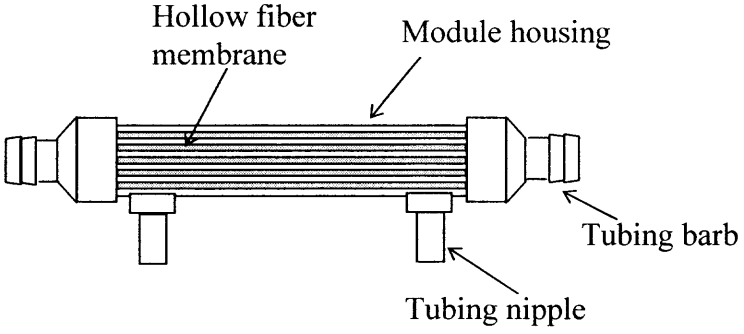

Figure 2.1 Hollow fiber module from A/G Technology.

Table 2.1 Parameters for Hollow Fiber Membrane Modules

Module		Fiber effective length (cm)	Shell space volume (ml)
Type	No.		
UF	1	24.5	19.8
	2	25.4	20.5
MF	3	25.6	20.7

The new membrane modules were soaked in ethanol solution overnight to remove the glycerol and displace any air in the membrane pores. The modules were then rinsed with deionized water and flushed with 4L warm deionized water at 60°C.

2.1.1.2 Crossflow Module with Two Sets of Hollow Fibers. To reduce the flow resistance at the permeate side having the chromatographic media packing, a small but complete crossflow module (Module No. 4) with two sets of hollow fibers was made in-house. The module configuration is shown in Figure 2.2. During operation, both of the shell-side ports remain closed. The permeate flowing out from the feed hollow fiber flows through the module shell space in a direction perpendicular to the module axis, and is collected by the permeate hollow fiber (hollow fiber 2). The two sets of hollow fibers can be different or same in so far as the membrane type and pore size are concerned. Two microfiltration hollow fibers from A/G Technology (Needham, MA), having a pore size of 0.2 μm, ID of 1 mm and OD of 1.6 mm, were used to make this module. The two hollow fibers were carefully aligned to be parallel to each other throughout the length of the whole module, with a distance of 1 cm between them. A 14 cm diameter transparent polypropylene (PP) tube was used as the module shell. The effective hollow fiber length was 13.6 cm.

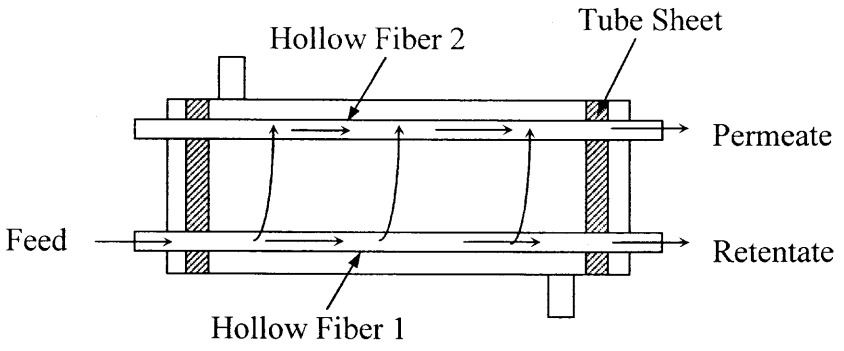

Figure 2.2 Two different sets of hollow fiber-based crossflow module.

2.1.2 Chromatographic Media

DEAE (diethylaminoethyl) Sepharose Fast Flow beads were from Amersham Biosciences (Piscataway, NJ). The weak anion exchange functional groups are covalently grafted to the pore surface of the highly cross-linked porous agarose beads. The highly cross-linked agarose beads provide greatly improved physical and chemical stability compared to Sepharose CL-6B ion exchange media, allowing the Sepharose Fast Flow beads to be used at higher flow rates required for large-scale chromatography. The structure of the bead and the functional group for anion exchange are shown in Figure 2.3. The characteristics of the anion exchanger are listed in Table 2.2.

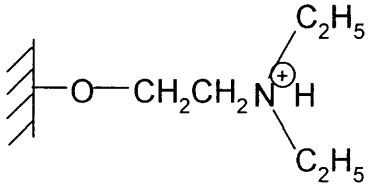

Figure 2.3 Structure of DEAE Sepharose Fast Flow beads.

Table 2.2 Characteristics of DEAE Sepharose Fast Flow Anion Exchange Beads (Amersham Pharmacia Biotech 2000)

Total ionic capacity	0.11 - 0.16 mmol/ml gel
Available capacity	100 mg/ml for α-lactalbumin
Bead structure	6% highly cross-linked agarose
Bead size range	45 - 165 μm
Mean bead size	90 μm
Max. linear flow rate	750 cm/h
Max. operating pressure	0.3 MPa (42 psi)
pH working range	3 - 9
pH stability (long term)	3 - 12
pH stability (short term)	1 - 14
Chemical stability	All commonly used aqueous buffers, 1 M NaOH, 8M urea, 70% ethanol, etc.
Physical stability	Negligible volume variation due to changes in pH or ionic strength
Autoclavable	With counterions (Cl^-) at 121°C, pH 7 for 30 min.
Storage	20% ethanol at 4°C

2.1.3 Proteins, Adsorbent, and Process Chemicals

Myoglobin (Mb, MW 17566, pI 7.3 (Radola 1973)), α-lactalbumin (α-LA, MW 14175, pI 4.2-4.5 (Kronman and Andreotti 1964)), bovine serum albumin (BSA, MW 66430, pI 4.7 (Longsworth and Jacobsen 1949)) and sebacoyl chloride ($C_{10}H_{16}Cl_2O_2$, MW 239.14) were purchased from Sigma (St. Louis, MO). 1,6-hexanediamine ($C_6H_{16}N_2$, MW 116.2) was purchased from ACROS (Geel, Belgium). Octane solvent was purchased from EM Science (Cherry Hill, NJ). Tris-HCl, Tris-base and NaCl were purchased from Sigma (St. Louis, MO). 20 mM Tris-HCl buffer at pH 8.5 was prepared by dissolving 3.536 g of

Tris-HCl and 6.976 g of Tris-base in 4 L deionized water and used as the starting buffer in all of the experiments.

2.1.4 Cells and Synthetic Fermentation Broth Preparation

Yeast strain (*S. Cerevisiae* NRRLY-12636) was purchased from the United States Department of Agriculture (Peoria, IL). Yeast extract, malt extract, peptone and glucose for the YM medium broth were all from Sigma (St. Louis, MO). YM medium broth was prepared by dissolving 3 g yeast extract, 3 g malt extract and 5 g peptone together in 600 ml water, 10 g glucose in 400 ml water separately, autoclaving at 121°C (15-16 psig steam) for 20 min, and then mixing the two solutions after cooling down. Yeast cells were cultured in 50-60 ml YM medium broth in a shaker incubator (New Brunswick Scientific, Edison, NJ) at 30°C for 20-24 hours. The yeast broth was centrifuged using an IEC Clinical Centrifuge (International Equipment Co., Needham HTS, MA) at 3000 *g* for 3 min. The supernatant was discarded and the cells were washed and centrifuged 3 times with deionized water and finally with the starting buffer.

2.2 Device Fabrication

2.2.1 Packing the Beads into the Shell Side of the Hollow Fiber Module

The ethanol solution in the bead storage container was replaced with the starting buffer. The beads were washed with the starting buffer 3 times and then equilibrated with the starting buffer. The dilute bead slurry was degassed for 5 min in a Cole-Parmer 8850 ultrasonic bath (Chicago, IL).

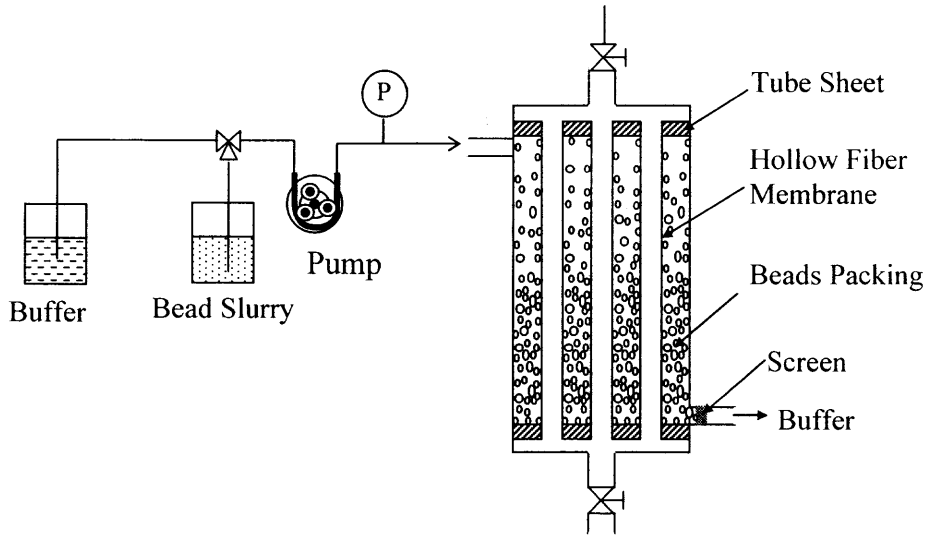

Figure 2.4 Packing the beads into the shell side of the membrane module.

Before packing the beads into the shell side, the module was thoroughly cleaned and washed with the starting buffer. With both tube-side ports closed and the shell-side outlet port covered with a 21 μm polyester mesh, the starting buffer was pumped through the shell-side inlet port using a peristaltic pump at a flow rate of 4-6 ml/min. Then the feed was switched to the dilute bead slurry. The beads were densely packed in the shell side of the module from the bottom to the top while the buffer flowed out. After the whole shell-side space was full of beads, the feed was switched back to the clear starting buffer to flush the packing for 10 more minutes.

2.2.2 Interfacially Polymerized Coating on the Hollow Fiber Inner Skin Near the Outlet Zone

The membrane filtration-cum-chromatography devices using either UF or MF membranes fabricated in the last section were first tested for pure water permeation flux, hydrodynamic parameters, and protein loading-elution behaviors. After these experiments

were completed, the modules were cleaned thoroughly. To prevent early protein leakage and improve the loading capacity and protein separation, the bottom part of the hollow fiber membranes near each module outlet was coated with a thin interfacially-polymerized nylon 6-10 polyamide film. The following solutions were prepared first for interfacial polymerization:

Organic phase: 1% sebacoyl chloride in octane;

Aqueous phase: 1% 1, 6 – hexanediamine in deionized water.

When such an aqueous phase and the corresponding organic phase meet together at the phase interface, the sebacoyl chloride in the organic phase will polymerize with the hexanediamine in the aqueous phase, forming a thin polyamide film. The reaction is shown in Figure 2.5. The condensation polymerization happens at room temperature quickly, giving off HCl as the by-product. Small amount of alkalis (such as Na_2CO_3, NaOH etc.) can be added in the aqueous phase to absorb the released HCl and promote higher degree of polymerization. The sebacoyl chloride is highly reactive and could destroy the polysulfone membrane if the organic solution was allowed to contact the membrane surface directly. The membrane surface should be thoroughly wetted with the aqueous solution before the introduction of the organic solution.

Before carrying out the interfacial polymerization, the whole module was thoroughly flushed with deionized water to remove the Tris-HCl buffer. The schematic of the coating device is shown in Figure 2.6. With both shell side ports closed and the shell side filled with water, the interfacial polymerization was performed as follows.

1. The 1,6-hexanediamine containing aqueous solution was injected from the bottom of the tube-side port to fill the fiber lumen fully above the height of the desired coating level (say, 5 cm) with a syringe and was held there for 5 min.

2. The aqueous solution was drained next from the tube-side outlet port. The remaining aqueous solution in the tube side was blown out using compressed air.

3. The organic phase was then introduced from the bottom of the module into the fiber lumen with a feed side adjustable U shaped tube to control the organic phase level at 5 cm above the effective bottom of the hollow fibers. After 1 min, the organic phase was drained. Then the hollow fiber lumen was blown with compressed air again to remove any remaining organic phase.

4. With the tube side outlet port fully open, the module tube side was rinsed slowly with deionized water at a flow rate of 7.5 ml/min for 30 min at room temperature.

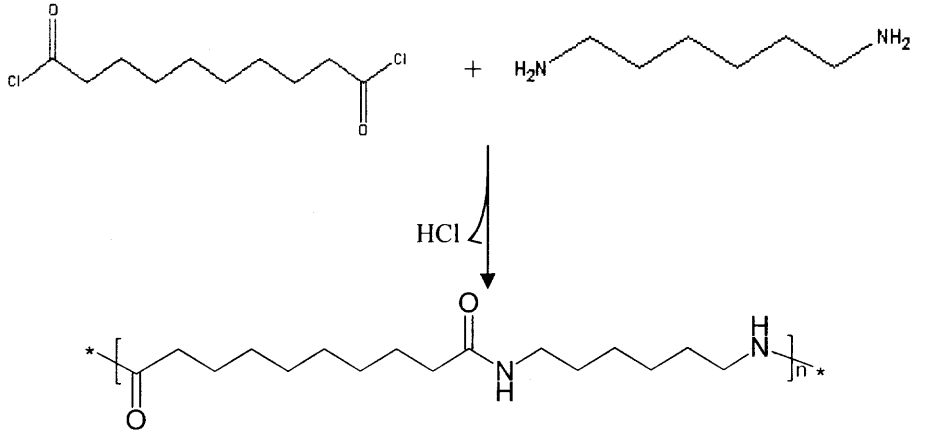

Figure 2.5 Interfacial polymerization reaction.

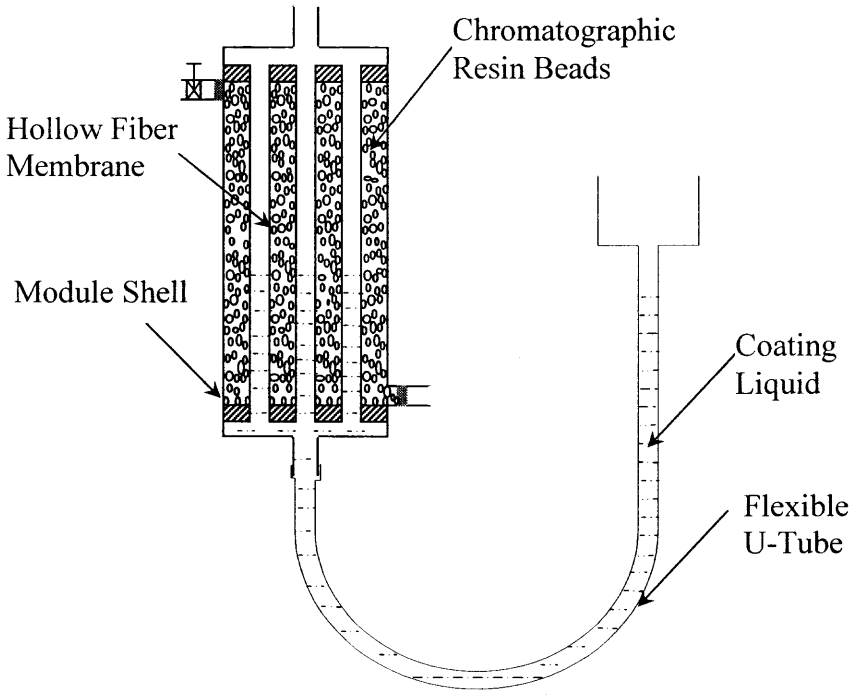

Figure 2.6 Device for partial coating of the hollow fiber membranes by interfacial polymerization.

5. The tube side was further flushed with warm water at 60°C for 30 min, then with 0.5 N NaOH solution at 60°C for 30 min at a flow rate of about 20 ml/min (this heat treatment allowed the interfacial polymerization reaction to go to completion so that the mechanical strength and solvent resistance of the coating will be improved).

6. The module was then cooled down and flushed first with deionized water and then with 20 mM Tris-HCl buffer (pH 8.5) at room temperature.

The coating length was about 6 cm, which is about 1/5-1/4th of the total effective fiber length depending on the module.

2.3 Experimental Setup

The experimental setup shown in Figure 2.7 was used for measurement of the membrane water permeation flux and protein transmission as well as the cleaning, loading and washing of the module with/without bead packing. The liquid in the feed reservoir was pumped to the module tube side inlet by a Masterflex 7518-60 peristaltic pump (Cole Parmer, Chicago, IL) at the desired flow rate. The operating pressure was controlled by the valve at the tube-side outlet. The permeate flow rate was regulated by the valve at the permeate outlet. Pressures at the tube-side inlet and outlet as well as the shell side were indicated by pressure gauges. Both the retentate and the permeate can be recycled if necessary.

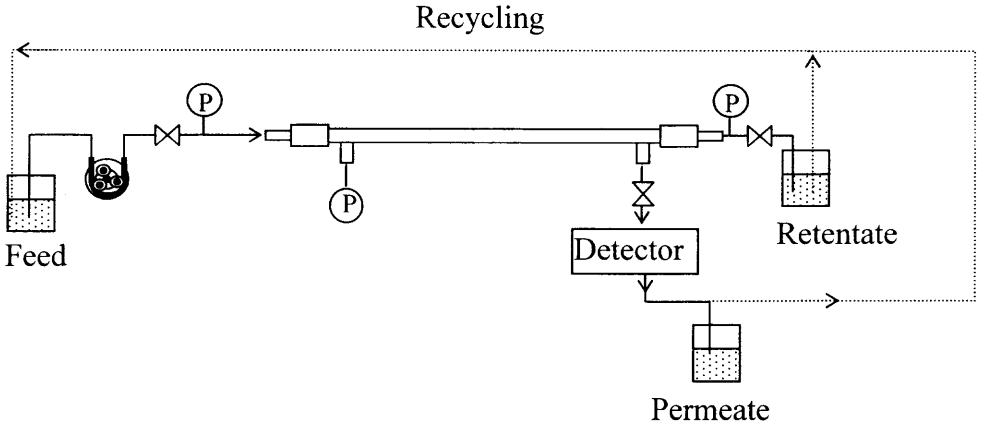

Figure 2.7 Setup for membrane filtration and loading of the integrated device.

Crossflow operation was used in all experiments. When starting a crossflow operation, the permeate outlet valve should be totally closed and the retentate outlet valve should be fully open at the beginning. Then the feed pump was turned on, the feed flowed through the membrane tube side without backpressure and the retentate was recycled to the feed reservoir. After flow in the tube side had stabilized, the permeate side outlet

valve was slowly opened and the retentate valve was slowly closed to the extent necessary to get the permeate flow at the desired operating pressure. The permeate flow rate was determined by measuring the permeate volume collected within a measured time interval using a graduated cylinder.

2.4 Membrane Characterizations and Protein Transmissions

The pure water fluxes for various membrane modules were measured using the setup shown in Figure 2.7 under different transmembrane pressure differences. Water feed flow rate was 200 ml/min for all tests. Steady state crossflow condition was built up with total recycling of the permeate and the retentate for 5 min. Then the permeate flow rate was measured. For the MF module, the pure water fluxes were measured under very low transmembrane pressure difference because a high permeate flow rate will cause significant shell-side pressure drop. The transmembrane pressure difference was measured using an inverted U-tube manometer between the tube-side and shell-side ports at the inlet side. The manometer was filled with air as the manometric fluid, while the tubing between the pressure taps and the U-tube was filled with water.

Protein transmissions for the UF module with or without beads packing were determined using the same setup. Protein solutions were fed to the module tube side at a flow rate of 200 ml/min and pressure of 34.5 kPag. Permeate flow control was used to obtain the protein transmission for different value of the permeate flux. Crossflow filtration was started with total recycle of the permeate and retentate. Then the permeate outlet control valve was slowly opened and adjusted to the desired permeate flow rate. When the total permeate volume reached two times the module shell-space volume,

steady state was assumed to have been achieved. Samples of feed, permeate and retentate were taken at steady state, and assayed for the protein concentrations.

2.5 Filtration-cum-Chromatography Operation: Single Cycle Run

2.5.1 Cleaning, Loading and Washing Setup and Operations

Before the experiment, the cartridge was cleaned by recycling the 0.5 M NaOH and 0.5 M NaCl cleaning solution at a flow rate of 200 ml/min, pressure of 34.5 kPag and temperature of 50°C for 1 hr; the cartridge was then flushed with deionized water at 50°C, regenerated with 0.5 M NaCl solution, and equilibrated with the starting buffer at room temperature. During loading, the protein containing feed solution was introduced to the module tube side at a flow rate of 200 ml/min. The operating feed pressure was maintained at 34.5 kPag. The retentate was recycled. The permeate from the shell-side outlet port was collected and measured for total volume. Both the permeate and the retentate were sampled and assayed for their protein concentrations. After loading, the protein solution remaining in the fiber lumen was drained and the lumen was washed with 50 ml starting buffer while the tube-side outlet valve was fully open and both of the shell-side ports were closed.

2.5.2 Elution

After protein loading and washing, tube-side elution was performed using a GradiFrac System from Amersham Biosciences (Piscataway, NJ). The system consisted of a gradient solvent delivery system, a LKB UV monitor at 280 nm wavelength, a conductivity monitor, a REC 102 recorder and a GradiFrac fraction collector. The

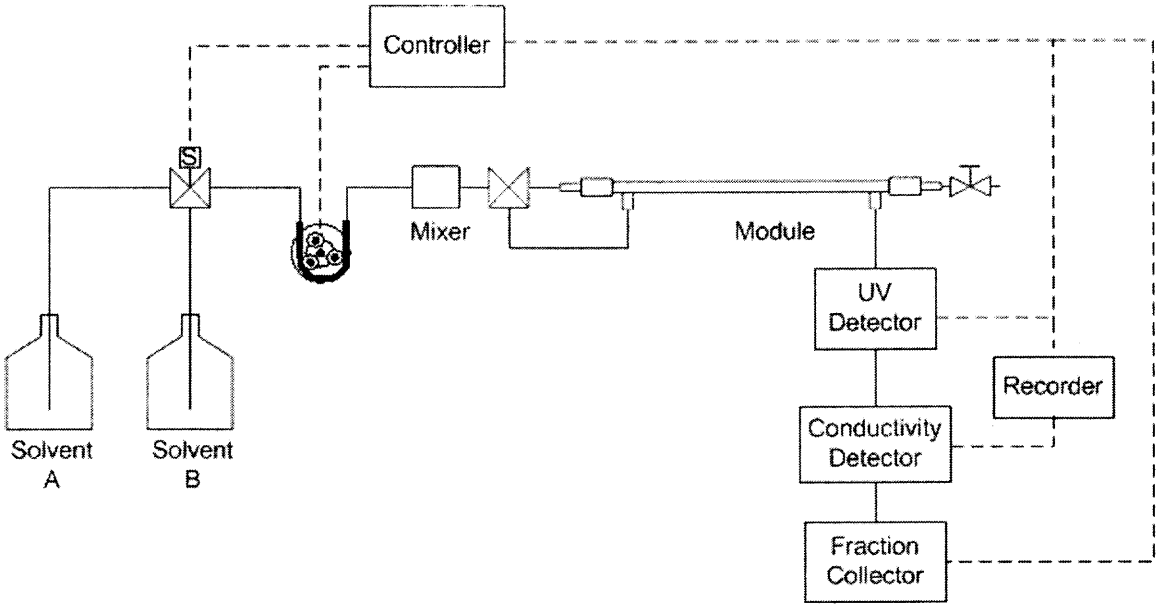

Figure 2.8 System for step-wise and gradient elution.

schematic of the setup is shown in Figure 2.8. Solvent A (starting buffer) and solvent B (0.5 M NaCl in the starting buffer) were pumped by a LKB1 pump and completely mixed in a mixer forming the elution buffer. The percentage of the solvent B, hence the ionic strength of the elution buffer, was adjusted by the opening of a PSV-50 control valve at the pump inlet. The elution buffer flowed into either the tube-side or the shell-side inlets of the module while the tube-side outlet was closed. The eluate came out through the shell-side outlet. Fractions were collected every 2.5 min using the GradiFrac fraction collector and assayed for protein concentrations using an UV spectrophotometer. In stepwise elution, initially, an elution buffer with lower ionic strength was used for a period of time to elute out the weaker charged protein, then a step-change of the ionic strength of the elution buffer was made by increasing the percentage of solvent B to elute

out the other more highly charged protein. In gradient elution, the eluent salt concentration was increased linearly from an initial low value to a higher value at a specific time. Multiple segments with different gradients can be used. The eluent flow rate was 2.5 ml/min for all elution experiments.

2.6 Cyclic Filtration-cum-Chromatography Operation: Multiple Cycles

Cyclic runs were performed using the MF-cum-chromatography device having a coated zone in a loading-washing-elution-reequilibration cyclic mode without cleaning in between as shown in Figure 2.9. Synthetic fermentation broth was also used in the cyclic run to demonstrate the feasibility of getting purified proteins directly from an unclarified feed.

Fresh yeast cells obtained from the fermentation step described in section 2.1.4 were added into the protein mixture solution to obtain synthetic fermentation broths having a cell density of 0.3 – 0.8 g/L. The synthetic fermentation broth was fed directly to the tube-side inlet of the device at a flow rate of 200 ml/min and pressure of 34.5 kPag. The retentate was recycled. After loading, the cells and protein solution remaining in the membrane tube side and the system dead volume were drained. With the permeate outlet valve totally closed, the membrane lumens were washed with 50-60 ml starting buffer. The device loaded with protein mixture was then switched to the elution system shown in Figure 2.8. Tube-side stepwise elution was performed. The eluate fractions were collected and assayed for protein concentrations. After elution, the device was reequilibrated with the starting buffer and another cycle was started.

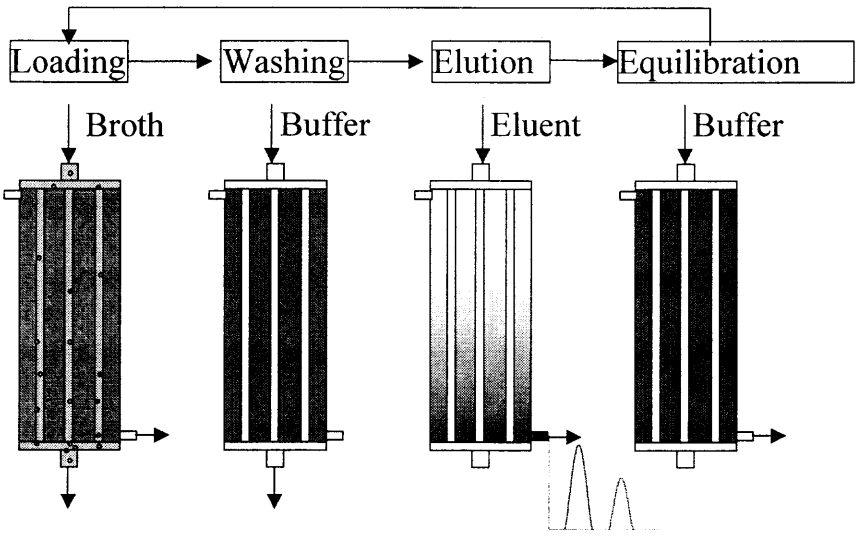

Figure 2.9 Cyclic operation.

2.7 Protein Concentration and Cell Density Assay

Protein concentrations were measured using a Hitachi U-2000 (Danbury, CT) UV-Vis spectrophotometer. S-10 quartz cuvets (10 mm path length) from Sigma (St. Louis, MO) were used in the spectrophotometer. The spectrum of Mb shows one peak at 280 nm and the other peak at 410 nm. Both α-LA and BSA have maximum absorbance at 280 nm, but negligible absorbance at 410 nm. Standard curves obtained at different wavelengths for various pure protein solutions are shown in Figures 2.10-2.12, and the calibration equations as well as their corresponding linear ranges are listed in Table 2.3.

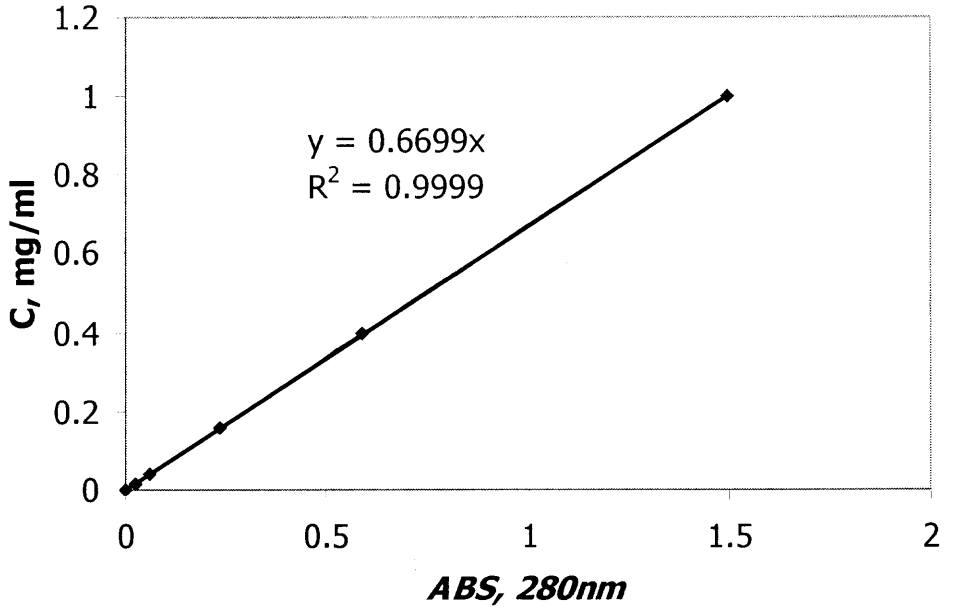

Figure 2.10 Standard curve for Mb at 280 nm.

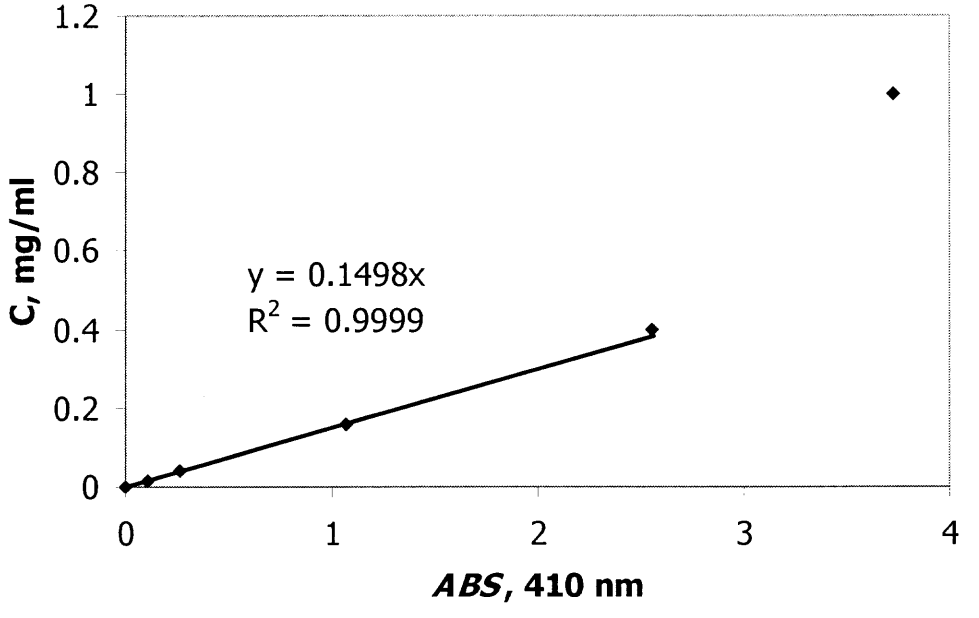

Figure 2.11 Standard curve for Mb at 410 nm.

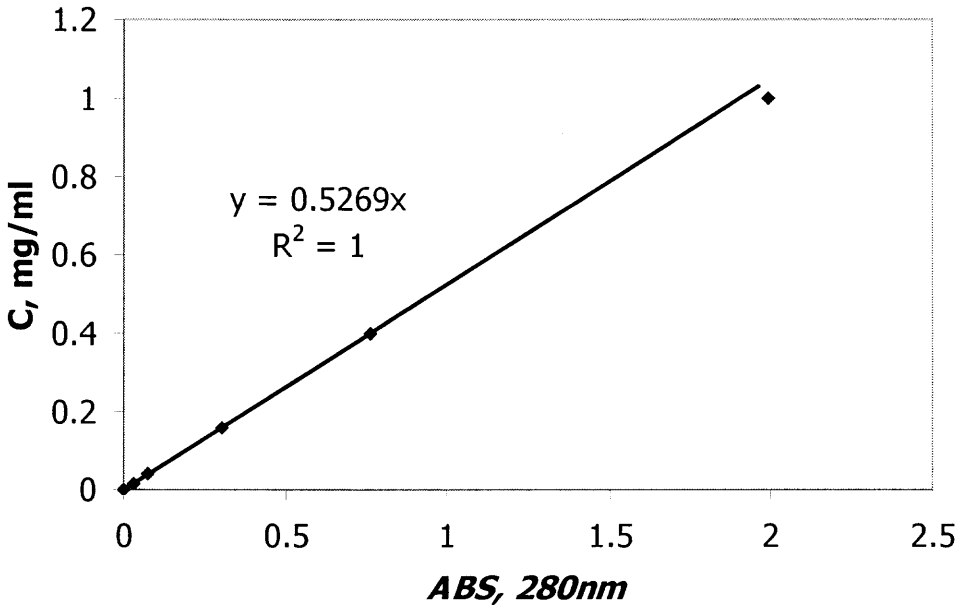

Figure 2.12 Standard curve for α-LA solution.

Table 2.3 Standard Curves for Protein Solutions

Wavelength / Protein	280 nm	410 nm
Myoglobin	$C = 0.6699\,ABS$	$C = 0.1498ABS$
	Linear range: 0-1 mg/ml	Linear range: 0-0.4 mg/ml
α-LA	$C = 0.5269ABS$	–
	Linear range: 0-1 mg/ml	
BSA	$C = 0.1253ABS - 0.0034$	–
	Linear range: 0-0.6 mg/ml	

The protein concentrations in a binary mixture were determined by the dual-wavelength method at 410 nm and 280 nm corresponding to their maximum absorbance. Absorbance of the protein mixture was measured at 410 nm and 280 nm, respectively. The Mb concentration was determined directly from the absorbance at 410 nm. The other protein concentration in the binary mixture was then determined by the absorbance of the mixture at 280 nm by subtracting the contribution from Mb.

For those feed or eluate samples whose protein concentrations were beyond the upper linear limits, the samples were diluted with the starting buffer before measurement.

Yeast cell culture optical density was measured by the spectrophotometer at a wavelength of 540 nm. The dry cell density was calculated using the calibration curve developed by Kang (1989).

CHAPTER 3

RESULTS AND DISCUSSION ON SEPARATION IN THE MODIFIED INTEGRATED DEVICE

In this chapter, the results of membrane characterization experiments of the integrated device and the extensive experiments on subsequent loading and elution experiments with various protein mixtures are presented and discussed. These results cover both the uncoated as well as the partially coated integrated device. Further, the hollow fiber membranes studied include both UF and MF membrane. While most of the results are based on clean mixtures of two proteins, results are also presented on synthetic solution of proteins containing yeast cells at various density levels. The protein mixtures whose separations have been studied are: Mb/α-LA and Mb/BSA.

3.1 Membrane Water Permeance

Membrane water permeance was measured for new membrane modules and modules thoroughly cleaned after protein transmission experiments. Water permeation flow rates were measured under different transmembrane pressure (TMP) differences. The permeance was calculated as the slope of water flux vs. TMP. For the two ultrafiltration membrane modules, the water permeance recovered around 80% of their original values after cleaning and remained at the same level after many rounds of experiments. For the MF membranes, the water permeability of the cleaned module recovered its original value. This is because the larger pores of the microfiltration membrane are much less likely to be blocked by contaminants or air and can be thoroughly cleaned.

Table 3.1 Water Permeance of Hollow Fiber Membranes

Module	New ($\times 10^{-10}$ $m^3/m^2/Pa/s$)	Cleaned ($\times 10^{-10}$ $m^3/m^2/Pa/s$)
#1 UF	8.49	7.15
#2 UF	6.09	4.86
#3 MF	85.9	86.1

3.2 Testing of the Partially Coated Fiber Module

The integrity of the coating was verified first by water permeation at 34.5 kPag. As shown in Table 3.2, the water permeation rates declined by about 25% corresponding to the extent of loss of the permeable membrane area; this value agrees very well with the decrease in the permeable fiber length after coating. The water permeation results indicate that the coating layer was essentially impermeable to water at the operating pressure.

Table 3.2 Water Permeation Results from Hollow Fiber Membrane modules

Module		Before coating	After coating	Percentage reduction
UF #1	Permeable fiber length (cm)	24.5	18.5	24.5%
	Water flux at 34.5 kPag (ml/min)	7.2	5.2	27.8%
MF #3	Permeable fiber length (cm)	25.6	19.6	23.4%
	Water flux at 34.5 kPag (ml/min)	10.0	7.8	22.0%

The coating layer was chemically and mechanically stable under the commonly used conditions in loading, elution, cleaning and sterilization operations. Especially during the cleaning operation, the coating layer could endure the hot, caustic cleaning solution and high shear stress. Both coated modules were used for more than a year in the experiments. They are still functioning very well as of the thesis preparation time.

3.3 Protein Separations in the Device using an UF Hollow Fiber Membrane

3.3.1 Effect of the Coated Zone on Mb Breakthrough

Figure 3.1 shows the Mb breakthrough behaviors of two devices made from identical UF modules (UFP-100-E-4A). Both modules have essentially identical amounts of resin beads on the shell side of the module. However, the adsorption capacity for the module having a coated zone was much higher. For the UF module without a coated zone, due to the hydrodynamic characteristics of this configuration, permeate flux increased along the flow direction and reached a maximum at the outlet point. There is only a thin layer of beads in the shell space near the module outlet, which is quickly saturated by the protein molecules permeating through the membrane near the outlet. Breakthrough (when the protein concentration in the permeate reaches 10% of the feed concentration) happened quickly (10 minutes after loading.). However, the Mb breakthrough time for the UF module with a coated zone happened after 50 minutes, signifying 5 times higher capacity. The operational conditions were identical for both modules.

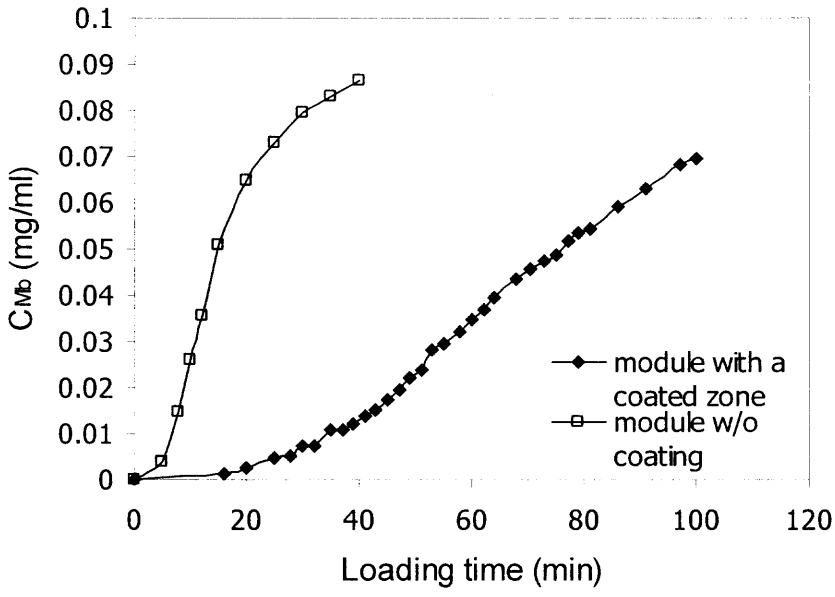

Figure 3.1 Mb breakthrough results from the conventional UF module and the module with a coated zone. (Feed: C_{Mb} 0.25 mg/ml, flow rate 200 ml/min, pressure 34.5 kPag)

After the coating layer was introduced on the membrane inner skin in the module outlet zone, the membrane pores at the coated zone were blocked. Neither protein molecules nor water could permeate to the shell side along the coated zone. Proteins permeating through the membrane in the upper unmodified section would be captured by the beads packed around the hollow fibers in situ and any leaked protein will be captured by the beads in the coated zone. Breakthrough would not happen until all the beads in the coated zone were saturated. This new configuration increased the loading capacity drastically without increasing the flow resistance of the packing encountered in the extended section of Dai et al. (1999).

3.3.2 Protein Separation Behavior of the Device with or w/o a Coated Zone

In Figures 3.2a and 3.2b, it is first shown that, for the conditions usually employed in Dai et al. (1999), the performance of the partially coated module (Figure 3.2b) was very close to that of the uncoated module (Figure 3.2a) for the elution-separation of Mb and α-Lactalbumin (α-LA). Note that the tube-side loading in each case was for 15 minutes and the peak profiles for the two proteins are essentially identical for the partially coated module and the conventional uncoated module. These conditions, however, are such that the uncoated module was close to having a breakthrough of the proteins.

On the other hand, Figures 3.3a and 3.3b illustrate the elution profiles for the same two proteins (Mb and α-LA) from the module having partially coated fibers for two different conditions: the first one (Figure 3.3a) where the loading was carried out for 55 minutes under feed conditions similar to that of Figure 3.2; the second one (Figure 3.3b) where the loading was carried out for 25 minutes under the same feed flow rate as in Figure 3.2 but the feed protein concentrations were five times larger than those in Figures 3.2a and 3.2b. As a result, both conditions in Figures 3.3a and 3.3b show much higher protein concentrations in the eluate. In fact, the total protein recovered in Figure 3.3b is about seven times higher for Mb as well as for α-LA compared to those in Figure 3.2a. Yet there was no breakthrough of the proteins from the partially coated fiber-based columns in spite of the high amount of protein loading.

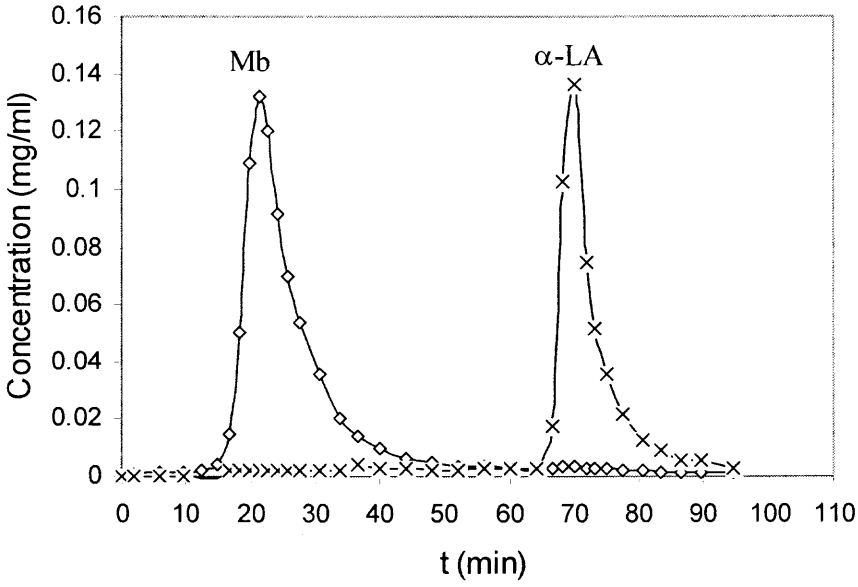

(a) Before coating: 0.0561 mg/ml Mb and 0.0422 mg/ml α-LA in feed.

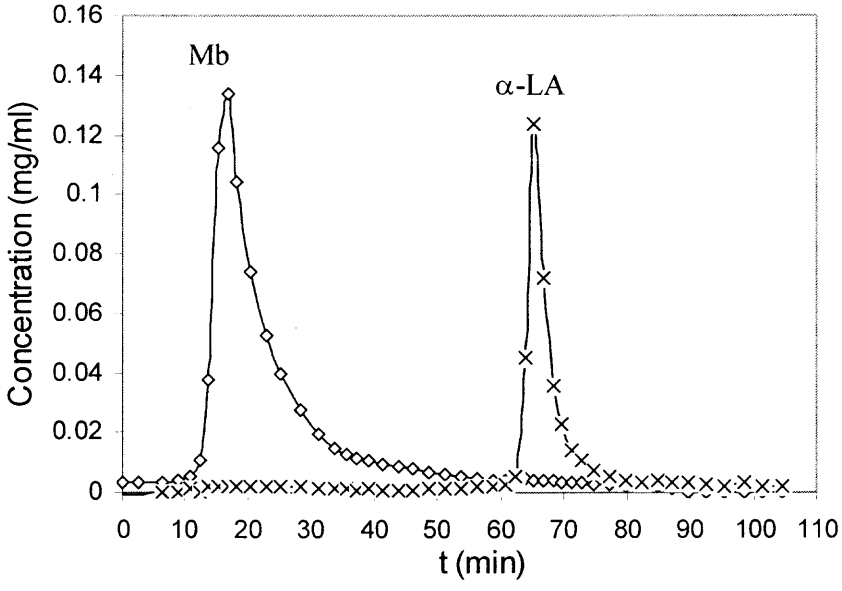

(b) After coating: 0.0548 mg/ml Mb and 0.0502 mg/ml α-LA in feed.

Figure 3.2 Comparison of Mb/α-LA separation behaviors at similar loading conditions for an UF module. (Loading time: 15 min. Elution: 0-50 min 0.05 M NaCl, 50-100 min 0.5M NaCl in Tris buffer.)

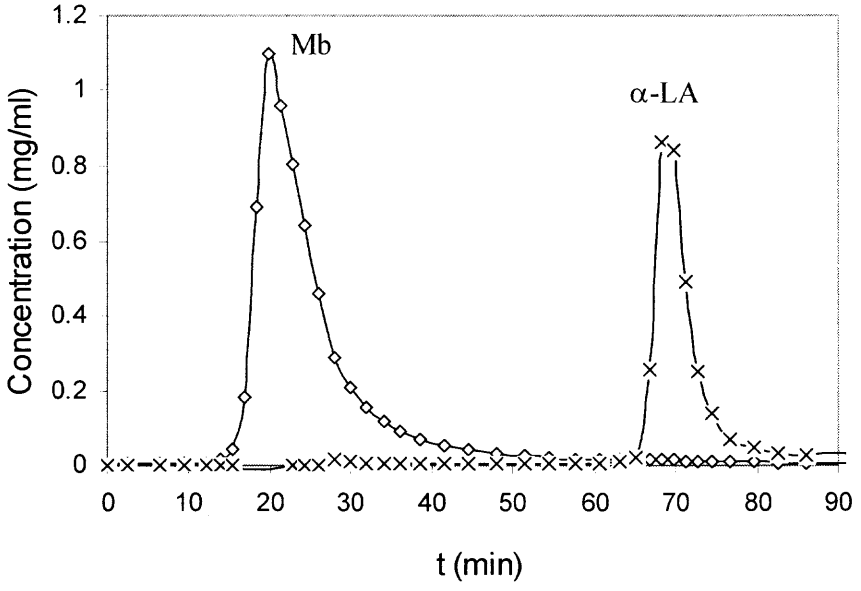

a. Longer loading time, 55min. 0.0548 mg/ml Mb and 0.538 mg/ml α-LA in feed.

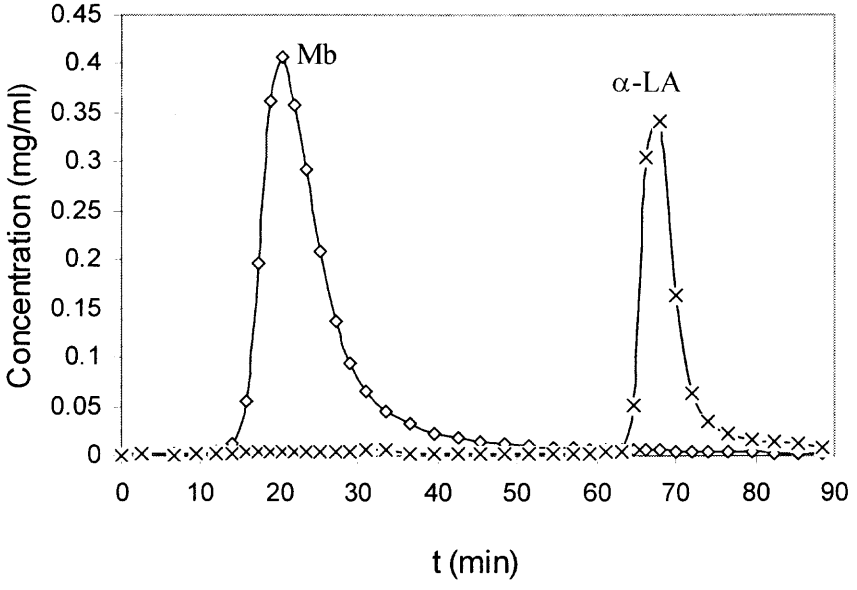

b. Higher loading concentration. 0.2857 mg/ml Mb and 0.2811 mg/ml α-LA in feed; loading time: 25 min.

Figure 3.3 Loading capacity enhancement in the UF module having a coated zone for Mb-α-LA separation. (Elution: 0-50 min 0.05 M NaCl, 50-90 min 0.5M NaCl in Tris buffer.)

The effect of the partial fiber coating on the reduction of protein leakage and increase in protein loading capacity as observed in the above experiments is reviewed in Table 3.3.

Table 3.3 Experimental Conditions and Protein Loading Results for the UF Modules

Item		Before coating	After partial coating		
		Fig. 3.2a	Fig. 3.2b	Fig. 3.3a	Fig. 3.3b
Feed conc. (mg/ml)	Mb	0.0561	0.0548	0.0548	0.2857
	α-LA	0.0422	0.0502	0.0538	0.2811
Loading time (min)		15	15	55	25
Permeate flow rate (ml/min)		5.9	5.3	5	4.52
Ave. Mb conc. in permeate (mg/ml)		0.00097	0.00056	0.0011	0.00090
Total Mb loaded (mg)		3.4	3.3	10.4	25.1
Total α-LA loaded (mg)		1.5	2.3	5.1	13.0

An even higher loading capacity was achieved using a high feed concentration as well as longer loading time. As shown in Figure 3.4, 51.34 mg of Mb and 14.13 mg of α-LA were loaded and separated completely. The average Mb concentration in the permeate was 0.01 mg/ml. Mb leaking level was allowed to be higher than that of the previous loading experiments shown in Table 3.3 because the feed concentration for this high loading capacity run was much higher, and therefore the breakthrough concentration would be correspondingly higher. The total amount of the leaked Mb is relatively small compared to the high loaded amount of Mb.

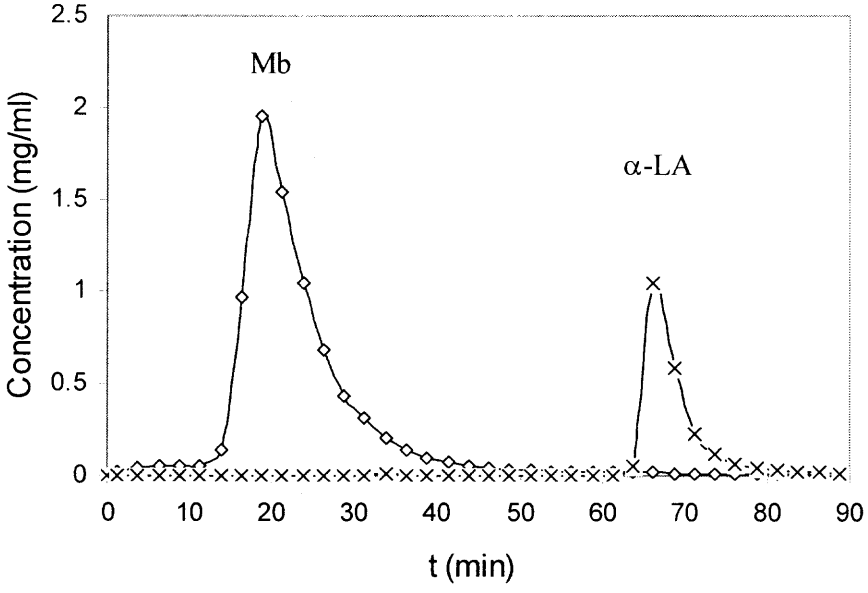

Figure 3.4 High loading capacity of Mb-α-LA for module 1 with a coated zone.
(Feed: 0.505 mg/ml Mb, 0.467 mg/ml α-LA; Loading time: 35 min; Tube-side step-wise elution. Total protein loaded: Mb 51.34 mg, α-LA 14.13 mg)

The effect of the coating on the separation results for another pair of proteins, namely, myoglobin and bovine serum albumin (Mb/BSA), is similar to that of Mb/α-LA. Figure 3.5a illustrates the protein separation profiles obtained from the conventional module (w/o coating). On the other hand, Figure 3.5b shows the significantly increased loading capacity after the membrane pores in the outlet zone were shut down by interfacial polymerization-based coating. The loading amount of BSA is apparently smaller than that of Mb due to its larger molecular size. The total separation result is a combination of membrane fractionation and shell-side chromatographic separation. If Mb (the smaller protein) is the target protein, the rejection of the BSA by the membrane provided a preliminary fractionation saving most of the shell-side bead adsorption capacity for Mb and simplifying the chromatographic separation.

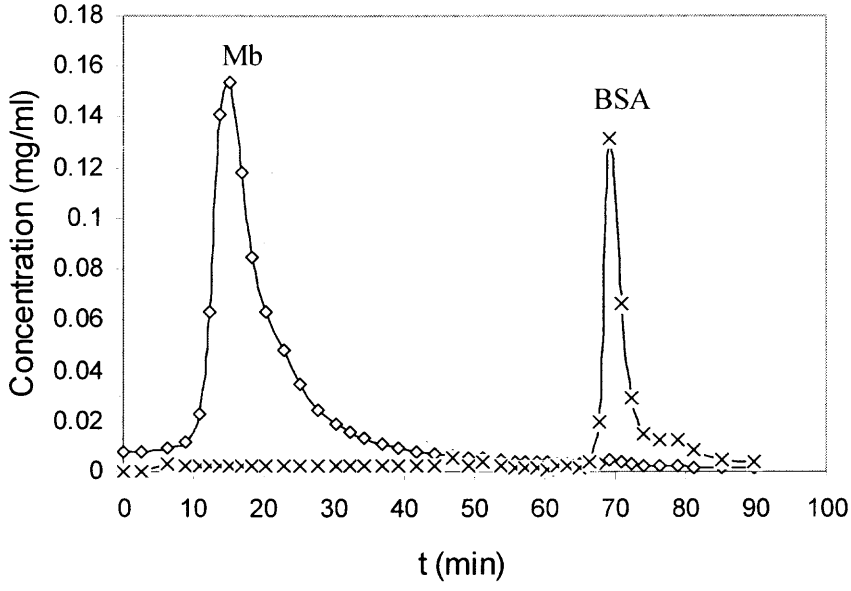

(a). Before coating, 0.0536 mg/ml Mb and 0.0505 mg/ml BSA in feed. Total protein loaded: Mb 4.1 mg, BSA 1.6 mg.

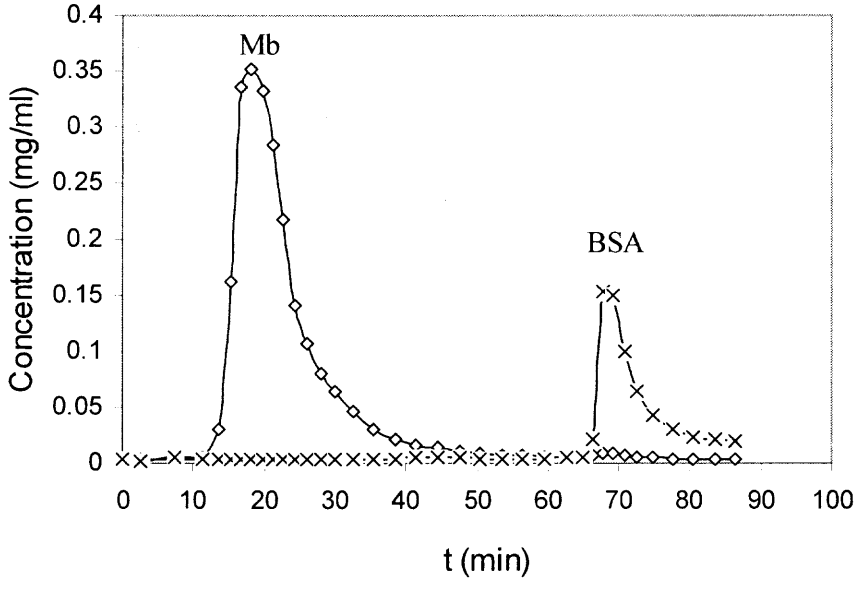

(b). After coating, 0.0518 mg/ml Mb and 0.0506 mg/ml BSA in feed. Total protein loaded: Mb 10.0 mg; BSA 3.5 mg.

Figure 3.5 Effect of coating on Mb/BSA separation for an UF module. (Loading time: a: 15 min; b: 55 min. Elution: 0-50 min 0.05 M NaCl , 50-90 min 0.5M NaCl in Tris buffer.)

3.3.3 Comparison of Different Elution Conditions

Different elution conditions were tried for both shell-side and tube-side elution in the coated device. The loading conditions were the same for all the runs shown in the following Figures 3.6 to 3.8. The protein feed solution containing 0.05 mg/ml Mb and α-LA was circulated through the hollow fiber tubeside under 34.5 kPag and a flow rate of 200 ml/min for 15 min. Next, the protein solution remained in the system dead volume was drained, and the hollow fiber lumen was washed with the starting buffer. Eluents with different salt concentrations were then introduced either through the tube-side or the shell-side to elute the proteins out.

Figures 3.6a and 3.6b illustrate the elution profiles of Mb and α-LA using shell-side gradient elution. Under gradient 1, where NaCl concentration in the eluent started from 0.05 M and increased linearly to 0.5 M in 50 min, α-LA started to came out at 20 min, causing a significant overlap with the Mb peak. As shown in Figure 3.6a, Mb and α-LA were not totally separated.

Lowering the salt concentration in the initial eluent to 0.02 M and using a two segment gradient as shown in Figure 3.6b, a good separation of Mb and α-LA was achieved in a shorter time. Elution was completed in 55 min, $1/3^{rd}$ shorter than the time used for tube-side step-wise elution.

The results of tube-side gradient elution using gradient 2 employed in the studies for Figure 3.6b are shown in Figure 3.7. The resolution is not as good as that from the shell-side gradient elution under the same elution condition. The eluent with increased NaCl concentration flowed through the hollow fiber lumen and reached the bottom part of the module, permeated through the membrane before the elution front from the upper

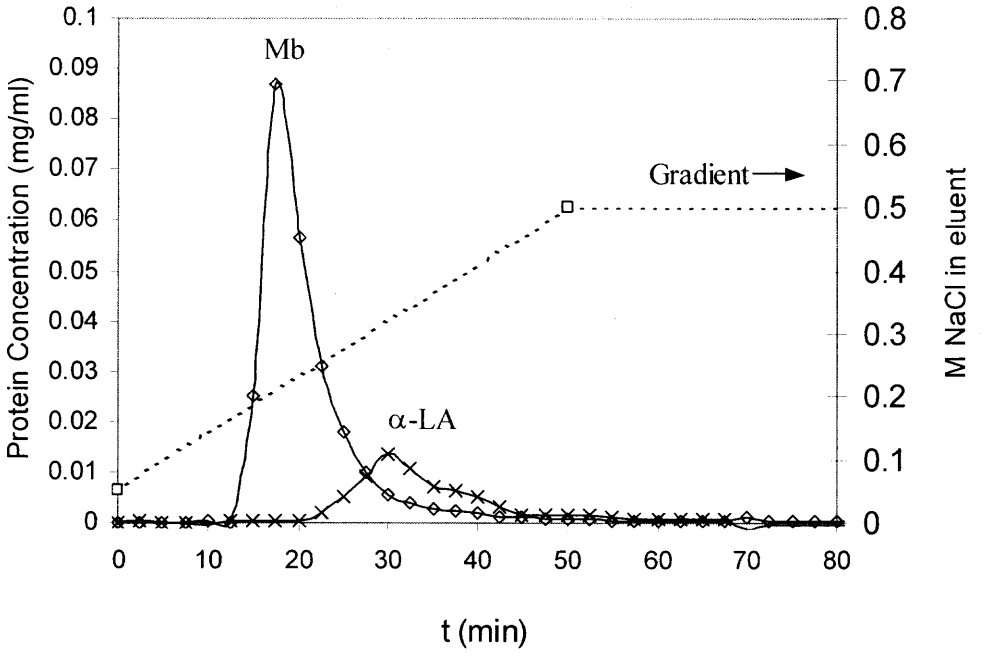

(a). Gradient 1: linear gradient from 0.05 M to 0.5 M NaCl in 50 min, followed by 0.5 M NaCl for 50 min (Feed concentration: Mb 0.0461 mg/ml, α-LA 0.0486 mg/ml).

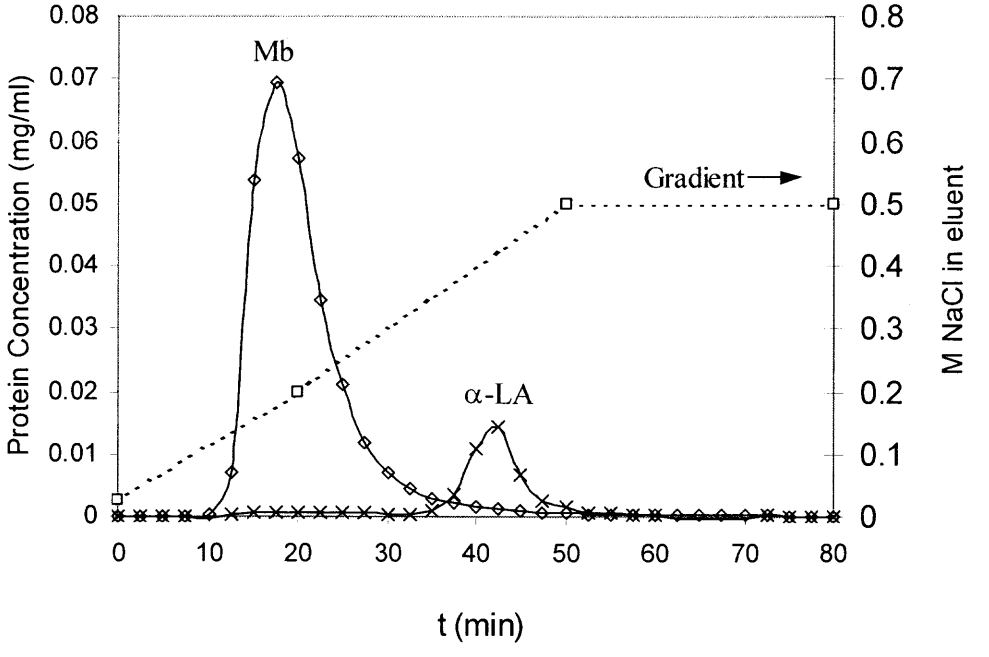

(b) Gradient 2: 0.02 M to 0.2 M NaCl in 20 min, followed 0.2 M to 0.5 M NaCl in 30 min, and then 0.5 M NaCl for another 30 min (Feed concentration: Mb 0.0524 mg/ml, α-LA 0.0531 mg/ml).

Figure 3.6 Shell-side gradient elution for mixture of Mb and α-LA using module 1 with a coated zone. (Loading time: 15 min.)

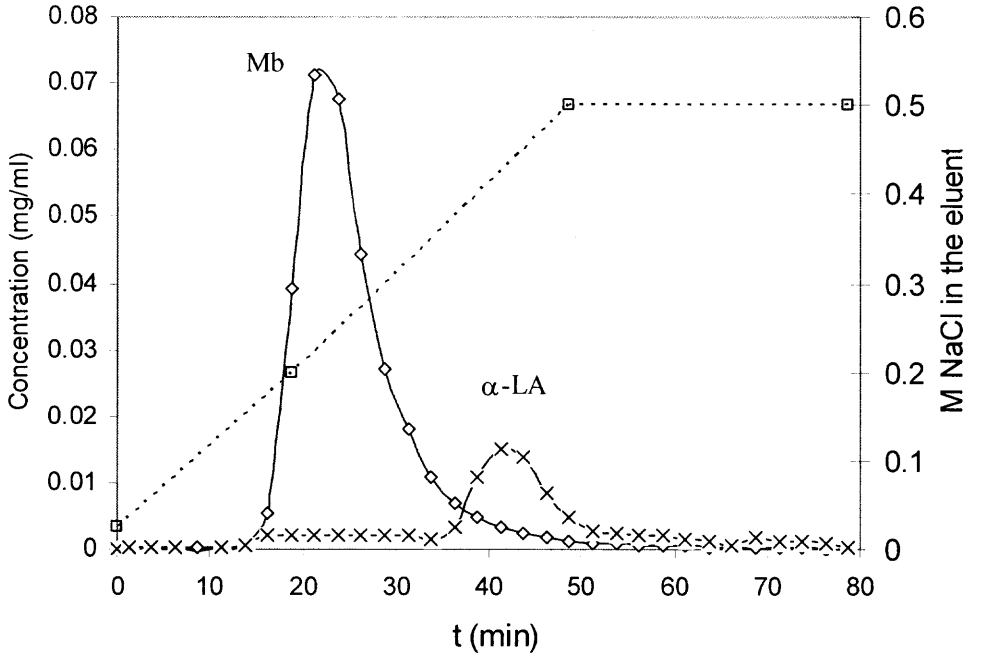

Figure 3.7 Tube-side gradient elution for Mb-α-LA separation. (Feed: Mb 0.0507 mg/ml, α-LA 0.0486 mg/ml; Loading time: 15 min; Elution: 0.02 M to 0.2 M NaCl in 20 min, followed 0.2 M to 0.5 M NaCl in 30 min, and then 0.5 M NaCl for another 30 min.)

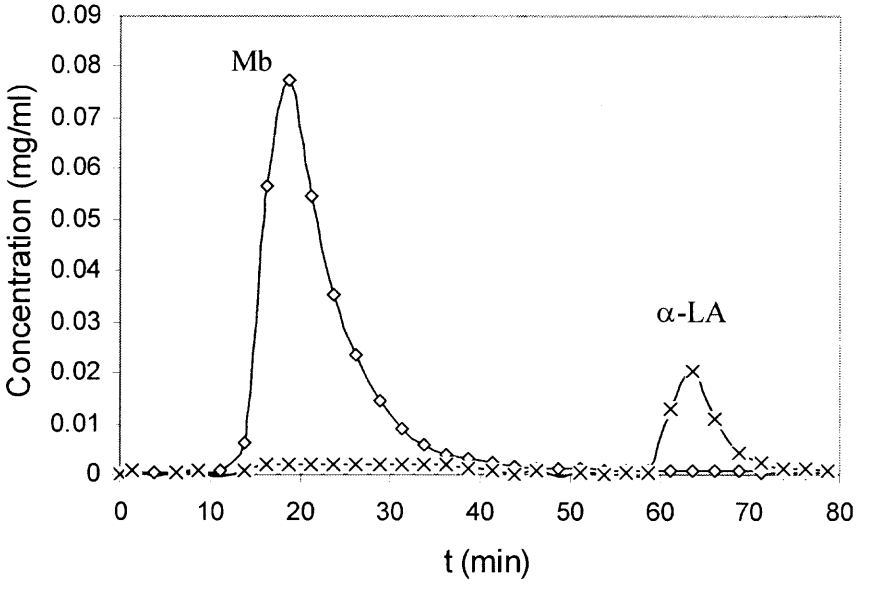

Figure 3.8 Tube-side step-wise elution for Mb-α-LA separation. (Feed: Mb 0.0509 mg/ml, α-LA 0.0495 mg/ml; Loading time: 15 min; Elution: 0-50 min 0.05 M NaCl , 50-80 min 0.5M NaCl in Tris buffer).

stream of the shell side. Higher salt concentration in the bottom part of the shell-side eluted the α-LA earlier, causing a broader α-LA peak and more overlap between the Mb and α-LA peaks.

However, the tube-side step-wise elution worked very well as shown in Figure 3.8, using a step change of 0.05 M NaCl for 50 min and then 0.5 M NaCl for 30 min. α-LA was completely separated from Mb.

3.3.4 Effect of the Feed Ionic Strength

It can be seen from the previous experimental results that the loaded amounts of α-LA were significantly lower than those of Mb. Considering that their molecular weight and size are similar, and their molecular size should be much smaller relative to the pore size of the 100K MWCO UF membrane, this high membrane rejection for α-LA should not be attributed to the molecular size itself. There must be some other factors dominating the α-LA transmission through the membrane.

Mb and α-LA feed solutions with different ionic strengths were loaded to the integrated device to investigate the effect of ionic strength on protein transmission. Figure 3.9a shows the separation result of Mb and α-LA with 0.001 M NaCl in feed. The loaded amount of α- LA (0.56 mg) doubled compared to that for no NaCl in the feed as shown in Figure 3.6b (0.28 mg). The loaded amount of Mb only increased slightly. As the NaCl concentration in the feed was increased to 0.01 M, the loaded amount of α-LA was increased drastically, by as much as 4 times, as shown in Figure 3.9b. However, the Mb broke through at relatively high concentrations during loading operation due to the

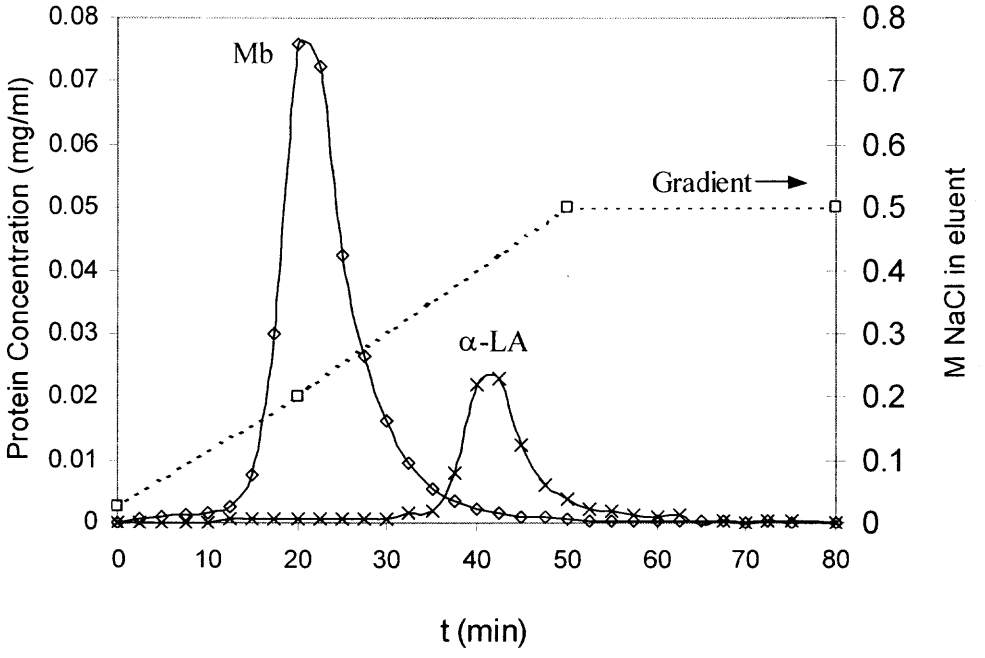

(a). 0.001 M NaCl (Feed concentration: Mb 0.0545 mg/ml, α-LA 0.0493 mg/ml)

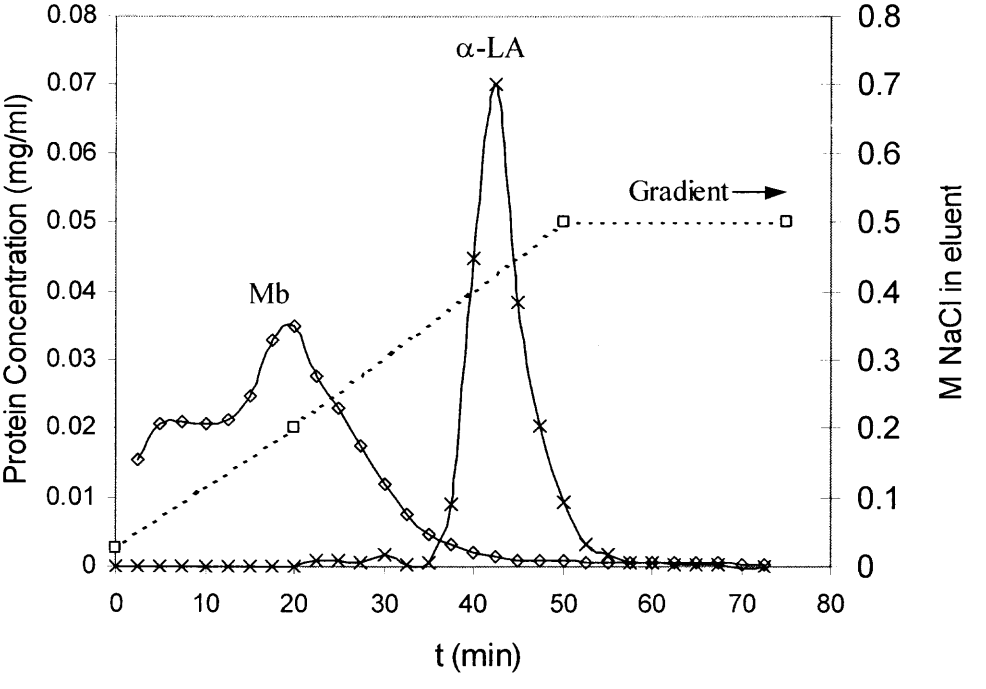

(b). 0.01 M NaCl (Feed concentration: Mb 0.0509 mg/ml, α-LA 0.0511 mg/ml)

Figure 3.9 Loading at different NaCl concentration in the feed for Mb-α-LA system. (Loading time: 15 min, pressure 35.4 kPa, Q_f = 200 ml/min. Shell-side gradient elution.)

Mb adsorption capacity decreasing as the ionic strength increased. The significant increase of the loaded amount of α-LA with increasing NaCl concentration in the feed solution shown in Figure 3.6b and Figures 3.9a and 3.9b suggests that the ionic strength of the protein feed solution not only affects the protein adsorption on the beads but also plays an important role in α-LA transmission through the UF membrane.

These results support that the polysulfone membrane is negatively charged under the loading condition (pH 8.5). With the α-LA (pI 4.2-4.5) being strong negatively charged, Donnan exclusion dominates the protein transport through the membrane pores.

Under very low ionic strength, the electrical double layers (EDL) of the charged surfaces of both membrane pore and protein molecule are thick, causing significant electrostatic interaction between the protein molecules and membrane surface. Under conditions of a higher ionic strength, the electrical double layer is suppressed by the small ions in the solution, and the electrostatic interaction was shielded, resulting in higher α-LA transmission. The Mb (pI, 7.3) is nearly neutral under the loading condition so that the electrostatic interaction is not as strong as that for α-LA; Donnan exclusion effect is not significant, and steric hindrance dominates the Mb transportation. More detailed discussions on the effect of the electrostatic interaction on protein transmission and permeate flux will be provided in Chapter 5.

The effect of the ionic strength of the feed solution provides one with an additional option to tailor the protein separations via the integrated device. If Mb is the target protein, loading at low ionic strength will help to reject α-LA, alleviating the adsorption burden of the packed beads at the shell side and simplifying the following elution separation. On the other hand, if α-LA is the target protein, loading at higher

ionic strength will increase the α-LA transmission, therefore the loaded amount. Mb adsorption on the bead is weak under high ionic strength, so that it will flow out with the permeate while α-LA is adsorbed on the beads.

3.4 Protein Separations in the Device Using a MF Hollow Fiber Membrane

3.4.1 Effect of the Coated Zone on Mb Breakthrough

Dai et al. (2003) have shown that the higher the membrane permeability, the more significant the nonuniform axial solvent flux distribution in a noncoated membrane module. High water flux near the module outlet and high protein transmission through the MF membrane will bring large amounts of proteins directly to the module outlet area. Protein breakthrough will happen much earlier than that in the device using a UF membrane. The Mb breakthrough curves for module #3 having a MF membrane with/without a coated zone are shown in Figure 3.10. Protein solutions containing 0.25 mg/ml Mb were circulated through the membrane tube side of the hollow fiber modules at a flow rate of 200 ml/min and pressure of 34.5 kPag. As was expected, breakthroughs for the MF module before coating and after coating happened earlier than those for the module having a UF membrane shown in Figure 3.1.

Similar to the case of the module having a UF membrane, blocking the membrane pores at the module bottom section using an interfacially polymerized coating layer extended the Mb breakthrough time by a factor of four. The interfacial polymerization coating on the MF membrane worked as well as that on UF membrane described in the last section.

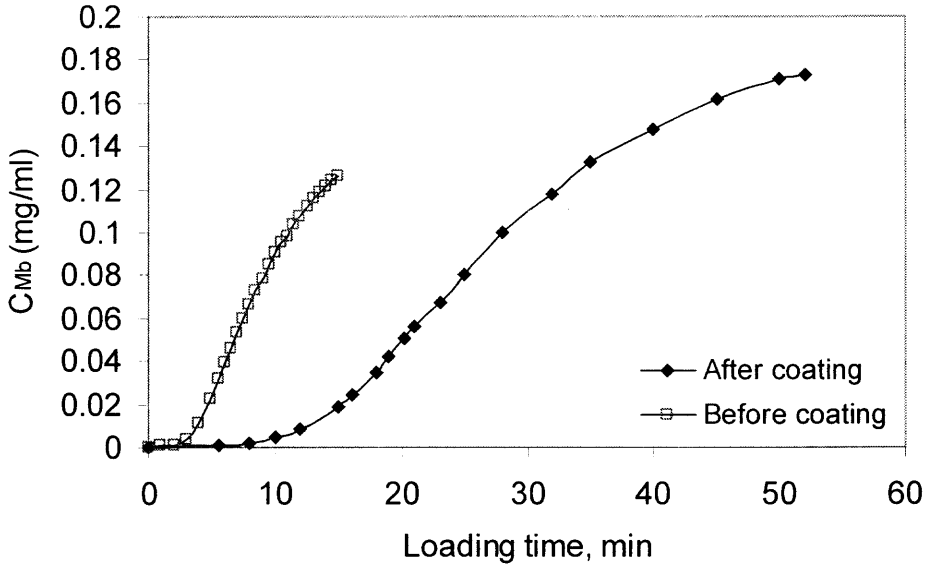

Figure 3.10 Mb breakthrough curves for a device using MF membrane. (Feed: Mb 0.25 mg/ml; Loading condition: pressure 34.5kPag, Q_f = 200 ml/min.)

3.4.2 Comparison of Protein Separations in the Device with or w/o a Coated Zone

In the protein separation experiments using the device made of UF membranes, α-LA and BSA encountered significant rejection due to their molecular size, shape or charge. In applications where both the smaller protein and the larger protein need to be recovered, membrane rejection for any of the proteins will be undesirable. Membranes with larger pores can be used in such situations. A module using MF hollow fiber membranes was fabricated, and the protein separation behaviors of the module before coating and after coating were investigated using two pairs of model proteins: Mb/α-LA and Mb/BSA. The results are shown in Figures 3.11 and 3.12.

The loaded amounts of α-LA and BSA were similar to that of Mb, and much higher than their loaded amounts in the UF module. The MF membrane did not provide any selection for different proteins since they are supposed to block only particles like

cells, cell debris and bacteria. The loaded amount of Mb in the MF module before coating was only about 2 mg, lower than that in the UF module without coating. This is due to the much lower flow resistance through the MF membrane causing a greater nonuniformity in the solvent flux distribution along the axial direction of the hollow fiber MF membrane compared to that in the hollow fiber UF membrane. Higher amounts of buffer solutions and proteins permeated through the bottom section of the MF membrane near the outlet port, leading to an early protein leakage.

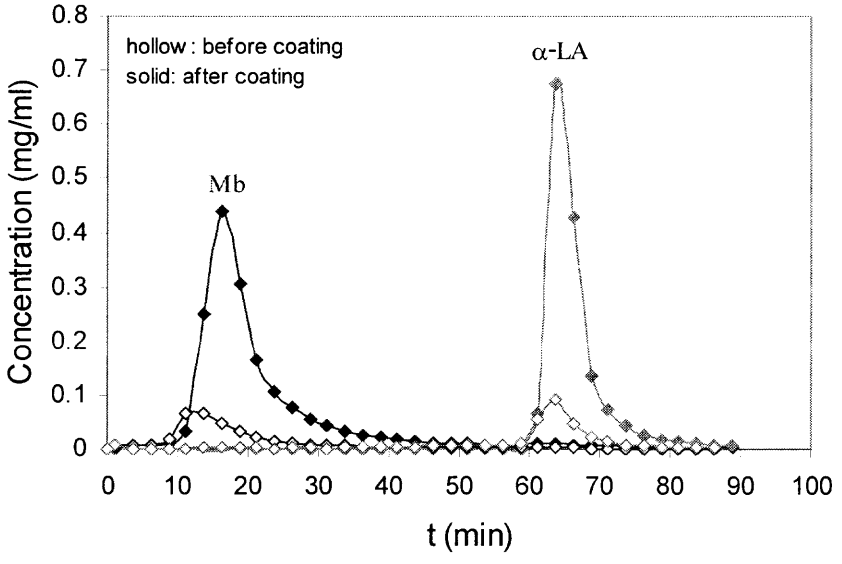

Figure 3.11 Effect of coating on Mb/α-LA separation for a MF module.
(Feed: 0.0587 mg/ml Mb and 0.0524 mg/ml α-LA before coating; 0.0545 mg/ml Mb and 0.052 mg/ml α-LA after coating. Loading time: 4 min before coating; 29 min after coating. Elution: 0-50 min 0.05 M NaCl, 50-90 min 0.5M NaCl in Tris buffer. Protein loaded amount: before coating, Mb 2.29 mg, α-LA 2.17 mg ; after coating, Mb 10.88 mg, α-LA 9.44 mg.)

Then the bottom section of the hollow fiber MF membrane near the module outlet was coated by a thin polyamide film using interfacial polymerization described earlier. The membrane pores in the coated zone were totally shut down for both buffer solution

and protein molecules. As has been observed ealier in the module containing the UF membrane, the loaded amounts of Mb, α-LA and BSA were all increased to around 10 mg, more than 4 times over that before coating. The loaded amount of Mb was similar to that in the UF module with a coated zone. But the loaded amounts of α-LA and BSA were significantly higher than that in the UF module with a coated zone. No protein rejection was observed for any of the three model proteins. The module using MF membrane can be used to recover and purify the larger protein or both smaller and larger protein at the same time.

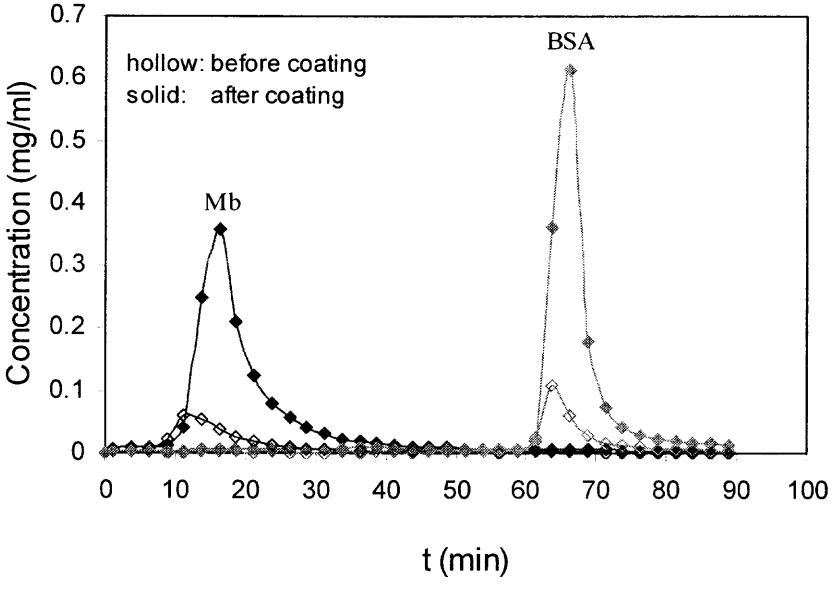

Figure 3.12 Effect of coating on Mb/BSA separation for a MF module.
(Feed: 0.0535 mg/ml Mb and 0.0475 mg/ml BSA before coating; 0.0533 mg/ml Mb and 0.049 mg/ml BSA after coating. Loading time: 4 min before coating; 25 min after coating. Elution: 0-50 min 0.05 M NaCl , 50-90 min 0.5M NaCl in Tris buffer. Protein loaded amount: before coating, Mb 1.93 mg, BSA 2.14 mg ; after coating, Mb 8.74 mg, BSA 9.59 mg.)

The improvement of the loading capacity for the module with a coated zone was further explored using much higher protein feed concentrations. The separation results for Mb/α-LA from a binary mixture of around 0.5 mg/ml of each protein are shown in Figure

3.13 and compared with the earlier results using lower feed concentrations in Table 3.4. The loading time was 16 min before breakthrough. 50.68 mg of Mb and 46.84 mg of α-LA were recovered in the fractions corresponding to two totally separated peaks. The average Mb concentration in the permeate was 0.0085 mg/ml, higher than that for the runs shown in Figure 3.11, because the breakthrough concentration is higher corresponding to the higher feed concentration. But the percentage of the total amount of leaked Mb in the permeate as a fraction of the total Mb loaded on the beads is actually lower compared to that in the runs shown in Figure 3.11. All such results are compared in Table 3.4.

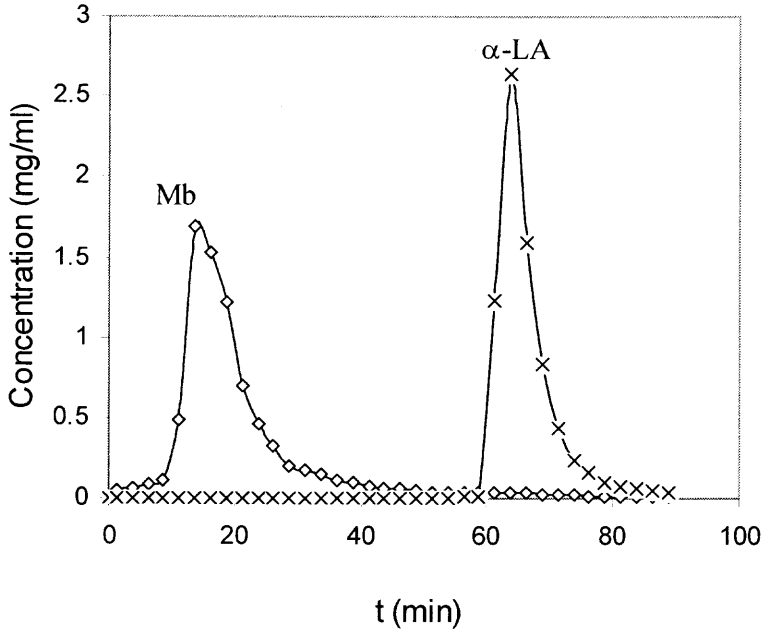

Figure 3.13 High loading capacity for Mb/α-LA separation for a MF module with coated zone. (Feed: 0.499 mg/ml of Mb and 0.461 mg/ml of α-LA. Loading time: 16 min. Elution: 0-50 min: 0.05 M NaCl , 50-90 min: 0.5 M NaCl in Tris buffer. Protein loaded amount: Mb 50.68mg, α-LA 46.84 mg.)

Table 3.4 Experimental Conditions and Protein Loading Results for the MF Modules

		Before coating	After partial coating	
		Fig. 3.11	Fig. 3.11	Fig. 3.13
Feed conc. (mg/ml)	Mb	0.0587	0.0545	0.499
	α-LA	0.0524	0.052	0.461
Loading time (min)		4	29	16
Permeate flow rate (ml/min)		9.5	7.2	7.1
Ave. Mb conc. in permeate (mg/ml)		.0022	0.0014	0.0085
Total Mb loaded (mg)		2.28	10.75	50.68
Total α-LA loaded (mg)		2.17	9.54	46.84

3.5 Adsorption Capacity Utilization

The actual amounts of protein loaded in the experiments described in the last two sections were compared to the maximum equilibrium adsorption capacities under the experimental conditions. The Mb equilibrium concentration in the beads was calculated using the isotherm determined by Dai (2000):

$$q^* = \frac{44.46 C_f}{1.02 + C_f} \tag{3.1}$$

where C_f is the protein concentration in the feed, and q^* is the equilibrium protein concentration in the solid phase, all in mg/ml.

Adsorption capacity utilized was calculated as the total amount of Mb loaded over the total equilibrium loading capacity of the adsorbent, e.g.,

$$Capacity\%utilized = \frac{W_t}{q^* V_s(1-\varepsilon)} \tag{3.2}$$

where W_t (mg) is the amount of protein loaded during the experiment, V_s (ml) is the total adsorbent volume, and $\varepsilon = 0.3$ is the void fraction of the packing in the shell side.

For the runs using a UF membrane without coating shown in Figure 3.2a, only 10.6% of the total adsorption capacity was utilized. For the same membrane with a coated zone, the run shown in Figure 3.3a utilized 33.1% of the total adsorption capacity under the same operating conditions and similar protein leakage but longer loading time.

Adsorption capacity utilization for the module containing a MF hollow fiber membrane was increased more significantly after a coated zone was formed on the same membrane. For the results of runs shown in Figure 3.11, the adsorption capacity utilization was 6.5% before coating and 29.2% after coating, an increase of almost five times. Around 22.1% of the adsorption capacity was utilized for the run shown in Figure 3.13 using a much higher feed concentration. Considering that the protein dynamic loading capacity is considerably lower than the equilibrium adsorption capacity in porous chromatographic media (Sofer and Hagel 1997), 20-30% of the equilibrium capacity utilization is acceptable in most biochromatographic separations (Natarajan and Cramer 2000).

3.6 Effect of Yeast Cells in the Feed

To demonstrate the direct recovery and separation of proteins from an unclarified feed and study the effect of cells in the feed, fresh yeast cells were added into the protein feed mixture to prepare a synthetic fermentation broth. The module containing a MF

membrane with a coated zone was used in the experiments using the synthetic fermentation broth as the feed solution during loading operation.

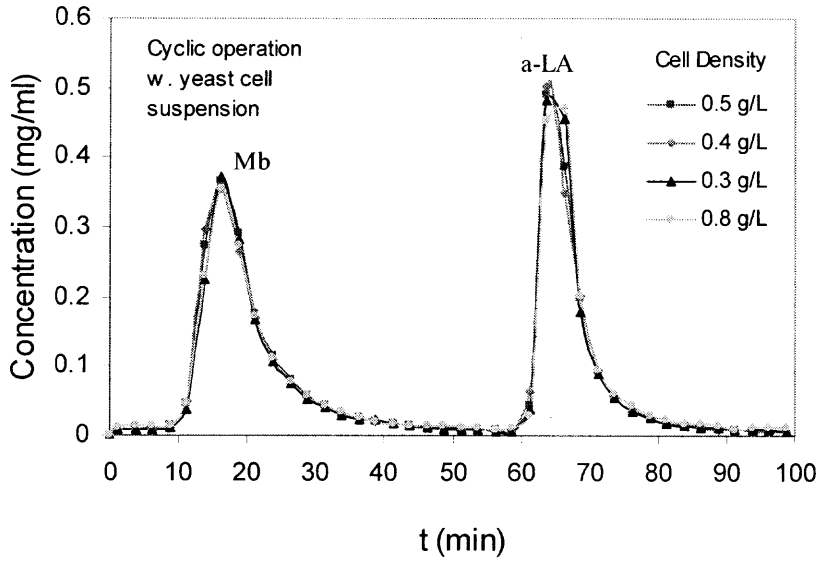

Figure 3.14 Cyclic runs for Mb/α-LA separation from synthetic yeast broths of different cell densities using the coated MF module. (Feed: 0.0515 mg/ml of Mb and 0.0466 mg/ml of α-LA with yeast cell suspension. Loading time: 29 min. Elution: 0-50 min: 0.05 M NaCl , 50-100 min: 0.5 M NaCl in Tris buffer.)

Four consecutive runs for Mb and α-LA separation from the synthetic yeast fermentation broths with different cell densities were performed in a loading-washing-elution-reequilibration cyclic mode without cleaning in between. The Mb and α- LA elution profiles for different runs, as shown in Figure 3.14, are similar to the profiles from the clear feed solution shown in Figure 3.11. The peak heights in Figure 3.14 are slightly lower than the peak heights in Figure 3.11 indicating a small decrease in protein transmission through the membrane. This might have been caused by cell-protein interactions and the presence of cells near the membrane surface blocking the movement of protein molecules. Elution profiles of the four consecutive runs are almost

superimposable, indicating that the washing and elution steps served as efficient periodic cleaning of external and internal membrane fouling. The membrane cleaning was integrated into the operational steps of the chromatographic separation. The device can be used repeatedly without further cleaning in each cycle.

CHAPTER 4

MODELING AND SIMULATION OF THE PARTIALLY COATED DEVICE PERFORMANCE

4.1 Hydrodynamics of the Coated Device

The hydrodynamics of the integrated filtration-cum-chromatogrpahy device with a coated zone near the module outlet will be analyzed in this section. A simplified physical model describing the fluid flow in the device is shown in Figure 4.1.

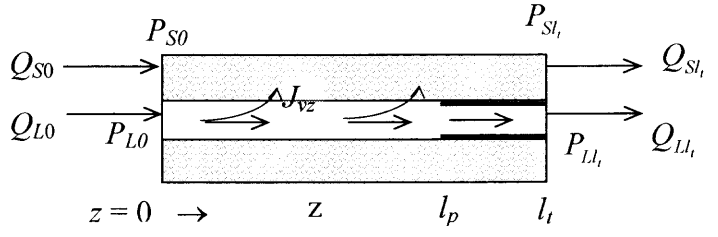

Figure 4.1 Fluid flow in the integrated device with a coated zone.

4.1.2 Basic Governing Equations

Local permeation flux along the axial direction:

For values of z between $z = 0$ and $z = l_p$, $0 \le z \le l_p$, the permeable zone, the local solvent permeation flux (volumetric flux) is

$$J_{vz} = A(P_{Lz} - P_{Sz}) \tag{4.1}$$

where A is the membrane water permeation parameter under the shell-side packing condition.

For values of z between $z = l_p$ and z = l_t, $l_p \le z \le l_t$, the coated zone,

$$J_{vz} = 0 \tag{4.2}$$

The axial gradient of change of the lumen-side volumetric flow rate due to permeation is:

$$\frac{dQ_{Lz}}{dz} = -N_0(\pi d_i J_{vz}) \tag{4.3}$$

where N_0 is the total number of fibers packed in the hollow fiber module and d_i is the inner diameter of the fiber lumen. An expression for the lumen-side local liquid flow rate is obtained by integrating Eq. 4.3:

$$Q_{Lz} = Q_{L0} - N_0 \pi d_i \int_0^z J_{vz} dz \tag{4.4}$$

Similarly, the shell-side local volumetric flow rate is obtained as

$$Q_{Sz} = Q_{S0} + N_0 \pi d_i \int_0^z J_{vz} dz \tag{4.5}$$

For laminar flow in the hollow fiber lumen, the pressure drop can be described by the Hagen-Poiseuille law (Apelblat, Katzir-Katchalsky et al. 1974):

$$\frac{dP_{Lz}}{dz} = -\frac{128\mu_L Q_{Lz}}{N_0 \pi d_i^4} = -\frac{128\mu_L}{d_i^3}\left(\frac{Q_{L0}}{N_0 \pi d_i} - \int_0^z J_{vz} dz\right) = -M_1\left(M_2 - \int_0^z J_{vz} dz\right) \tag{4.6a}$$

where $$M_1 = \frac{128\mu_L}{d_i^3}, \text{ and } M_2 = \frac{Q_{L0}}{N_0 \pi d_i} \tag{4.6b}$$

For laminar flow in the shell side packed with beads of diameter d_p and the bed void fraction of ε, the pressure drop can be described by the Blake-Kozeny law (Bird, Stewart et al. 1960):

$$\frac{dP_{Sz}}{dz} = -\frac{150(1-\varepsilon)^2}{d_p^2 \varepsilon^3} \mu_S u_{Sz} \tag{4.7a}$$

Here u_{Sz} is the superficial velocity of the fluid flow in the shell-side space of cross section area S_S

$$S_S = \frac{\pi}{4}\left(D_S^2 - N_0 d_0^2\right) \tag{4.7b}$$

where D_S is the module housing inner diameter, d_o is the hollow fiber outer diameter:

$$u_{Sz} = \frac{Q_{Sz}}{S_S} = \frac{4\pi N_0 d_i}{\pi(D_S^2 - N_0 d_o^2)}\left(\frac{Q_{S0}}{N_0 \pi d_i} + \int_0^z J_{vz} dz\right) = a\left(\frac{Q_{S0}}{N_0 \pi d_i} + \int_0^z J_{vz} dz\right) \tag{4.7c}$$

Here a is defined as the total membrane surface area over the corresponding unit shell-side space volume,

$$a = \frac{4N_0 d_i}{\left(D_S^2 - N_0 d_o^2\right)} \tag{4.7d}$$

Substituting Eq. 4.7c into Eq. 4.7a, one obtains

$$\frac{dP_{Sz}}{dz} = -\frac{150(1-\varepsilon)^2}{d_p^2 \varepsilon^3}\mu_S a\left(\frac{Q_{S0}}{N_0 \pi d_i} + \int_0^z J_{vz} dz\right) = -B\left(M_3 + \int_0^z J_{vz} dz\right) \tag{4.7e}$$

where $$B = \frac{150(1-\varepsilon)^2}{d_p^2 \varepsilon^3} a\mu_S \tag{4.7f}$$

and $$M_3 = \frac{Q_{S0}}{N_0 \pi d_i} \tag{4.7g}$$

4.1.3 Permeable Zone ($0 \le z \le l_p$)

By differentiating Eq. 4.1 and combining with Eqs. 4.6a and 4.7e, one can obtain the governing equation for the permeation flux in the permeable zone ($0 \le z \le l_p$)

$$\frac{dJ_{vz}}{dz} = A\left(\frac{dP_{Lz}}{dz} - \frac{dP_{Sz}}{dz}\right) = -AM_1 M_2 + ABM_3 + A(M_1 + B)\int_0^z J_{vz} dz \tag{4.8}$$

By differentiating Eq. 4.8 again, a second-order differential equation is obtained:

$$\frac{d^2 J_{vz}}{dz^2} = A(M_1 + B)J_{vz} \tag{4.9a}$$

Let $$\beta^2 = A(M_1 + B) \tag{4.9b}$$

The general solution of Eq. 4.9a is then:

$$J_{vz} = A_1 \cosh(\beta z) + A_2 \sinh(\beta z) \tag{4.10}$$

Therefore the following expressions can be developed:

$$\frac{dP_{Lz}}{dz} = -M_1 M_2 + \frac{M_1}{\beta}\{A_1 \sinh(\beta z) + A_2[\cosh(\beta z) - 1]\} \tag{4.11}$$

$$\frac{dP_{Sz}}{dz} = -BM_3 - \frac{B}{\beta}\{A_1 \sinh(\beta z) + A_2[\cosh(\beta z) - 1]\} \tag{4.12}$$

Integrating from z = 0 to z, one can get the expressions for the lumen-side and shell-side pressures:

$$P_{Lz} = P_{L0} - M_1(M_2 + \frac{A_2}{\beta})z + \frac{M_1}{\beta^2}\{A_1[\cosh(\beta z) - 1] + A_2 \sinh(\beta z)\} \tag{4.13}$$

$$P_{Sz} = P_{S0} - \left(BM_3 - \frac{BA_2}{\beta}\right)z - \frac{B}{\beta^2}\{A_1[\cosh(\beta z) - 1] + A_2 \sinh(\beta z)\} \tag{4.14a}$$

Representing P_{S0} with the shell-side pressure at the end of the permeable zone:

$$P_{S0} = P_{Sl_p} + \left(BM_3 - \frac{BA_2}{\beta}\right)l_p + \frac{B}{\beta^2}\{A_1[\cosh(\beta l_p) - 1] + A_2 \sinh(\beta l_p)\} \tag{4.14b}$$

Substituting Eq. 4.14b into Eq. 4.14a, one obtains:

$$P_{Sz} = P_{Sl_p} + \left(BM_3 - \frac{BA_2}{\beta}\right)(l_p - z) + \frac{B}{\beta^2}\{A_1[\cosh(\beta l_p) - \cosh(\beta z)] + A_2[\sinh(\beta l_p) - \sinh(\beta z)]\} \tag{4.14c}$$

Substituting Eq. 4.10 into Eq. 4.4 and Eq. 4.5, respectively and integrating; one can now get

$$Q_{Lz} = Q_{L0} - \frac{N_0 \pi d_i}{\beta}\{A_1 \sinh(\beta z) + A_2[\cosh(\beta z) - 1]\} \tag{4.15}$$

$$Q_{Sz} = Q_{S0} + \frac{N_0 \pi d_i}{\beta}\{A_1 \sinh(\beta z) + A_2[\cosh(\beta z) - 1]\} \tag{4.16}$$

4.1.4 Coated Zone ($l_p \le z \le l_t$)

In the coated zone near the module outlet, the membrane pores are blocked with the coating layer on the hollow fiber inner skin. Neither fluid nor other species can permeate through the membrane, therefore,

$$J_{vz} = 0 \tag{4.2}$$

The volumetric flow rates of the fluid in both the hollow fiber lumen and the shell side are constant and equal to their corresponding flow rates at the end of the permeable zone, e.g., $Q_{Lz} = Q_{Ll_p}$; $Q_{Sz} = Q_{Sl_p}$

The lumen-side pressure drop is

$$\frac{dP_{Lz}}{dz} = -\frac{128\mu_L Q_{Ll_p}}{N_0 \pi d_i^4} \tag{4.17}$$

Integrating from l_p to z, one obtains

$$P_{Lz} - P_{Ll_p} = -\frac{128\mu_L Q_{Ll_p}}{N_0 \pi d_i^4}\left(z - l_p\right) \tag{4.18}$$

Q_{Llp} can be obtained from Eq. 4.15,

$$Q_{Ll_p} = Q_{L0} - \frac{N_0 \pi d_i}{\beta}\left\{A_1 \sinh(\beta l_p) + A_2\left[\cosh(\beta l_p) - 1\right]\right\} \tag{4.19}$$

$$P_{Lz} - P_{Ll_p} = \left\{-M_1 M_2 + \frac{M_1}{\beta}\left\{A_1 \sinh(\beta l_p) + A_2\left[\cosh(\beta l_p) - 1\right]\right\}\right\}\left(z - l_p\right) \tag{4.20}$$

The shell-side pressure drop is

$$\frac{dP_{Sz}}{dz} = -\frac{150(1-\varepsilon)^2}{d_p^2 \varepsilon^3}\mu_S \frac{4Q_{Sl_p}}{\pi(D_S^2 - N_0 d_o^2)} = -\frac{B}{N_0 \pi d_i} Q_{Sl_p} \tag{4.21}$$

where Q_{Slp} can be obtained from Eq. 4.16,

$$Q_{Sl_p} = Q_{S0} + \frac{N_0 \pi d_i}{\beta}\left\{A_1 \sinh(\beta l_p) + A_2\left[\cosh(\beta l_p) - 1\right]\right\} \tag{4.22}$$

Substitute Eq 4.22 to Eq. 4.21 and obtain after integration and rearrangement,

$$P_{Sz} - P_{Sl_p} = -\left\{ BM_3 - \frac{BA_2}{\beta} + \frac{B}{\beta}\left[A_1 \sinh(\beta l_p) + A_2 \cosh(\beta l_p)\right]\right\}\left(z - l_p\right) \tag{4.23a}$$

Let $z = l_t$. Then rearrange it and obtain:

$$P_{Sl_p} = P_{Sl_t} + \left\{ BM_3 - \frac{BA_2}{\beta} + \frac{B}{\beta}\left[A_1 \sinh(\beta l_p) + A_2 \cosh(\beta l_p)\right]\right\}\left(l_t - l_p\right) \tag{4.23b}$$

4.1.5 Determination of A_1 and A_2

Boundary conditions:

At $z = 0$, $$J_{v0} = A_1 = A(P_{L0} - P_{S0}) \tag{4.24}$$

At $z = l_p$, $$J_{vl_p} = A_1 \cosh(\beta l_p) + A_2 \sinh(\beta l_p) = A(P_{Ll_p} - P_{Sl_p}) \tag{4.25}$$

From Eq. 4.24 – Eq. 4.25, one can get,

$$P_{S0} - P_{Sl_p} - (P_{L0} - P_{Ll_p}) = \frac{A_1}{A}\left[\cosh(\beta l_p) - 1\right] + \frac{A_2}{A}\sinh(\beta l_p) \tag{4.26}$$

The pressure differences can also be expressed directly from Eqs. 4.13 and 4.14a:

$$\begin{aligned} P_{S0} - P_{Sl_p} - (P_{L0} - P_{Ll_p}) &= \frac{B}{\beta^2}\left\{A_1\left[\cosh(\beta l_p) - 1\right] + A_2 \sinh(\beta l_p) - A_2 \beta l_p\right\} + BM_3 l_p \\ &- M_1\left(M_2 + \frac{A_2}{\beta}\right)l_p + \frac{M_1}{\beta^2}\left\{A_1\left[\cosh(\beta l_p) - 1\right] + A_2 \sinh(\beta l_p)\right\} \\ &= \frac{A_1}{A}\left[\cosh(\beta l_p) - 1\right] + \frac{A_2}{A}\sinh(\beta l_p) + BM_3 l_p - \frac{BA_2 l_p}{\beta} - M_1\left(M_2 + \frac{A_2}{\beta}\right)l_p \end{aligned} \tag{4.27}$$

Substituting Eq. 4.26 into Eq. 4.27, one can obtain using Eq. 4.9b,

$$A_2 = \frac{\beta\left[BM_3 - M_1 M_2\right]}{B + M_1} = \frac{A\left[BM_3 - M_1 M_2\right]}{\beta} \tag{4.28}$$

Substitute Eq. 4.14b into Eq. 4.24,

$$A_1 = A(P_{L0} - P_{S0})$$
$$= A\left\{P_{L0} - P_{Sl_p} - BM_3 l_p - \frac{B}{\beta^2}\left\{A_1\left[\cosh(\beta l_p) - 1\right] + A_2 \sinh(\beta l_p) - A_2 \beta l_p\right\}\right\} \quad (4.29)$$

Replace P_{Sl_p} with P_{Sl_t}, the pressure at the module shell outlet via Eq. 4.23b; Eq. 4.29 can be rewritten as

$$A_1 = A\left\{\begin{array}{l} P_{L0} - P_{Sl_t} - BM_3(l_t - l_p) - \frac{B}{\beta}\left\{A_1 \sinh(\beta l_p) + A_2\left[\cosh(\beta l_p) - 1\right]\right\}(l_t - l_p) \\ - BM_3 l_p - \frac{B}{\beta^2}\left\{A_1\left[\cosh(\beta l_p) - 1\right] + A_2 \sinh(\beta l_p) - A_2 \beta l_p\right\} \end{array}\right\} \quad (4.30)$$

Reorganize and solve for A_1 to obtain,

$$A_1 = \frac{\beta^2(P_{L0} - P_{Sl_t} - BM_3 l_t) + \beta BA_2 l_t - \beta BA_2(l_t - l_p)\cosh(\beta l_p) - BA_2 \sinh(\beta l_p)}{M_1 + \beta B(l_t - l_p)\sinh(\beta l_p) + B\cosh(\beta l_p)} \quad (4.31)$$

4.1.5.1 Case 1. Tube-side Loading. For tube-side loading, from Eq. 4.7g $M_3 = 0$; therefore from Eqs. 4.28 and 4.31

$$A_2 = -\frac{AM_1M_2}{\beta} \quad (4\text{-}32)$$

$$A_1 = \frac{\beta^2(P_{L0} - P_{Sl_t}) - ABM_1M_2 l_t + ABM_1M_2(l_t - l_p)\cosh(\beta l_p) + \frac{ABM_1M_2}{\beta}\sinh(\beta l_p)}{M_1 + \beta B(l_t - l_p)\sinh(\beta l_p) + B\cosh(\beta l_p)} \quad (4\text{-}33)$$

When $l_p = l_t$, corresponding to the no-coating situation, the expression for A_1 can be reduced to

$$A_1 = \frac{\beta^2(P_{L0} - P_{Sl_t}) - ABM_1M_2 l_t + \frac{ABM_1M_2}{\beta}\sinh(\beta l_t)}{M_1 + B\cosh(\beta l_t)} \quad (4.34)$$

which is the same as the equation Dai et al. (1999) obtained for the integrated device without any coating.

4.1.5.2 Case 2. Tube-side Elution. Boundary conditions:

$$Q_{L0} = Q_{Sl_t} = Q_{Sl_p} \tag{4.35}$$

$$Q_{Ll_t} = Q_{S0} = 0 \tag{4.36}$$

The constant A_2 is the same as shown in Eq. 4.32. The constant A_1 can be determined using Eqs. 4.35, 4.36, 4.32 and 4.22:

$$A_1 = \frac{AM_2\left[B + M_1 \cosh\left(\beta l_p\right)\right]}{\beta \sinh\left(\beta l_p\right)} \tag{4.37}$$

In the permeable zone, $0 \le z \le l_p$, from Eqs 4.16 and 4.36

$$Q_{Sz} = \frac{N_0 \pi d_i}{\beta}\left\{A_1 \sinh(\beta z) + A_2\left[\cosh(\beta z) - 1\right]\right\} \tag{4.38}$$

In the coated zone, $l_p \le z \le l_t$,

$$Q_{Sz} = Q_{L0} \tag{4.39}$$

$$Q_{Lz} = Q_{Ll_p} = 0 \tag{4.40}$$

4.1.5.3 Case 3. Shell-side Elution. Boundary conditions:

$$Q_{L0} = Q_{Ll_t} = Q_{Ll_p} = 0 \tag{4.41}$$

$$Q_{S0} = Q_{Sl_t} = Q_{Sl_p} \tag{4.42}$$

$$A_2 = \frac{ABM_3}{\beta} \tag{4.43}$$

Applying the boundary conditions to eq. 4.24, we obtain A_1.

$$A_1 = \frac{ABM_3\left[\cosh\left(\beta l_p\right) - 1\right]}{\beta \sinh\left(\beta l_p\right)} \tag{4.44}$$

In the permeable zone,

$$J_{vz} = -A_1 \cosh(\beta z) - A_2 \sinh(\beta z) \tag{4.45}$$

$$Q_{Sz} = Q_{S0} - \frac{N_0 \pi d_i}{\beta} \{A_1 \sinh(\beta z) + A_2 [\cosh(\beta z) - 1]\} \tag{4.46}$$

In the coated zone,

$$J_{vz} = 0$$

$$Q_{Sz} = Q_{S0} \tag{4.47}$$

4.1.6 Estimation of the Parameters *A* and *B*

The two quantities A and B are parameters describing respectively the flow resistance through the membrane and the packed bed; A accounts for the membrane permeance under the shell-side packing condition and B is a characteristic parameter accounting for the beads and the hollow fiber packing. These two parameters need to be known for solving the equations describing the hydrodynamic behavior of the integrated device. Parameters A and B can be estimated from experimental hydrodynamic data. A 'cold' loading run using the tris-buffer only was performed on module #1 packed with beads before coating. The feed pressure P_{L0}, shell-side inlet pressure P_{S0}, and the permeate flow rate Q_{Slp} were measured. Equations 4.14b and 4.16 were used to calculate P_{S0} and Q_{Slp} respectively using the initial guess values of A and B. The sum of least squares of the relative deviation between the experimental data and the calculated values of P_{S0} and Q_{Slp} was used as the optimization function. The optimal value of A and B for the integrated device shown in Table 4.1 were calculated using the Generalized Reduced Gradient (GRG2) nonlinear optimization algorithm (Beklaitis, Ravindran et al. 1983) by Excel solver:

$$\min\left[\left(\frac{P_{S0}^{\exp}-P_{S0}^{cal}}{P_{S0}^{\exp}}\right)^2+\left(\frac{Q_{Sl_p}^{\exp}-Q_{Sl_p}^{cal}}{Q_{Sl_p}^{\exp}}\right)^2\right] \tag{4.48}$$

Table 4.1 Hydrodynamic Experimental Data and Estimated Parameters for Module #1

Q_{L0} (ml/min)	P_{L0} (kPa)	P_{S0} (kPa)	Q_{Slp} (ml/min)	A (m/s/Pa)	B (Pa•s/m^3)	ε
200	35.2	27.6	7.2	2.4×10^{-10}	2.65×10^{11}	0.374

As one can see, parameter A is only about 1/4th of the original membrane permeance and 1/3rd of the cleaned module permeance obtained earlier (Table 3.1) for the UF module without the shell-side packing. One of the possible reasons is that some membrane pores at the shell-side membrane surface were blocked by the beads, introducing more flow resistance through those membrane pores. In cases where the pore was not blocked, there is a possibility of an additional resistance in the fluid exit due to the presence of a nearby bead. Another contribution to the deviation is caused by the radial flow that was neglected in the present one dimensional model. The pressure at the membrane shell-side interface is actually a little higher than the radial average pressure across the packing used in our model. The void fraction of the shell-side packing was calculated from Eq. 4.7e using the value of B shown in the table. Typical void fractions for packed beds are 0.35-0.5 (LeVan, Carta et al. 1997). Dai et al. (Dai, Luo et al. 1999) found A, B, ε to be 1.857×10^{-10}, 4.724×10^{11}, 0.3248 respectively for a similar device, and 3.255×10^{-10}, 3.003×10^{11}, 0.3622 respectively for another similar device.

4.2 Protein Loading Behaviors in the Device with a Coated Zone

The following assumptions were used in the model:

1. Fluid flow and membrane filtration are at steady state.
2. The permeate flow rate is much smaller than the lumen-side feed flow rate so that the observed protein transmission through the membrane τ_{ob} along the permeable fiber length can be considered as constant.
3. Hollow fibers are distributed evenly in the module housing.
4. Chromatographic beads are packed homogeneously in both axial and radial directions in the shell side.
5. Mass transport in the mobile phase in the shell side can be described by an one dimensional axial dispersion model.
6. Linear adsorption equilibrium exists everywhere between the mobile phase and the stationary phase in the shell side (Dai, Majumdar et al. 2003).

4.2.1 Lumen-Side Material Balance

The observed protein transmission of protein i through the membrane in a conventional membrane filtration τ_{obi} is defined as the shell-side permeate concentration over the lumen-side feed bulk concentration, where the concentration polarization effect at the feed side was lumped:

$$\tau_{obi} = \frac{C_{Si}}{C_{Li}} \tag{4.49}$$

For the same cross flow velocity and the permeation flux, τ_{obi} for a membrane is constant. In this study, we assume τ_{obi} is a constant along the membrane length. From the conventional membrane theory (Ho and Sirkar 1992), the concentration of species i along the membrane length can be calculated using the following equation

$$C_{Lzi} = C_{L0i}\left(\frac{Q_{L0}}{Q_{Lz}}\right)^{1-\tau_{obi}} \tag{4.50}$$

When τ_{obi} = 0, the species can not pass through the membrane, and total amount of species i in the lumen feed side will not change along the membrane length. If the membrane is permeable to the solvent, species i will get concentrated along the membrane length. If the membrane is not permeable to the solvent either, as in the coated zone section in the integrated device of this study, the concentration of species i will not change along the membrane length.

4.2.2 Shell-Side Material Balance

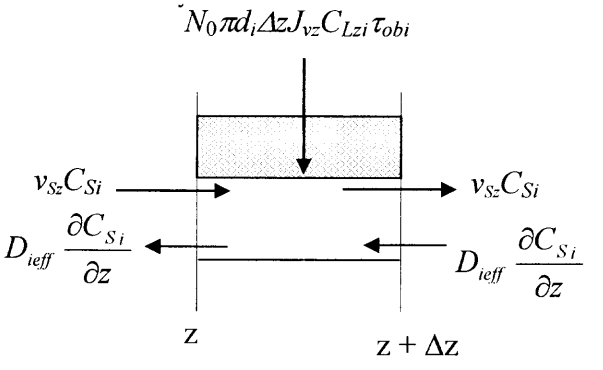

Figure 4.2 Mass transport in and out of a differential control volume in the shell side.

The material balance for species i over the control volume of Figure 4.2 is

$$\begin{aligned} &S_S \Delta z\left[\varepsilon\frac{\partial C_{Si}}{\partial t} + (1-\varepsilon)\frac{\partial q_{Si}}{\partial t}\right] \\ &= \varepsilon S_S\left[v_{Sz}C_{Si} - D_{ieff}\frac{\partial C_{Si}}{\partial z}\right]_{z,t} - \varepsilon S_S\left[v_{Sz}C_{Si} - D_{ieff}\frac{\partial C_{Si}}{\partial z}\right]_{z+\Delta z,t} + N_0\pi d_i \Delta z J_{vz} C_{Lzi}\tau_{obi}\Big|_{z,t} \end{aligned} \tag{4.51}$$

Here q_{Si} is the concentration of species i in the adsorbed phase; D_{ieff} is a lumped effective axial dispersion coefficient of species i; v_{Sz} is the interstitial fluid velocity in the shell side and is equal to the superficial velocity u_{Sz} divided by the void fraction ε,

$$v_{Sz} = \frac{u_{Sz}}{\varepsilon} \tag{4.52}$$

Substitute Eq. 4.52 into Eq. 4.51 and divide both sides by $\varepsilon S_S \Delta z$; one obtains

$$\frac{\partial C_{Si}}{\partial t} + \frac{1-\varepsilon}{\varepsilon}\frac{\partial q_{Si}}{\partial t} = \frac{u_{Sz}C_{Si}\big|_{z,t} - u_{Sz}C_{Si}\big|_{z+\Delta z,t}}{\varepsilon \Delta z} - \frac{D_{ieff}\left.\frac{\partial C_{Si}}{\partial z}\right|_{z,t} - D_{ieff}\left.\frac{\partial C_{Si}}{\partial z}\right|_{z+\Delta z,t}}{\Delta z} + \frac{N_0 \pi d_i J_{vz} C_{Lzi} \tau_{obi}\big|_{z,t}}{\varepsilon S_S} \tag{4.53}$$

Substitute Eq. 4.7b in to Eq. 4.53 and take the limit of $\Delta z \rightarrow 0$; one gets the governing differential equation:

$$\frac{\partial C_{Si}}{\partial t} + \frac{1-\varepsilon}{\varepsilon}\frac{\partial q_{Si}}{\partial t} + \frac{1}{\varepsilon}\frac{\partial (u_{Sz}C_{Si})}{\partial z} = \frac{\partial}{\partial z}\left(D_{ieff}\frac{\partial C_{Si}}{\partial z}\right) + \frac{aJ_{vz}C_{Lzi}\tau_{obi}}{\varepsilon} \tag{4.55}$$

4.2.2.1 Governing Equation in the Permeable Zone. Here the superficial axial velocity u_{Sz} varies along the axial direction due to the solvent permeation through the membrane in the permeable zone, and the gradient of the u_{Sz} can be obtained by differentiating Eq 4.7c

$$\frac{du_{Sz}}{dz} = aJ_{vz} \tag{4.56}$$

The effective axial dispersion coefficient D_{ieff} is a function of v_{Sz}, thus varies along the axial direction too. It was found that D_{ieff}/v_{Sz} is constant regardless of the flow rate and the type of gel particles and solutes, and is a unique function of the particle size of the gel (Yamamoto, Nakanishi et al. 1983a; 1983b), e.g.,

$$D_{ieff} = C_D \frac{u_{Sz}}{\varepsilon} \tag{4.58}$$

Dai et al.(2003) adopted $C_D = 7.83 \times 10^{-4}$ for an integrated device using the same kind of ultrafiltration membrane module and chromatography beads:

$$\frac{dD_{ieff}}{dz} = \frac{C_D}{\varepsilon}\frac{du_{Sz}}{dz} = \frac{C_D}{\varepsilon} aJ_{vz} \tag{4.59}$$

The second term on the right hand side of Eq 4.55 is a source term representing the permeation of species i through the membrane from the lumen side:

$$\frac{\partial C_{Si}}{\partial t} + \frac{1-\varepsilon}{\varepsilon}\frac{\partial q_{Si}}{\partial t} = D_{ieff}\frac{\partial^2 C_{Si}}{\partial z^2} + \frac{\left(aC_D J_{vz} - u_{Sz}\right)}{\varepsilon}\frac{\partial C_{Si}}{\partial z} + \frac{aJ_{vz}\left(C_{Lzi}\tau_{obi} - C_{Si}\right)}{\varepsilon} \tag{4.60}$$

4.2.2.2 Governing Equation in the Coated Zone. However, in the coated zone, the right hand side source term of Eq 4.55 becomes zero, and u_{Sz} remains constant. Therefore, Eq 4.55 reduces to the governing equation valid for a conventional chromatography column:

$$\frac{\partial C_{Si}}{\partial t} + \frac{1-\varepsilon}{\varepsilon}\frac{\partial q_{Si}}{\partial t} + \frac{u_{Sz}}{\varepsilon}\frac{\partial C_{Si}}{\partial z} = D_{ieff}\frac{\partial^2 C_{Si}}{\partial z^2} \tag{4.61}$$

4.2.3 Boundary Conditions and Initial Conditions

Boundary conditions:

z = 0: $$P_{Lz} = P_{L0},\ Q_{Lz} = Q_{L0},\ C_{Lzi} = C_{L0i} \tag{4.56}$$

$$\left.\frac{\partial C_{Si}}{\partial z}\right|_{z=0} = 0 \tag{4.57}$$

At the module exit, the concentration in the mobile phase will not change after the fluid leaves the packed bed, thus

$$z = l_t \qquad P_{Sz} = P_{Sl_t}, \quad \left.\frac{\partial C_{Si}}{\partial z}\right|_{z=l_t} = 0 \tag{4.58}$$

Initial conditions:

$$\text{At } t = 0, \qquad C_{Szi} = 0, \quad 0 \le z \le l_t \tag{4.59}$$

$$q_{Szi} = 0, \quad 0 \le z \le l_t \tag{4.60}$$

4.3 Adsorption Isotherm and Protein Transmission Parameters

Due to the high adsorption capacity of the DEAE Sepharose beads, most of the proteins permeating through the membrane will be adsorbed in the stationary phase during loading. As a result, the mobile phase equilibrium protein concentrations in the shell side are relatively low in the loading step. The equilibrium isotherms for Mb and α-LA fall in the linear range (Dai 2000).

$$q_{Si} = K_i C_{Si} \tag{4.61}$$

Dai et al.(2003) reported K_i for Mb and α-LA to be 43.4 and 31009, respectively, in the Tris-buffer of pH 8.5. The extremely high adsorption capacity for α-LA indicates that α-LA binds very strongly with the DEAE Sepharose Fast Flow beads under the experimental conditions.

The observed protein transmission through the membrane lumped the feed side concentration polarization, membrane intrinsic protein transmission and mass transfer enhancement effect due to the adsorption at the permeate side (for the latter, see Chapter 5 that follows). It is determined by the pseudo-permeate concentration, i.e., the total loaded amount of a specific protein divided by the total permeate volume in the loading period, over the feed bulk protein concentration. A more detailed analysis of observed

protein transmission through the membrane in this integrated device will be presented in Chapter 5.

Table 4.2 Isotherm and Protein Transmission Parameters

Protein	K_i	τ_{ob}
Mb	43.4	0.48
α-LA	31099	0.88

* Data for K_i were obtained from Dai et al. (2003).

4.4 Numerical Solution Procedure

The above partial differential equations (PDEs) were solved using a public PDE solver package PDECOL (Madson and Sincovec 1979). The solution method uses finite element collocation based upon piecewise polynomials for spatial discretization to reduce the PDEs into ordinary differential equations (ODEs) in the time domain. The resulting ODEs then are solved by a general purpose ODEs solver package. The original Fortran 77 code was rewritten to be used on PC and errors were corrected according to Madsen and Sincovec ((Madson and Sincovec 1992)). For simulation of the device without any coating, the whole module length was divided into 100 subintervals. The Fortran 77 code is listed in Appendix A. For simulation of the device with a coated zone, the permeable zone of the module was divided into 75 subintervals and the coated zone was divided into 25 subintervals respectively. The corresponding governing equations for the fluid flow and the material balance for each specific zone were called upon during use. The Fortran 77 code is listed in Appendix B.

4.5 Results and Discussion

4.5.1 Protein Loading in the Non-Coated Module

Figure 4.3 shows the flow rate, pressure and flux profiles during loading in module #1 without coating. The lumen-side pressure decreases only slightly along the module length. But the shell-side pressure decreased much faster due to the high flow resistance of the packed bed. As a result, the transmembrane pressure increases significantly along the flow direction, and reaches the maximum at the module exit. The permeate flux profile shows clearly that more solvent permeates through the membrane at the module downstream section. The higher solvent permeate flux will bring more protein molecules through the membrane at the downstream section, causing uneven protein loading across the module.

Figure 4.4 shows the simulated protein concentration profiles after 15 min loading corresponding to the hydrodynamic operating conditions shown in Figure 4.3. The protein feed concentrations used in the simulation were 0.0509 mg/ml for Mb and 0.0495 mg/ml for α-LA. As was expected from the hydrodynamic profiles, the protein concentrations in the stationary phase and the mobile phase are highly uneven along the module length. While Mb already starts leaking and the beads near the module exit have been saturated by the Mb, the beads at the upstream section are still far away from being saturated. The adsorption capacity of the whole module could not be fully utilized. The profile for α-LA concentration in the beads are similar to that for Mb, but at a lower level. The α-LA concentration in the liquid along the whole module is very low due to the extremely high adsorption capacity of the beads for α-LA. The curve for α-LA

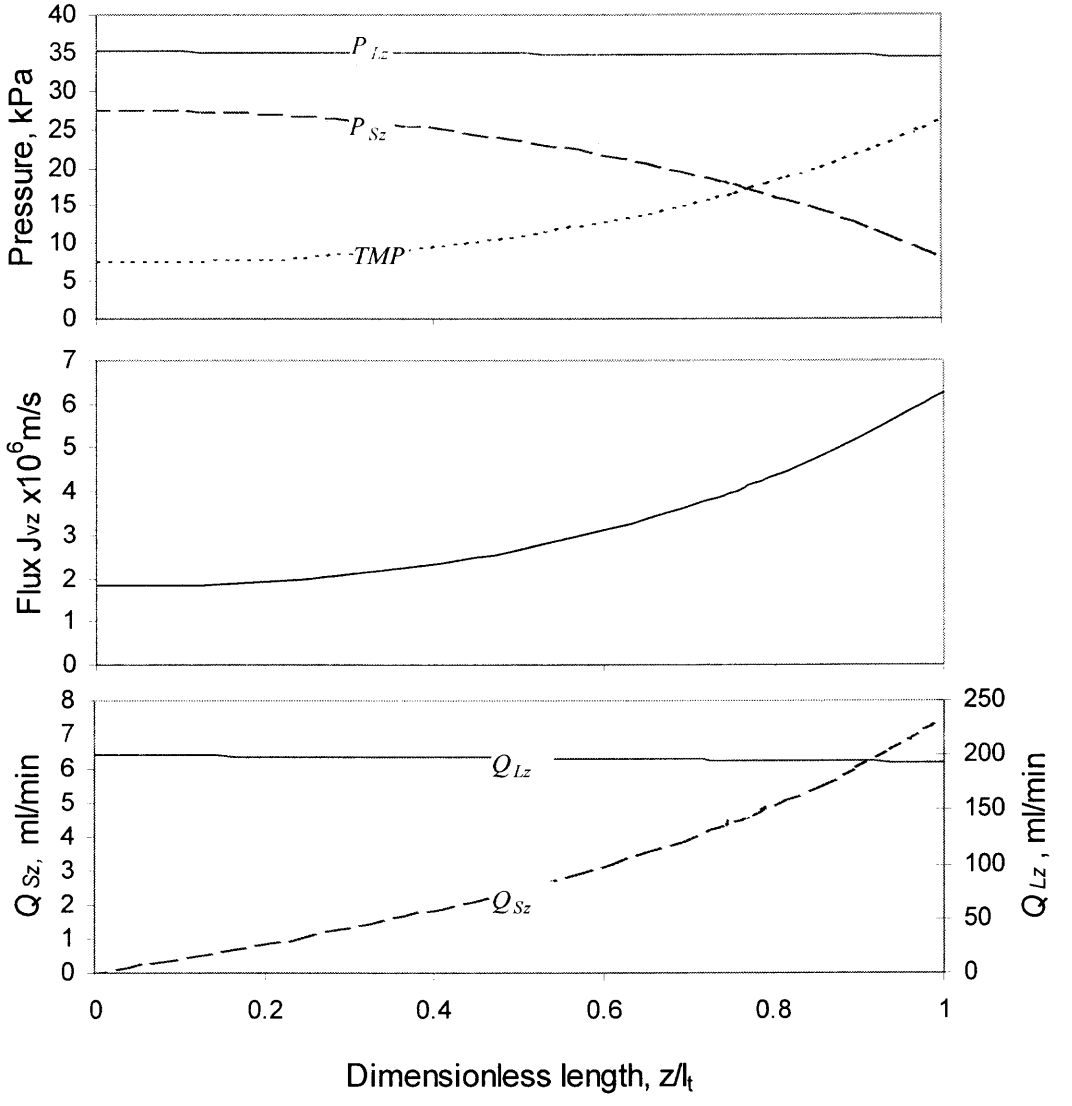

Figure 4.3 Pressure, solvent flux and flow rate profiles during loading in module #1 without coating. (Tube-side feed: flow rate 200 ml/min, pressure 35.4 kPag.)

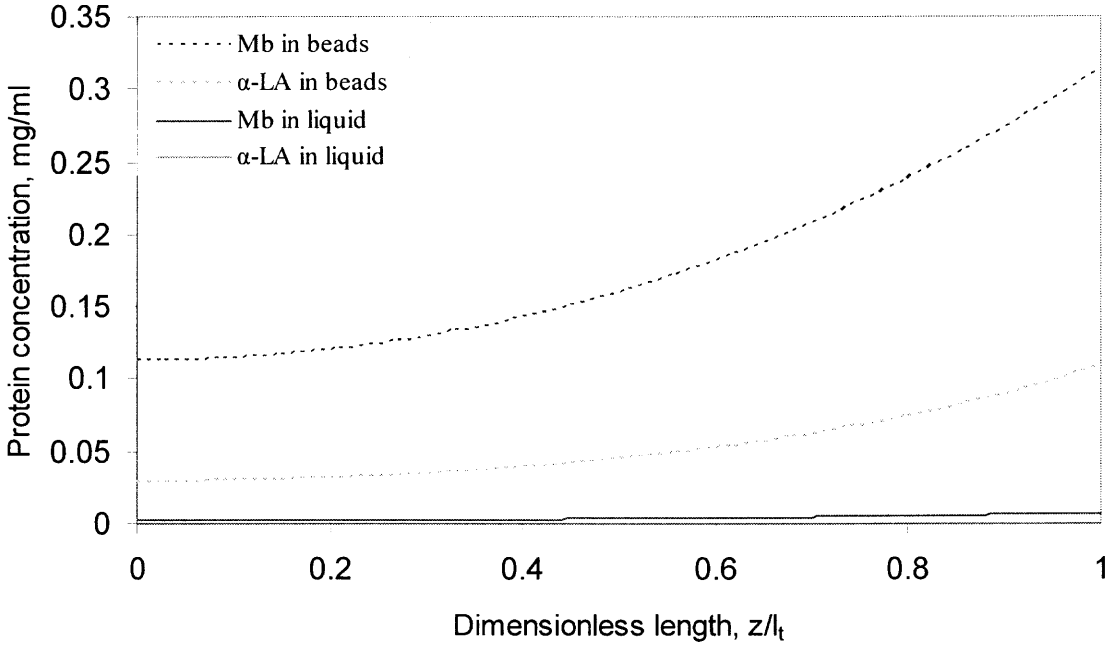

Figure 4.4 Protein concentration profiles along module #1 without coating at the end of loading. (Feed concentration: Mb 0.0509 mg/ml, α-LA 0.0495 mg/ml. Loading condition, tube-side feed flow rate 200 ml/min, pressure 35.4 kPag. Loading time 15 min.)

concentration in the liquid almost lies on the x-axis in the plot. But strictly speaking, there will still be trace amount of α-LA (in equilibrium with the α-LA concentration in beads at the module exit) leaking from the module during loading and the first elution step for Mb elution. These simulation results provide insight into the reasons for early protein leakage in Dai et al. (2003) and the lower loading capacity observed in the experiments using a device without a coated zone.

4.5.2 Loading of the Module with a Coated Zone

However, when a coated zone of 6 cm length is formed near the module outlet by interfacial polymerization, neither solvent nor protein molecules can permeate through the membrane to the shell side through the coated zone. As shown in Figure 4.5, the permeate flux through the membrane becomes zero along the coated zone. Correspondingly, the permeate flow rate remains constant in the coated zone. Although the total permeate flow rate drops due to loss of the permeable membrane area, its rate of decrease is less than the corresponding permeable membrane area reduction rate. This is because the lower downstream permeate flow rate leads to a lower pressure build up in the bed. Therefore, the upstream TMP becomes larger and more solvent permeates through the membrane in the upstream region. This effect can be seen more clearly if we compare the flux profile in Figure 4.5 with that in Figure 4.3.

Simulations of the protein loading in the integrated device having a coated zone were performed under the same operating conditions as those for the experiment shown in Figure 3.8. The simulated protein concentration profiles for the loading time of 15 min shown in Figure 4.6a are significantly different from that in Figure 4.4. A clear shock front layer is formed in the front of the profiles in the coated zone. Ahead of the shock layer of the Mb, the beads are still fresh. There will not be any protein leakage before the Mb shock layer reaches the module exit. The upstream protein concentration in the beads is higher than that in the module without a coated zone shown in Figure 4.4. The total loaded amounts of the proteins from the simulation are 1.89 mg Mb and 0.47 mg α-LA, very close to the experimental results.

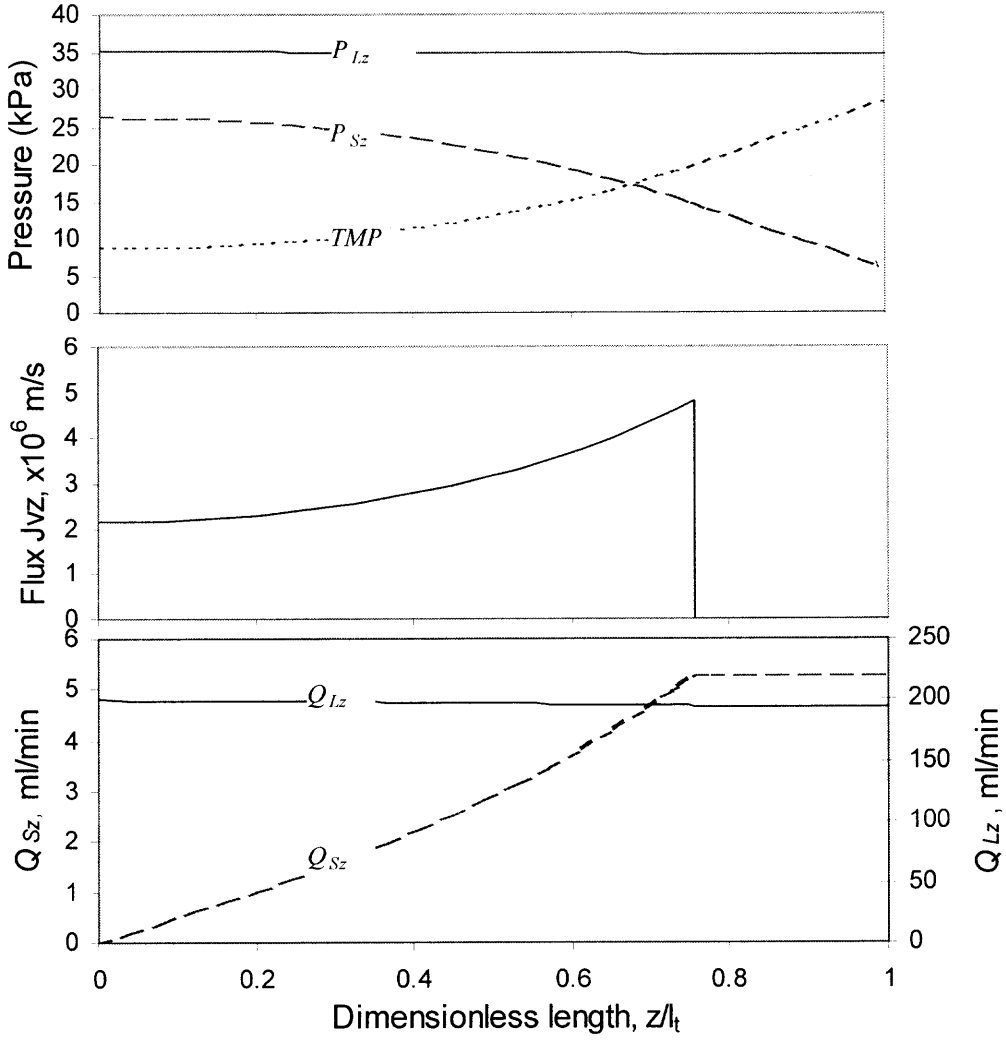

Figure 4.5 Pressure, solvent flux and flow rate profiles during loading in a module having a coated zone. (Tube-side feed: flow rate 200 ml/min, pressure 35.4 kPag.)

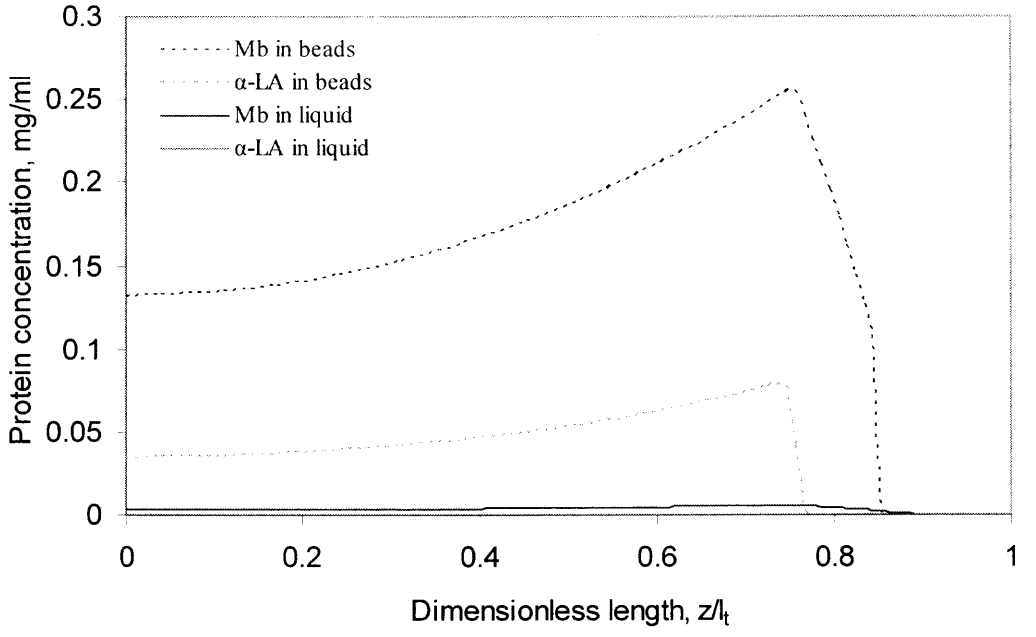

a. Loading time 15 min

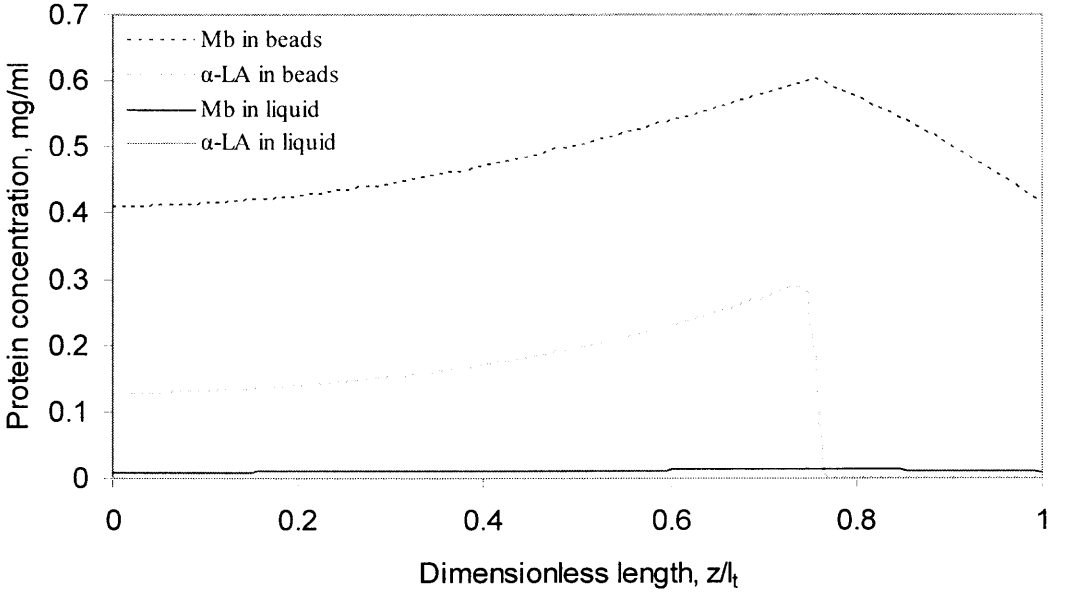

b. Loading time 55 min

Figure 4.6 Protein concentration profiles along the module #1 with a coated zone. (Feed concentration: Mb 0.0509 mg/ml, α-LA 0.0495 mg/ml. Loading condition, tube-side feed flow rate 200 ml/min, pressure 35.4 kPag.)

With the loading continuing, the protein concentration in the beads behind the shock layer will increase and the shock layer front will propagate forward. Figure 4.6b shows the protein concentration profiles at the loading time of 55 min. The Mb shock layer front reached the module exit, and breakthrough happened at a similar level as that in Figure 4.4 for the module without any coating. But the protein concentrations in the beads along the whole module are much higher than that in Figure 4.4. Further the protein concentration profiles are much more uniform along the bed length. The Mb concentration in the beads at the module inlet is almost four times that in Figure 4.4.

More importantly, the α-LA shock layer front is still remaining at the beginning of the coated zone, far away from the module outlet. The adsorption of α-LA on the beads is much stronger than that of Mb so that the α-LA shock layer front propagates much more slowly toward the module outlet. Before the α-LA shock layer front reaches the module exit, there will not be any α-LA leakage at all. It will also be much easier to get complete separation of Mb and α-LA in the elution step. In addition, the concentration of α-LA in the fresh permeate (just out of the membrane pores, before adsorption take place) is much lower than that of Mb, due to the higher membrane rejection for α-LA. The higher membrane rejection for the non-targeted protein will alleviate the adsorption burden of the beads at the shell-side.

Simulations were also performed for the high feed concentration, high loading capacity run shown in Figure 3.4 in the experimental results section. The feed concentrations were 0.505 mg/ml for Mb and 0.467 mg/ml for α-LA (Figure 4.7). The loading time was 35 min. The total loaded amounts of proteins from simulation are 42.84 mg for Mb and 10.32 mg for α-LA, somewhat less than the experimental values, which

are 51.34 mg for Mb and 14.13 mg for α-LA. One of the reasons for the deviation is that constant feed concentrations were adopted as the boundary condition. But the experiment was performed in the retentate recycle mode to save the total amount of protein used in the experiment. With every pass-through across the module, the retentate became more concentrated due to the membrane rejection of the protein molecules. The feed concentrations increased with the loading time while the retentate was recycled into the feed reservoir.

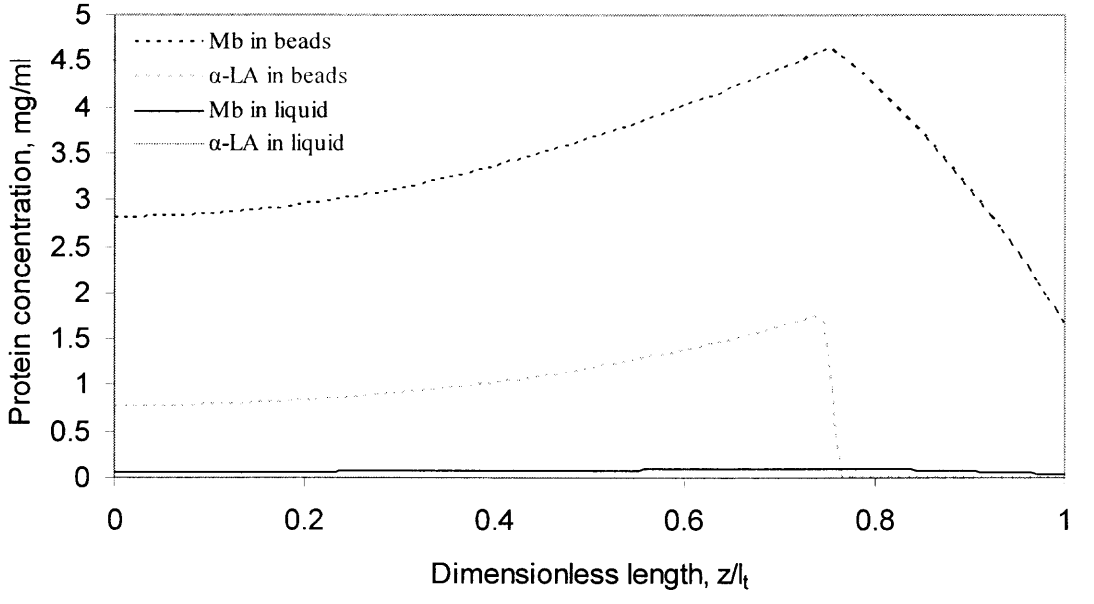

Figure 4.7 Protein concentration profiles at the end of loading, for the high feed concentration, high loading capacity run. (Feed concentration: Mb 0.505 mg/ml, α-LA 0.467 mg/ml. Loading condition, tube-side feed flow rate 200 ml/min, pressure 35.4 kPag. Loading time 35 min.).

In all of the above protein concentration profiles from simulation, both Mb and α-LA concentrations in the mobile phase remained very low during the whole loading process. This validates the use of the linear isotherm in the model and simulations.

4.5.3 Simulation of the Breakthrough Behavior of the Integrated Device, with and without a Coated Zone

The same program was used to simulate the experimental breakthrough curves shown in Figure 3.1. The simulation results along with the experimental data points are shown in Figure 4.8. The lighter curve is the simulated breakthrough curve for the module without any coated zone. The black curve is the simulated breakthrough curve for the module having a 6 cm coated zone near the module outlet. The simulated curves fit the experimental data fairly well and the breakthrough points were correctly predicted.

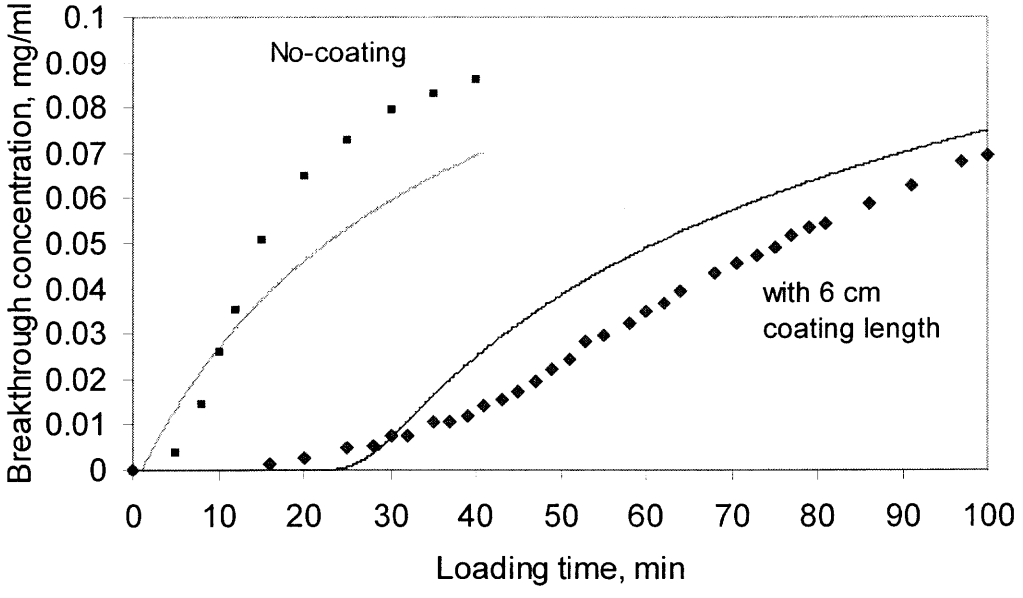

Figure 4.8 Comparison of the simulation results with the experimental breakthrough curves. (Loading conditions described in Figure 3.1).

4.5.4 Optimal Length of the Coated Zone

When the integrated device is operated in a loading-washing-elution-reequilibration cyclic mode, the productivity is defined as the protein product output per day. Since the washing, elution and reequilibration times are relatively constant in a cycle, optimizing the loading step to get the maximum productivity is important. If the loading time is very short, and the protein loaded amount is low, most of the time spent to produce the proteins will be consumed by the washing-elution-reequilibration steps, resulting in low productivity. As has been shown in the previous sections, introducing a coated zone in the integrated device can increase the loading time and thus the loading capacity. A simulation of the device productivity for different lengths of the coated zone was performed. The time for washing-elution-reequilibration in a cycle was assumed to be 90 min. The same loading operating conditions as shown in Figure 3.4 have been used. As the coating length is increased, more beads on the shell side can be fully utilized, but more membrane permeable area will be lost. As the total protein amount obtained per loading is increased, the time for loading is increased too. So the optimal length of the coated zone will be a trade off between the beads' adsorption capacity utilization and the available membrane permeable area. At the beginning, with the increase of the coating length, the productivity increases. At 12 cm length of the coated zone, about half of the total fiber length, the productivity of the device reaches maximum. Extending the coating beyond the optimal length will cause the productivity to decline. The loading time becomes too long and the increase in the loading capacity is not significant enough to compensate for the increased time for loading.

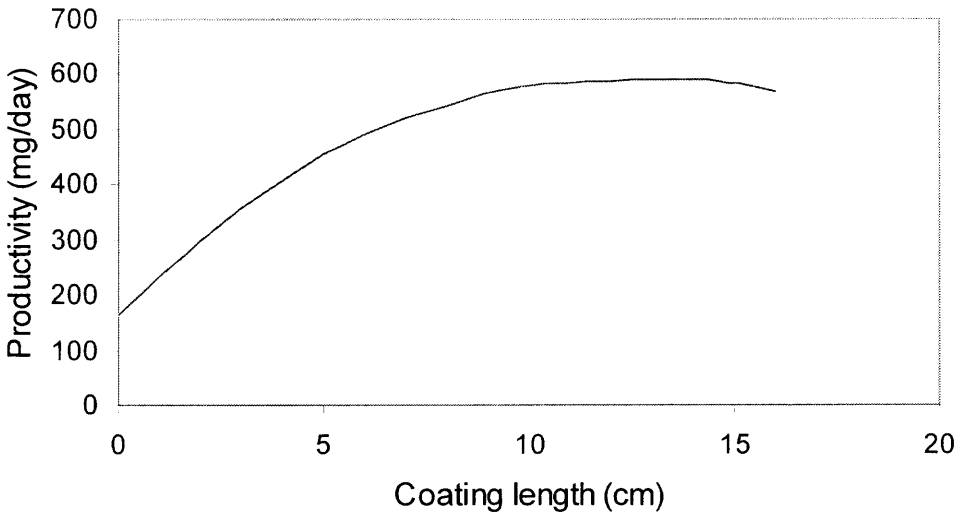

Figure 4.9 Optimal length of the coated zone.

CHAPTER 5

MASS TRANSFER ENHANCEMENT ANALYSIS

5.1 Introduction

Dai et al. (1999), as well as Dai (2000) observed that the protein transmission rate through the membrane was enhanced somewhat by protein adsorption on ion exchange beads packed in the shell side of the ultrafiltration membrane module. The mechanism of this protein transmission enhancement phenomenon was not given and could not be found in literature. Neither did they consider the effect of the potential protein transmission enhancement on the behavior of the integrated filtration-cum-chromatography device [(Dai, Majumdar et al. 2003)].

It is useful to conduct a theoretical analysis of the protein transmission enhancement due to permeate side protein adsorption. This may identify the regions of operation where such an effect may be important. A pseudo-steady state convection-diffusion model to describe protein mass transfer through the membrane with permeate side protein adsorption will be developed now. The mass transfer enhancement factor due to permeate side protein adsorption for different membrane fluxes and protein diffusivities can be evaluated for a single protein as well as a binary protein mixture. The significance of diffusional contributions to the protein transmission will be considered.

5.2 Theoretical Development

Consider a crossflow membrane-based protein filtration process with the adsorbent beads packed at the permeate side of the membrane surface as illustrated in Figure 5.1. The feed protein solution flows along the membrane surface in the feed side at a

pressure higher than that in the permeate side. Protein molecules permeating through the membrane are adsorbed by the adsorbent beads. The protein concentration of the liquid

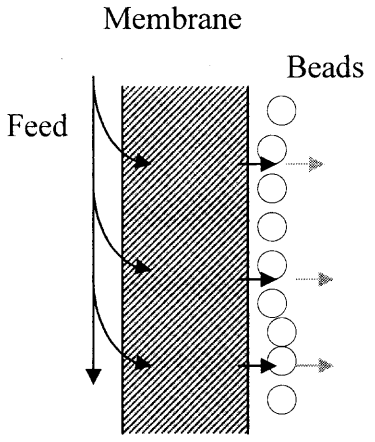

Figure 5.1 Crossflow membrane filtration with adsorbent at the permeate side.

near the adsorbent surface can be much lower than that near the membrane interface due to the adsorption equilibrium. The concentration gradient formed in the permeate side boundary layer can increase the diffusional transport rate, and therefore, increase the protein mass transfer rate through the permeate side boundary layer. This means that the protein concentration at the permeate side membrane interface will be lowered and the driving force for protein diffusion through the membrane pores will be increased. The significance of protein transmission enhancement for this process depends on the relative contributions of diffusion and convection to the total mass transport.

The crossflow filtration-cum-adsorption process described above is a dynamic process because the protein concentration near the adsorbent surface will be changing with time due to adsorption equilibration. The dynamic filtration-cum-adsorption process is complicated for simulation purposes. To explicitly determine the permeate side protein

adsorption effect, we can assume that the adsorbent is a huge protein sink having a large enough capacity so that the dynamic process can be approximated by a pseudo-steady state model. Figure 5.2 illustrates the steady state concentration profiles in the protein transport process in the feed side boundary layer, the microporous membrane and the permeate side boundary layer. The permeate bulk concentration is constant under pseudo-steady state conditions.

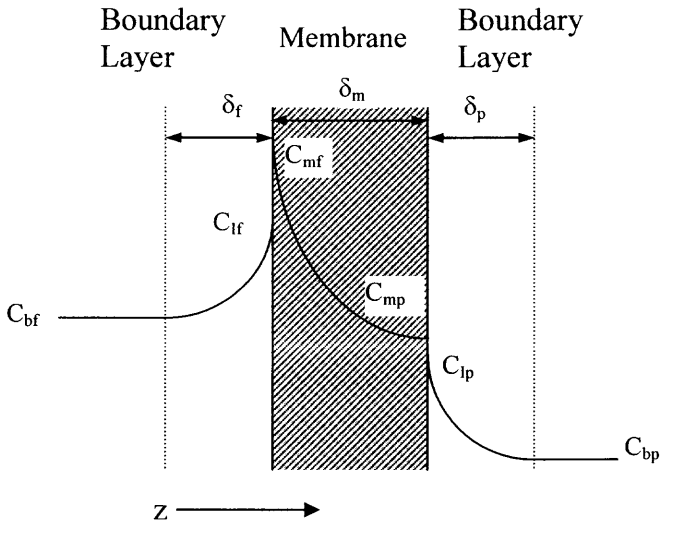

Figure 5.2 Pseudo-steady state protein transport mechanism: concentration profiles.

A mass balance in the feed side boundary layer for the protein solute at any z leads to

$$N_s = J_v C - D_0 \frac{dC}{dz} \tag{5.1a}$$

Boundary conditions:

$$z = 0, \quad C = C_{bf}; \quad z = \delta_f, \quad C = C_{lf} \tag{5.1b}$$

Integrating:

$$\int_{C_{bf}}^{C_{lf}} \frac{dC}{C - N_s/J_v} = \int_0^{\delta_f} \frac{J_v}{D_0} dz$$

$$\frac{C_{lf} - N_s/J_v}{C_{bf} - N_s/J_v} = \exp\left(J_v/k_f\right) = E_f \tag{5.1c}$$

where $k_f = D_0/\delta_f$ is the protein mass transfer coefficient, and J_v/k_f is the Peclect number in the feed side boundary layer. An alternate form is

$$\frac{N_s}{J_v} = \frac{C_{bf}E_f - C_{lf}}{E_f - 1} \tag{5.1d}$$

Consider now the mass flux through the porous membrane; locate the z-coordinate origin at the feed-membrane interface going toward the permeate side:

$$N_s = K_c J_v C_m - \varepsilon K_d D_0 \frac{dC_m}{dz} \tag{5.2a}$$

where ε is the membrane skin layer porosity, K_c is the convective hindrance factor, and K_d is the diffusive hindrance factor (Opong and Zydney 1991, Anderson and Quinn 1974).

Boundary conditions:

$$z = 0,\ C_m = C_{mf} = \phi C_{lf}; \qquad z = \delta_m,\ C_m = C_{mp} = \phi C_{lp} \tag{5.2b}$$

Here ϕ is the partition coefficient for the protein between the external solution and the membrane and is assumed to be the same at both interfaces.

Integrating equation (5.2a) between the two limits:

$$\int_{C_{mf}}^{C_{mp}} \frac{dC_m}{C_m - N_s/(J_v K_c)} = \int_0^{\delta_m} \frac{K_c J_v}{\varepsilon K_d D_0} dz$$

$$\frac{\phi C_{lp} - N_s/(J_v K_c)}{\phi C_{lf} - N_s/(J_v K_c)} = \exp\left(\frac{K_c J_v \delta_m}{\varepsilon K_d D_0}\right) = \exp\left(\frac{\tau_\infty J_v \delta_m}{D_{eff}}\right) = \exp(Pe_m) = E_m$$

Here $\tau_\infty = \phi K_c$, is the asymptotic intrinsic membrane transmission; $D_{eff} = \phi \varepsilon K_d D_0$, is the effective solute diffusivity in the pore; Pe_m is the membrane Peclet number.

Rearranging one gets

$$\frac{N_s}{J_v} = \frac{\tau_\infty C_{lf} E_m - \tau_\infty C_{lp}}{E_m - 1} \tag{5.2c}$$

For a conventional ultrafiltration process, both C_{lp} and N_s/J_v are equal to C_p, the permeate protein concentration. One can get the same expression for the intrinsic membrane transmission τ_i from equation (5.2c) as what Quinn et al. (Anderson and Quinn 1974) got using a classical membrane transport theory (Opong and Zydney 1991, Burns and Zydney 1999); τ_i will approach τ_∞ at very high J_v.

$$\tau_i = \frac{C_p}{C_{lf}} = \frac{\tau_\infty E_m}{\tau_\infty + E_m - 1} \tag{5.2d}$$

In addition to the feed side boundary layer, the observed transmission or sieving coefficient for a conventional ultrafiltration process has been described by Zydney et al. (Saksena and Zydney 1994, Opong and Zydney 1991, Burns and Zydney 1999) using a stagnant film model (Michaels 1968) and a hydrodynamic model (Deen 1987, Anderson and Quinn 1974) as follows:

$$\tau_{ob} = \frac{C_p}{C_{bf}} = \frac{\tau_\infty E_m E_f}{(\tau_\infty - 1)(1 - E_m) + \tau_\infty E_m E_f} \tag{5.2e}$$

Here k_f is the mass transfer coefficient on the feed side. At large values of Pe_m and negligible concentration polarization ($J_v << k_f$), $\tau_{ob} \rightarrow \tau_\infty$. For a membrane filtration-cum-adsorption process, the protein mass transfer through the permeate side boundary layer can also be described by the stagnant film theory. Here the protein diffusion is in the same direction as the convective transport so that diffusion enhances the protein mass transfer rate, which is different from the concentration polarization in the feed side boundary layer. Considering the three mass transfer resistances in series, one can derive an expression for the observed transmission for the ultrafiltration-cum-adsorption process.

Consider next the mass balance for the permeate side boundary layer. Locate the z-coordinate at the membrane-permeate interface going away from the membrane:

$$N_s = J_v C - D_0 \frac{dC}{dz} \tag{5.3a}$$

Boundary conditions:

$$z = 0, \quad C = C_{Ip}; \qquad z = \delta_p, \quad C = C_{bp} \tag{5.3b}$$

Integrating:

$$\int_{C_{Ip}}^{C_{bp}} \frac{dC}{C - N_s/J_v} = \int_0^{\delta_p} \frac{J_v}{D_0} dz$$

$$\frac{C_{bp} - N_s/J_v}{C_{Ip} - N_s/J_v} = \exp\left(J_v/k_p\right) = E_p$$

$$\frac{N_s}{J_v} = \frac{C_{Ip} E_p - C_{bp}}{E_p - 1} \tag{5.3c}$$

where $k_p = D_0/\delta_p$ is the protein mass transfer coefficient, and J_v/k_p is the Peclect number in the permeate side boundary layer.

At steady state, the protein flux and the solvent flux do not change along the three resistances in series from the feed boundary layer to the permeate boundary layer through the porous membrane. Therefore, the values of N_s/J_v via equations (5.1d), (5.2c) and (5.3c) should be identical.

Equating N_s/J_v from equations (5.2c) and (5.3c), one obtains

$$C_{lp} = \frac{\tau_\infty C_{lf} E_m (E_p - 1) + C_{bp}(E_m - 1)}{E_p (E_m - 1) + \tau_\infty (E_p - 1)} \tag{5.4}$$

Equating N_s/J_v for (5.1d) = (5.2c) and substituting C_{lp} from equation (5.4), one gets:

$$C_{lf} = \frac{C_{bf} E_f (E_m - 1) + \dfrac{\tau_\infty C_{bp}(E_m - 1)(E_f - 1)}{E_p (E_m - 1) + \tau_\infty (E_p - 1)}}{E_m - 1 + \tau_\infty E_m (E_f - 1) - \dfrac{\tau_\infty^2 E_m (E_f - 1)(E_p - 1)}{E_p (E_m - 1) + \tau_\infty (E_p - 1)}} \tag{5.5}$$

Substituting this expression for C_{lf} in equation (4.1d), one can calculate N_s/J_v. Thus one can get the observed transmission for the UF-cum-adsorption process as:

$$\tau_{ob} = \frac{N_s / J_v}{C_{bf}} \tag{5.6}$$

The quantity N_s/J_v provides an estimate of the pseudo permeate solute concentration as if the transmitted protein were totally dissolved in the permeate liquid.

5.3 Simulation Results and Discussion

Opong and Zydney (1991) studied the transmission of BSA (MW 69,000 Da) through different MWCO polyethersulfone asymmetric UF membranes. Table 5.1 shows the membrane properties and the corresponding BSA transport parameters. The BSA diffusivity in free solution, D_0, was reported to be 6.7×10^{-11} m^2/s (Opong and Zydney

1991). The BSA observed transmissions for different membrane processes under different running conditions can be calculated using equations (5.2e) and (5.6). The simulation results will now be presented and discussed.

Table 5.1 Membrane Properties and the Corresponding BSA Transport Parameters (Opong and Zydney 1991)

Membrane MWCO	τ_∞	$\varepsilon\phi K_d (\times 10^{-2})$	δ_m (μm)
50 K	0.001	0.0033	0.5
100K	0.037	0.4	0.5
300K	0.48	5.0	0.5

5.3.2 Effects of the Enhanced Transport on the Permeate Side

The variations of the observed protein transmission with the permeate flux J_v for conventional ultrafiltration and two UF-cum-adsorption runs operated at different permeate bulk concentrations are shown in Figure 5.3. At low values of permeate flux (< 5×10^{-6} m/s), all observed transmissions decrease with an increase of permeate flux due to the reduction of the relative contribution of diffusion. They go through a minimum at a permeate flux value of 5×10^{-6} m/s and then increase with the permeate flux due to the high protein concentration at the feed side membrane interface caused by the high degree of concentration polarization. At low permeate flux, diffusion dominates the mass transfer. The observed transmissions of the UF-cum-adsorption process are much larger than that of conventional ultrafiltration and much larger than 1. This means that the total protein transmission was enhanced by the permeate side concentration gradient created by protein adsorption. The pseudo permeate concentration is much higher than the feed concentration. With an increase in the permeate flux, more and more proteins pass

through the membrane due to the convective flow. The diffusional contribution takes less and less part in the total protein transmission, and the τ_{ob} for UF-cum-adsorption approaches the τ_{ob} for conventional ultrafiltration.

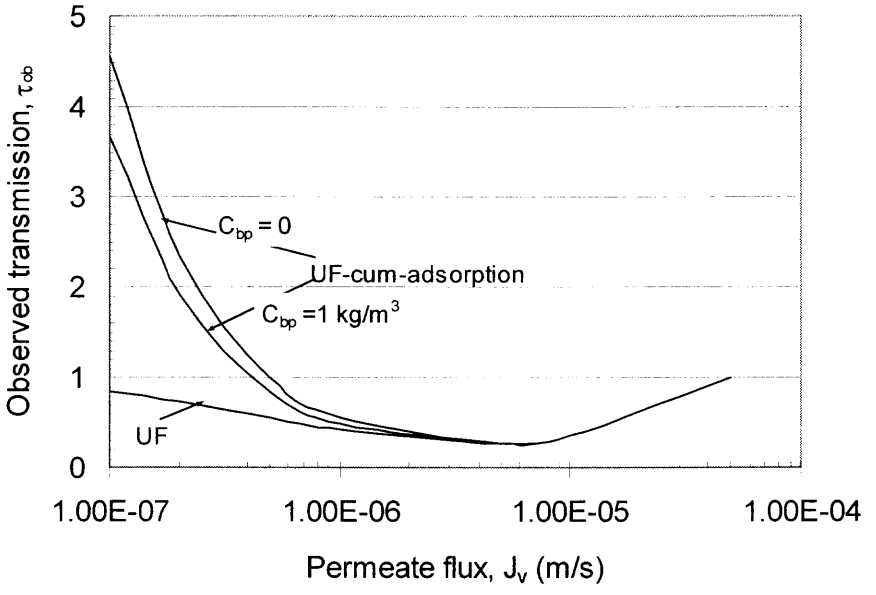

Figure 5.3 Observed transmission vs. permeate flux at different bulk permeate concentrations. 100K membrane, (C_{bf}=5 kg/m^3, $k_f = k_p$ = 5.2×10^{-6} m/s.)

One can see from Figure 5.3 that the τ_{ob} for C_{bp} = 0 and C_{bp} = 1 kg/m^3 at the same feed bulk concentration C_{bf} of 5 kg/m^3 are not much different. In real loading operation of the UF–cum-adsorption process, the permeate concentration is usually much lower than 1 kg/m^3. So the pseudo-steady state assumption is valid for the purpose of estimating the protein transmission. However, for a typical UF-cum-adsorption operation, the permeate flux ranges from 2×10^{-6} to 1×10^{-5} m/s [(Dai, Luo et al. 2000)], which is beyond the region of diffusion-dominated operation. The mass transfer enhancement effect due to the permeate side concentration gradient will not then be important.

5.3.3 Effect of Membrane Pore Size

The membrane asymptotic transmission τ_∞ and the hindered diffusion factor $\varepsilon\phi K_d$ are both strong functions of the ratios of the molecular radius to the membrane pore radius. But $\varepsilon\phi K_d$ decreases much faster than τ_∞ does with a decrease of the membrane pore size as shown in Table 5.1. Figures 5.4 (a) and (b) show clearly the very different observed transmission behaviors for a 300K MWCO and a 50K MWCO polyethersulfone membrane respectively. The nominal pore size of the 50K membrane is smaller than the dimensions of the BSA molecule. Very little protein can permeate through the membrane; thus a very low observed transmission is obtained (Figure 5.4b). The total protein mass transfer rate is dominated absolutely by the membrane skin layer. The permeate side enhanced protein diffusion almost has no effect on the observed transmission. For the 300K membrane, the average pore size is several times larger than the BSA molecule. Protein molecules can diffuse much more easily through the membrane pores so that the permeate side enhanced diffusion effect is very significant at low permeate fluxes. But as shown in Figure 5.3 for the 100K membrane, the τ_{ob} for the UF-cum-adsorption process approaches τ_{ob} for conventional UF after the permeate flux becomes greater than 5×10^{-6} m/s. Convection dominates the mass transfer process at high permeate flux.

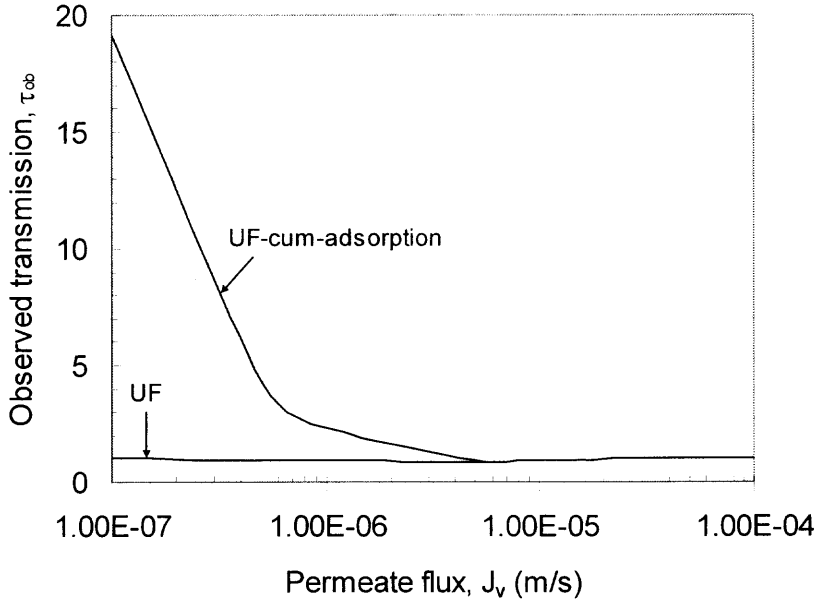

(a). 300K membrane, C_{bf}=5 kg/m^3, C_{bp} =0, k_f= k_p = 5.2×10^{-6} m/s.

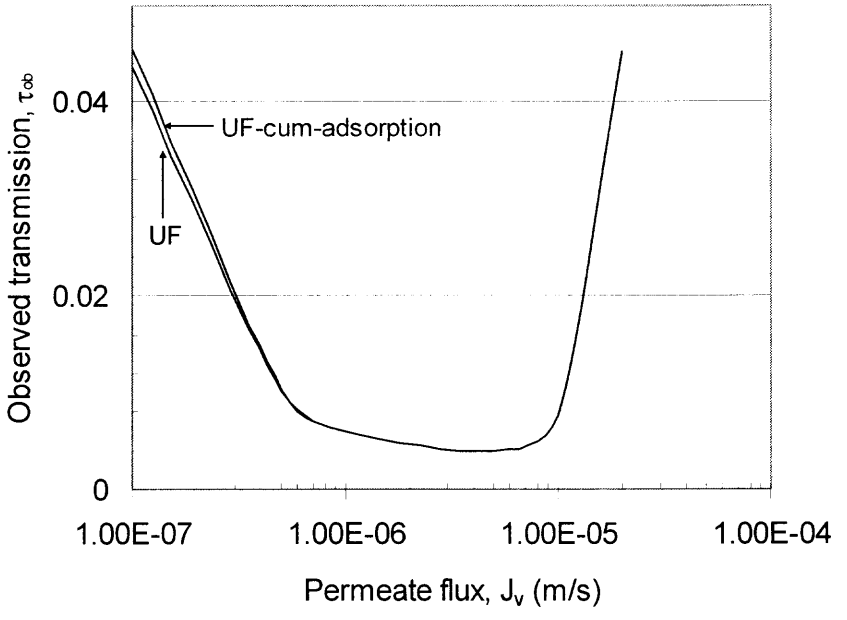

(b). 50K membrane, C_{bf}=5 kg/m^3, C_{bp}=0, k_f= k_p = 5.2×10^{-6} m/s.

Figure 5.4 Observed transmission vs. permeate flux for different pore size membranes.

5.3.4 Effect of the Permeate Side Mass Transfer Coefficient

Figure 5.5 illustrates the observed transmission for the UF-cum-adsorption process for different values of k_p. As expected, the protein transmission enhancement becomes stronger as the permeate side mass transfer coefficient is increased. The quantity k_p is inversely proportional to the thickness of the permeate side boundary layer. For BSA, a value of $k_p = 1 \times 10^{-5}$ m/s corresponds to a permeate boundary layer thickness of 6.7 μm, significant protein transmission enhancement effect can be seen in a wide range of the permeate flux (1×10^{-7} m/s ~ 5×10^{-6} m/s). At the permeate flux value of 1×10^{-7} m/s, where diffusion contributes a lot to the total transmission, the observed protein transmission for the UF-cum-adsorption process is almost 5 times greater than that for a conventional UF. Whereas $k_p = 1 \times 10^{-7}$ m/s corresponds to a much thicker permeate boundary layer of 670 μm, not only the range of the permeate flux where enhancement occurs is much narrower (1×10^{-7} m/s ~3×10^{-7} m/s), but also the extent of enhancement is much smaller. The thickness of the permeate side boundary layer may be controlled by adjusting the effective distance between the adsorbent particle and the membrane surface. Using finer particles will leave less space between the membrane and the particle surfaces, thus leading to a higher mass transfer coefficient. However, very fine particle packing will cause significant flow resistance. The practical particle size should be optimized considering both mass transfer and the hydrodynamics of the packed bed.

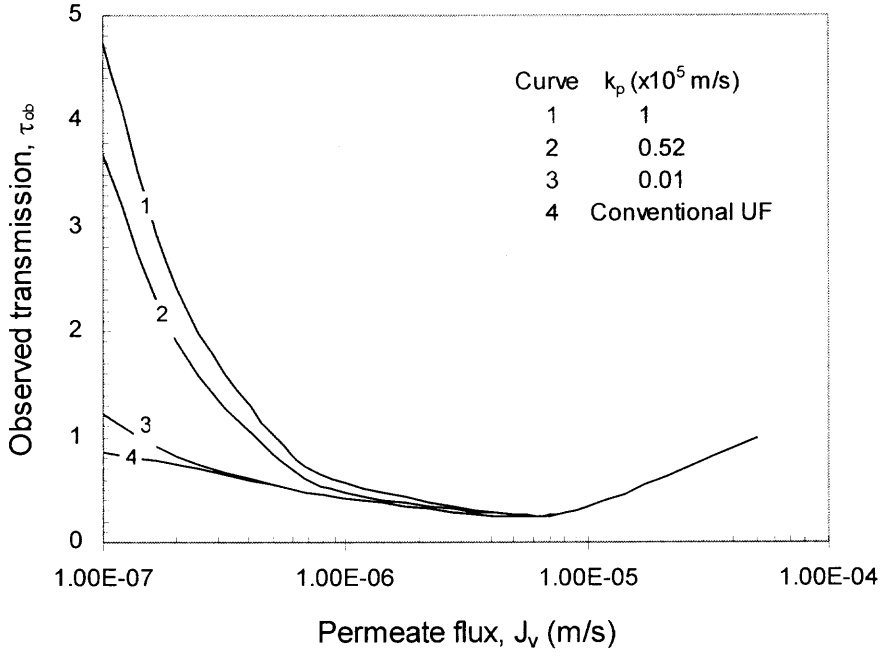

Figure 5.5 Effect of the mass transfer coefficient in the permeate side boundary layer on the observed transmission. (100K membrane, C_{hf} = 5 kg/m^3, C_{hp}=0 kg/m^3)

5.3.5 Effect of Membrane Skin Layer Thickness

Figure 5.6 illustrates the simulated value of τ_{ob} for a 5 μm skin layer 100K MWCO membrane. When compared with the results shown in Figure 5.3 for the same condition (except a thinner skin layer (0.5 μm)), the observed transmissions for both processes declined significantly for a thicker skin layer. Also the transport enhancement effect due to permeate side protein adsorption is much less than that in Figure 5.3. This is because an increase in membrane thickness increases the membrane Peclet number, thus the

membrane layer mass transfer becomes the limiting step for the total protein transmission.

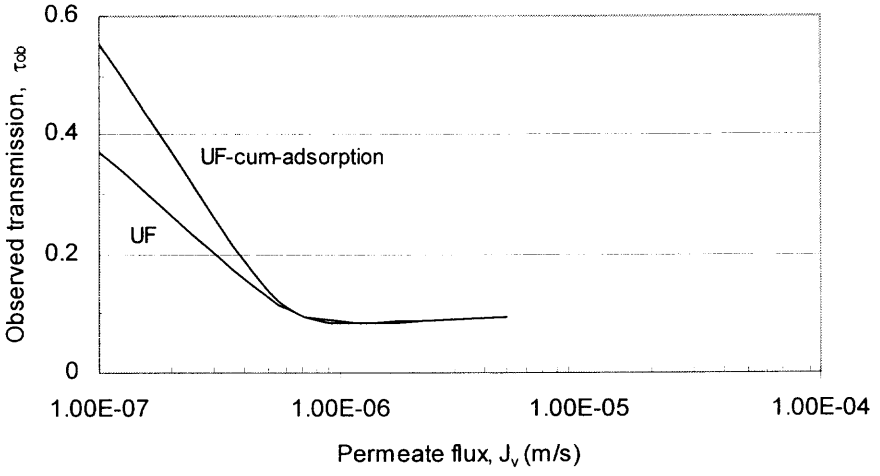

Figure 5.6 Effect of membrane skin layer thickness on τ_{ob}. (100 K membrane, $k_f = k_p = 5.2\times10^{-6}$ m/s, $\delta_m = 5$ μm, C_{bf}=5 kg/m^3, $C_{bp} = 0$ kg/m^3.)

5.3.6 Protein Transmissions for a BSA and IgG Mixture

For the UF-cum-adsorption as a separation device, it would be of significant interest to explore the protein transmission behaviors for a protein mixture. Two model proteins, BSA and IgG (MW 155,000), were used in the simulation of the binary mixture separation. Protein transport parameters on an OMEGA 100 K polyethersulfone membrane with a skin thickness of 0.5 μm were reported to be $\tau_\infty = 0.016$, $D_{eff} = 1.0\times10^{-13}$ m^2/s for BSA and $\tau_\infty = 0.0026$, $D_{eff} = 4.0\times10^{-15}$ m^2/s for IgG respectively (Burns and Zydney 1999). The diffusivity of IgG in the free solution is estimated from (Young, Carroad et al. 1980)

$$D_0 = 8.34 \times 10^{-15} \left(\frac{T}{\mu M^{1/3}} \right) \tag{5.7}$$

Figure 5.7 shows the simulated values of the enhanced transmission for BSA and IgG assuming that both of them bind to the adsorbent and there are no interactions between protein molecules. Under the same operating conditions, the observed transmission of BSA, the smaller protein, for a UF-cum-adsorption process will be promoted significantly in the permeate flux range of 1×10^{-7} m/s to 5×10^{-6} m/s. However,

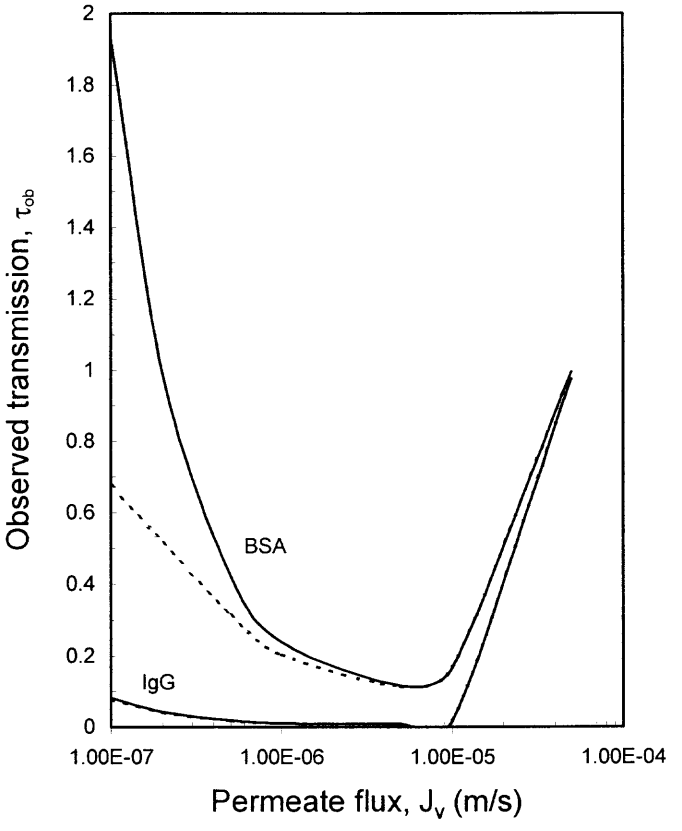

Figure 5.7 Observed transmission enhancement for BSA and IgG. (100 K membrane, k_f = 5.2×10^{-6} m/s, k_p = 1×10^{-5} m/s, δ_m = 5 μm, C_{bf} =5 kg/m^3, C_{bp} = 0 kg/m^3. Solid line: UF-cum-adsorption; Dotted line: UF.)

very limited transmission enhancement of IgG, a much larger protein, can be seen even under very low permeate flux. IgG molecule, with an intrinsic membrane transmission of only 0.0026, is much larger than the average membrane pore size; therefore only a very small fraction of the IgG molecules can go through the very small number of larger membrane pores. As in the case of BSA permeating through a 50K membrane in section 3.2, the mass transfer resistance through the membrane is the limiting step in the total protein transmission. The permeate side mass transfer enhancement will not contribute much to the total protein transmission.

If one can choose an adsorption media with selective binding to the desired protein, for example, an affinity media, there will be a transmission enhancement for the desired protein only. All other protein transmissions are going to be as in conventional ultrafiltration. The selective transmission enhancement will enlarge the membrane selectivity. This is potentially an ideal situation in the UF-cum-adsorption process.

In many other situations, where both proteins will bind to the adsorbent, the favored operating conditions are different for the smaller protein and the larger protein. If a smaller protein is the target product, like BSA in this analysis, the advantages, of both, the membrane fractionation and the mass transfer enhancement due to the permeate side adsorption, can be obtained. Operating at a lower permeate flux will benefit selective protein transmission. Rejecting the larger proteins can simplify the adsorption separation in the permeate side. If a larger protein is the target product, like IgG in this analysis, operating at the transmission enhancement range should be avoided. Instead, one should choose the high permeate flux operating condition where the transmission enhancement effect is negligible and IgG observed transmission is much larger due to the concentration

polarization at the feed side. However, the highest permeate flux one can use is restricted by the fouling and protein aggregation, and precipitation due to the high concentration at the membrane feed side surface.

5.3.7 Protein Transmission Enhancement Observed in the Integrated Device Using UF Membrane.

The observed Mb transmissions under different permeate fluxes were measured for the UF module #2 with or without adsorbent at the permeate side. The experimental results and the simulation results are shown in Figure 5.8.

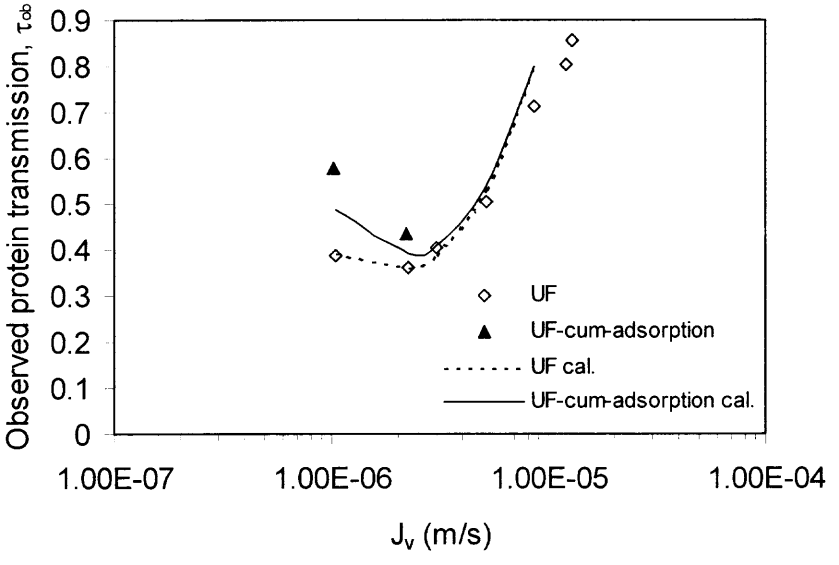

Figure 5.8 Mb observed transmission for a UF module w. or w/o adsorbent at the permeate side.

The diffusivity of Mb in the free solution was estimated using eq. 5.7. The permeate-side mass transfer coefficient was 1×10^{-4} m/s. The lumen-side mass transfer coefficient was estimated using correlation (Kulkarni, Funk et al. 1992)

$$Sh = 1.62\left[\mathrm{Re}\,Sc\left(d_i / l_i\right)\right]^{0.33} \tag{5.8}$$

The membrane skin layer thickness is 0.5 μm. The membrane transport parameters τ_∞ and $\varepsilon\phi K_d$ were regressed using eq 5.2e, to be 0.0716 and 0.00186 respectively. The experimental data of observed Mb transmission corresponding to the permeate fluxes from 1×10^{-6} to 1×10^{-5} m/s in the conventional UF were used in the regression. The two experimental points under higher permeate fluxes were abandoned because the membrane fouling becomes more significant at high permeate fluxes, resulting in lower observed protein transmissions, therefore not reflecting the true membrane transport parameters.

The theoretical values of the observed transmission for the conventional UF are shown as the dotted line. The solid line in Figure 5.8 shows the theoretical values of the observed transmission for the UF-cum-adsorption process calculated using eq. 5.6. One can see that the calculated value from the proposed convection-diffusion transport model somewhat underpredicted the experimental value. There are still other factors contributing to the protein transmission. The streaming potential formed by the electrolyte flowing through the charged membrane pores may be significant enough to facilitate the negatively charged protein molecules moving to the permeate side.

That the charged membrane surface affects the solute transport can be supported by another simple experiment, where the pure water flux variation is significant enough to be observed with the change of solution pH and ionic strength, indicating the electrokinetic phenomena is playing a role here. As shown in Figure 5.9, the pure water flux increases with the increase of the solution ionic strength but decreases with the increase of the solution pH. With more salt in the solution, the electrical double layers of

the ions and the membrane pores are compressed. With the increase of the pH of the solution, the extent of free charge at the membrane pore surface becomes stronger, causing more electroviscous effect.

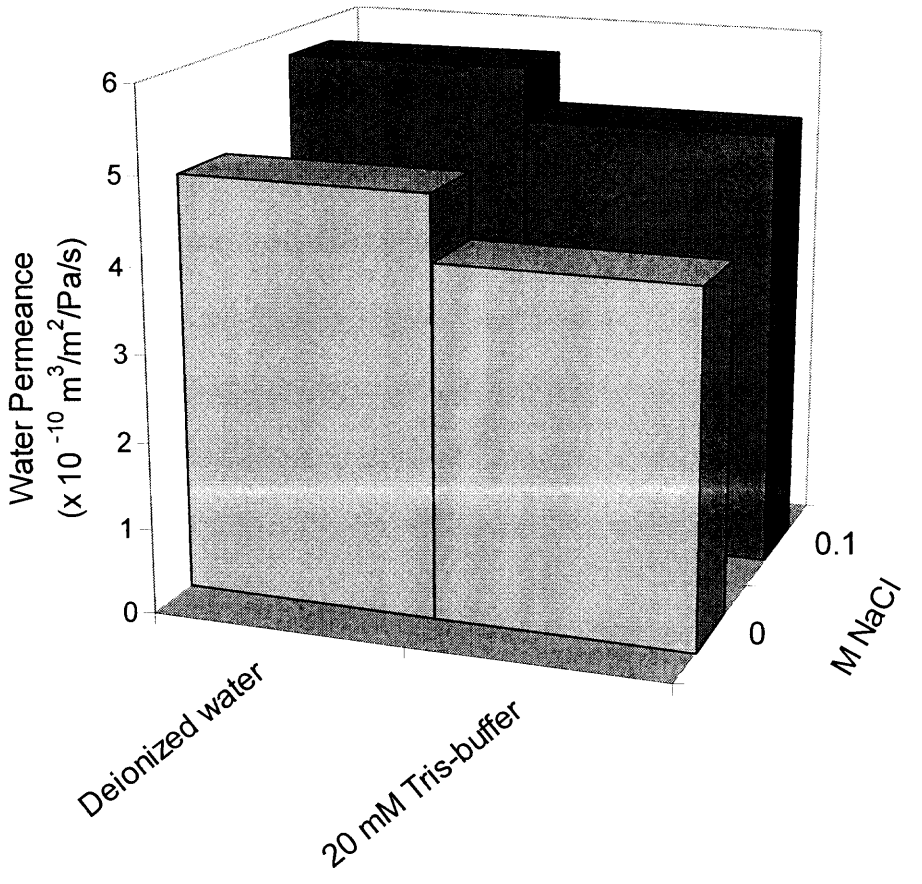

Figure 5.9 Salt effect on pure water permeance.

5.4 Concluding Remarks

In this chapter, the observed transmission in the UF-cum-adsorption process has been compared to that in the conventional UF process by simulating a model protein BSA permeating through different MWCO polyethersulfone membranes. The pseudo-steady state mass transfer model can explicitly show the observed transmission enhancement effect in the UF-cum-adsorption process. When diffusion makes a significant contribution to the transmembrane mass transfer, the total protein transmission can be enhanced considerably by the permeate side protein adsorption. During the protein loading period in a typical UF-cum-adsorption process, most protein molecules in the permeate side are captured by the adsorbent so that the protein concentration in permeate liquid phase is much lower than the feed bulk concentration. Simulation results show that the low permeate bulk protein concentration does not affect the enhancement effect much under this situation; therefore, the pseudo-steady state model can be used to describe the mass transfer behavior of the process. Larger membrane pore size and thinner membrane skin layer favor protein transmission enhancement effect due to permeate side protein adsorption. But the enhancement effect can be neglected at higher permeate flux when convection dominates the total mass transfer process or the proteins are very highly rejected by the membrane.

In the separation of protein mixtures, a media that selectively binds only the target protein will enhance the target protein transmission without affecting the transmissions of other proteins. The selective binding media can provide the fullest advantage of the UF-cum-adsorption process. If both proteins in a binary mixture bind to the adsorbent, smaller proteins will encounter more transmission enhancement. If the target protein is

the smaller one, operating at lower permeate flux where transmission enhancement is significant will enhance the membrane selectivity, a plus for the separation. If the target protein is the larger one, operating at the transmission enhancement range should be avoided by using higher permeate flux.

The diffusion-convection transport model underpredicts somewhat the experimental Mb observed transmission through the integrated device using UF membrane. The streaming potential formed while the electrolyte flowing through the membrane enhanced the protein transmission and need to be considered in the future modeling work. Electroviscous phenomenon is also observed on the polysulfone UF membrane, supporting the notion that the membrane surface is charged and electrokinetic phenomenon plays a significant role.

CHAPTER 6

CONCLUSIONS AND RECOMMENDATIONS FOR FUTURE STUDIES

A new membrane filtration-cum-chromatography device configuration was developed by coating part of the length of the hollow fibers near the module outlet with an essentially impermeable coating. Interfacially polymerized coating on part of the hollow fiber length was successfully developed on devices using either an UF or a MF membrane. The coating layer formed on the inner skin of the hollow fibers was shown to be mechanically and chemically stable. Through the upper section (about 3/4 - 4/5th of the length) of the device, the UF/MF hollow fibers behaved in a conventional fashion. The rest of the fiber length had an interfacially polymerized coating which essentially eliminated water permeation at transmembrane pressure drops used in UF/MF. Correspondingly, the permeation of proteins through the coated section of the fibers was eliminated. As a result, the intrinsically high protein adsorption capacity of the selected chromatographic resin beads on the shell side of the membrane device was fully utilized without any limitation of early protein breakthrough through the shell-side permeate outlet.

After coating the bottom section of the hollow fibers with an impermeable layer, dramatic increases of the protein loading capacities were demonstrated in both UF and MF modules in separation experiments for the following two systems: Mb/α-LA and Mb/BSA. In the integrated device using the UF membrane, α-LA and BSA encountered higher rejection than Mb due to their molecular sizes or charges. For applications where the more permeable protein molecule is the target product, the UF membrane can provide selective transmission of the proteins, alleviating the adsorption burden of the impurity proteins in the succeeding chromatographic separation steps. For applications where the

larger protein or both smaller and larger proteins are the products, membranes having larger pore size such as a MF membrane need to be used. The MF membrane is used to block particles like cells, cell debris and bacteria while the proteins permeate through the membrane and are loaded on the beads located in the shell side.

The ionic strength of the feed solution affects the α-LA transmission through the UF membrane significantly. At very low ionic strength, the α-LA was highly rejected by the UF membrane. With the increase of the ionic strength of the feed solution, the α-LA transmission through the membrane increased significantly because the Debye lengthes of the electrical double layers around the protein molecules and the membrane pores were compressed by the salt in the solution.

The proteins, Mb and α-LA, were recovered and totally separated from a synthetic fermentation broth using the device made of a MF module with a coated zone; it demonstrates the ability to recover and separate proteins directly from an unclarified feed. The elution profiles for four consecutive cyclic runs without cleaning in between were essentially superimposable. The integrated process provided self-cleaning of the membrane fouling via the washing and elution steps for chromatographic separation.

A mathematical model describing the hydrodynamic and protein loading behavior of the integrated device with a coated zone was developed. When the length of the coated zone becomes zero, the model will be reduced to the model for the integrated device without coating. Using linear isotherms for Mb and α-LA, numerical solutions of the pressure, solvent flux, solvent flow rate and the protein concentrations along the module were obtained. The simulation results show that the protein concentrations in beads for the integrated device with a coated zone are considerably higher than that for the module

without coating. Shock layers for the different proteins will be developed in the coated zone. The simulation results allow one to understand why the earlier device configuration (without coated zone) suffered from early protein leakage and low loading capacity, and provide insight into how the early protein leakage was avoided and loading capacity increased and the separation improved in the new configuration(with a coated zone near the module outlet). The simulated breakthrough curves of Mb on the device with and without coated zone fit the experimental data well. The optimal length of the coated zone for the UF module was found to be 12 cm, about half of the total effective hollow fiber length.

A theoretical analysis of the protein mass transfer enhancement due to the permeate-side adsorption was performed using a diffusion-convection model considering the feed-side concentration polarization and the permeate-side concentration gradient formed by the adsorption. The observed transmission in the UF-cum-adsorption process has been compared to that in the conventional UF process by simulating a pair of model proteins, BSA and IgG, permeating through different MWCO polyethersulfone membranes. When diffusion makes a significant contribution to the transmembrane mass transfer, the total protein transmission can be enhanced considerably by the permeate side protein adsorption. But the enhancement effect can be neglected at higher permeate flux where convection dominates the total mass transfer process or the proteins are very highly rejected by the membrane. The Mb transport parameters through the UF hollow membrane from A/G technology were determined from the conventional UF data. The observed Mb transmissions at different permeate fluxes from simulation using the diffusion-convection model are somewhat lower than the experimental values on the

integrated device #2. The streaming potential and the electrostatic interactions between the protein molecules and the membrane pore surface need to be considered in a more accurate model.

It can be seen from the protein transport analysis that the observed protein transmission is a function of the permeate flux. In our integrated device, the permeate flux varies along the module length, therefore, the observed protein transmission is actually a variable along the module. The mathematical model in Chapter 4 assumed a constant observed protein transmission for the whole device. In future, the local observed protein transmission influenced by the concentration polarization and the mass transfer enhancement due to the permeate-side adsorption should be combined with the model for loading behavior simulation in Chapter 4. This will lead to a more realistic model.

To further decrease the flow resistance caused by the packed bed, a new configuration of the integrated membrane filtration-cum-adsorption device is proposed. The new device consists of two sets of hollow fiber membranes carefully aligned in the module so that each fiber is surrounded by the hollow fibers belonging to the other set. Chromatographic beads are packed in the shell space between the hollow fibers. Feed stream flows through the lumen of one set of the hollow fiber, liquid and bioproduct permeate through the membrane and the thin packed bed in the radial direction, bioproduct will get adsorbed in the beads and the liquid will permeate into the lumen of the other set of hollow fiber and be collected. Complete cross flow is achieved in this configuration. The radial flow resistance across the packed bed between the two sets of hollow fibers is much less than that of the axial flow through the packed bed. As a result, finer adsorbent beads can be used leading to more available surface area and faster mass

transfer. Preliminary results show that the device can be loaded and eluted very fast. However, the hollow fibers need to be specially aligned and regularly distributed in the module to avoid any channeling. Further study on the hollow fiber packing arrangement and the device loading and elution need to be carried out in future.

APPENDIX A

FORTRAN 77 CODE FOR SIMULATION OF THE INTEGRATED DEVICE WITHOUT COATING

The program for simulating the loading step of the integrated membrane filtration-cum-chromatography device without coating is listed in this appendix.

```
C        Equilibrium dispersion model.
C        Binary mixture tube side feed. Tube side flow rate and conc.
profile using analytical solution.
C        Linear isotherm Csi=Ki*Ci
C        Output is the conc. profile along the module at the end of the
loading.
C        Unit: cm/g/s system.
C        created on 04/08/2001   MODIFIED 05/09/2001
C-----------------------------------------------------------------
         IMPLICIT DOUBLE PRECISION (A-H,O-Z)
         PARAMETER (NPDE=2,NINT=100,NPTS = NINT+1,KORD=4,NCC=2,MF=22,
     +    NCPTS=KORD*NINT-NCC*(NINT-1),IQUAD=0,
     +    ML=NPDE*(KORD+IQUAD-1)-1,MAXDER=5,LIWORK=NCPTS*(NPDE+1),
     +    LWORK=KORD+4*NPDE+9*NPDE*NPDE+NCPTS*(3*KORD+2)+NPDE*NCPTS*
     +           (3*ML+MAXDER+7))
         DOUBLE PRECISION U(NPDE,NPTS),XBKPT(NPTS),SCTCH(NINT)
         DOUBLE PRECISION WORK(LWORK)
         INTEGER          IWORK(LIWORK)
         DOUBLE PRECISION USOL(NPDE,NPTS), CS(2,NPTS),WS(2)
C//USOL: conc. in mobile phase l; CS: conc. in the stationary phase. WS:
total protein loaded
         DOUBLE PRECISION WK(2),C0(2),R(2)
C         DOUBLE PRECISION SUM1(2),SUM2(2),SUM3(2)
         COMMON /ENUPT/XLEFT,XRIGHT
         COMMON /GEARO/DTUSED,NC,NSTEPS,NF,NJ
         COMMON /ISOTHERM/WK
         COMMON /COF/CQ,CDL,CA,BETA,A1,A2,QF0,C0,R,EP,FAI,AS

C----------------------INPUT PROBLEM PARAMETERS-----------------------
         OPEN (UNIT=25,FILE='LOADING.DAT',STATUS='UNKNOWN')
C-----------------------------------------------------------------------
C     MEMBRANE MODULE PARAMETER
C// A: membrane permeability.
         DATA SN0,DI,DO,DS/50.D0,0.1,0.16,1.524/
C//SN0,total fiber number; DI,fiber inner diameter DO,fiber external
diameter; DS:shell inner diameter.
         DATA COLLEN/24.5/
C// COLLEN: column length (m).
C     packing parameters.
         DATA DP, EP/90.D-4, 0.374 /
C//DP: beads average diameter (cm); EP: bed void fraction,
```

```
          DATA A,B,R(1),R(2)/ 2.4D-9, 2.65D6, 0.52,0.88/
C//Parameter A: permeability (cm/(dyn/cm2)/s=0.1 m/pa/s), B:
packing(dyn/cm2).s/ml=1.D5Pa.S/m3), R: REJECTION FACTOR
          DATA QF0,C0(1),C0(2)/3.333D0,0.505D0, 0.467D0/
C//QF0, feed flow rate (ml/s). C01: feed conc(mg/ml).
          DATA PF0,PPL/3.516D5,8.328D4
C//PF0: tube side inlet gauge pressure (dyne/cm2=0.1 Pa) PPL: shell side
outlet gauge pressure.
          DATA WK(1), WK(2)/43.4, 31099./
C//Isotherm.
          DATA MIU,CDL/1.D-2, 7.83D-2/
C//Viscosity (poise), DL Dispersion coefficient constance. (cm)
          FAI=(1.D0-EP)/EP
C//EP: bed void fraction

C-----------------CALCULATION PARAMETERS-----------------------------

          write(*,*) 'liwork=',LIWORK, 'LWORK=',LWORK
          IWORK(1)=LWORK
          IWORK(2)=LIWORK
          INDEX=1
          TO=0.D0
          DT=1.D-10
          EPS=1.D-14
          DX=COLLEN/DBLE(NINT)
          DO 1 I=1,NPTS
              XBKPT(I)=DX*DBLE(I-1)
   1      CONTINUE
          XLEFT=XBKPT(1)
          XRIGHT=XBKPT(NPTS)

C-------------------------------------------------------------------------
          CM1=128.*MIU/DI**3
          AS=3.14159*(DS**2-SN0*DO**2)/4.
          CA=4.*DI*SN0/(DS**2-SN0*DO**2)
          CM2=QF0/SN0/3.14159/DI
C          B=150.*(1-EP)**2/DP**2/EP**3*MIU*CA
          BETA=DSQRT(A*(CM1+B))
          A2=-A*CM1*CM2/BETA
          A1=A*((PF0-CM1*CM2*COLLEN-PPL)
     +       -(CM1*COLLEN/BETA+B/BETA**2*DSINH(BETA*COLLEN))*A2)
     +       /(DCOSH(BETA*COLLEN)-A*CM1*(DCOSH(BETA*COLLEN)-1.)/BETA**2)

          CQ=SN0*3.14159*DI/BETA
C-------------------------------------------------------------------------

          DETAT=1.D0
          TOUT=0.0D0
          WRITE (6,241)
  241     FORMAT(//2X,'THE CALCULATION RESULTS ARE'//)

  51      TOUT=TOUT+DETAT
C-------------------CALL SUBROUTINE PDECOL----------------------------
          CALL PDECOL(TO,TOUT,DT,XBKPT,EPS,NINT,KORD,NCC,NPDE,MF,
     +    INDEX,WORK,IWORK)
          IF (INDEX .NE. 0) GOTO 105
```

```
C-----------------CALL SUBROUTINE TO GENERATE VALUES----------------
         CALL VALUES(XBKPT,USOL,SCTCH,NPDE,NPTS,NPTS,0,WORK)
         TTIME=TOUT
         IF ((TTIME .GE.405.)) GOTO 105
C//Compare to loading end time.
         GOTO 51
  105    WRITE (6,205) INDEX
  205    FORMAT (10X,'INDEX=',I5)
C-------------protein concentrations in the stationary phase---------

         DO 90 I = 1,NPTS
C//The concentrations in the stationary phase.
            CS(1,I)=USOL(1,I)*WK(1)
            CS(2,I)=USOL(2,I)*WK(2)
   90    CONTINUE

C___________Total protein loaded_____________________________________
         WS(1)=0.0
         WS(2)=0.0
         DO 95 I=2,NPTS
          WS(1)=WS(1)+(CS(1,I-1)+CS(1,I))/2.*AS*DX*(1.-EP)
          WS(2)=WS(2)+(CS(2,I-1)+CS(2,I))/2.*AS*DX*(1.-EP)
   95    CONTINUE
C------------Output-------------------------------------------------
         WRITE (6,151) TTIME
         WRITE (25,151)TTIME
  151    FORMAT (1X,'Loading time (s):', F10.4)
         WRITE (6, 153)
         WRITE (25,153)
  153    FORMAT (5X, 'X (cm)', 6X, 'C1 (mg/ml)',4X, 'C2(mg/ml)',5X,
     +           'CS1(mg/ml)',5X,'CS2(mg/ml)')
         DO 99 I=1,NPTS
          WRITE (6, 152)  XBKPT(I),USOL(1,I),USOL(2,I),CS(1,I),CS(2,I)
          WRITE (25, 152) XBKPT(I),USOL(1,I),USOL(2,I),CS(1,I),CS(2,I)
   99    CONTINUE
  152    FORMAT (1X, F10.4,4(4X, E10.4))
         WRITE(6,160)
         WRITE(25,160)
  160    FORMAT(1X, 'Total protein loaded (mg):')
         WRITE(6,161) WS(1), WS(2)
         WRITE(25,161) WS(1), WS(2)
  161    FORMAT(1X, 'WS1=', F10.4, 6X, 'WS2=',F10.4)

         STOP
         END
C
C
C------------SUBROUTINE FOR PDE AND ODE-------------------------------
         SUBROUTINE F(T,X,U,UX,UXX,FVAL,NPDE)
         IMPLICIT DOUBLE PRECISION (A-H,O-Z)
         DIMENSION U(2),UX(2),UXX(2),FVAL(2)
         DOUBLE PRECISION WK(2),C0(2),R(2)
         COMMON /COF/CQ,CDL,CA,BETA,A1,A2,QF0,C0,R,EP,FAI,AS
         COMMON /ISOTHERM/WK

         FJVZ=A1*DCOSH(BETA*X)+A2*DSINH(BETA*X)
         QPZ=CQ*(A1*DSINH(BETA*X)+A2*(DSINH(BETA*X)-1.))
```

```
      UP=QPZ/AS
      QFZ=QF0-QPZ
      C1FZ=C0(1)*(QF0/QFZ)**R(1)
      C2FZ=C0(2)*(QF0/QFZ)**R(2)

      FVAL(1)=(CDL*UP*UXX(1)+(CDL*CA*FJVZ-UP/EP)*UX(1)
     +         +CA*FJVZ*(C1FZ*(1.-R(1))-U(1))/EP)/(1.D0+FAI*WK(1))
      FVAL(2)=(CDL*UP*UXX(2)+(CDL*CA*FJVZ-UP/EP)*UX(2)
     +         +CA*FJVZ*(C2FZ*(1.-R(2))-U(2))/EP)/(1.D0+FAI*WK(2))
      RETURN
      END
C------------ SUBROUTINE FOR BOUNDARY CONDITIONS-----------------------
      SUBROUTINE BNDRY(T,X,U,UX,DBDU,DBDUX,DZDT,NPDE)
      IMPLICIT DOUBLE PRECISION (A-H,O-Z)
      DIMENSION U(2),UX(2),DBDU(2,2)
      DIMENSION DBDUX(2,2),DZDT(2)
      COMMON /ENUPT/XLEFT,XRIGHT
      COMMON /GEARO/DTUSED,NC,NSTEPS,NF,NJ

      DO 10 I=1,NPDE
         DZDT(I)=0.0D0
      DO 10 J=1,NPDE
         DBDU(I,J) =0.0D0
         DBDUX(I,J)=0.0D0
10    CONTINUE
      DBDUX(1,1)=1.D0
      DBDUX(2,2)=1.D0

      RETURN
      END
C--------------SUBROUTINE FOR INITIAL CONDITIONS----------------------
      SUBROUTINE UINIT(X,U,NPDE)
      IMPLICIT DOUBLE PRECISION (A-H,O-Z)
      DIMENSION U(2)
          U(1)=0.0D0
          U(2)=0.0D0
C          U(3)=0.0D0
C          U(4)=0.0D0
      RETURN
      END
C------------------OPTION SUBROUTINE---------------------------------
      SUBROUTINE DERIVF(T,X,U,UX,UXX,DBDU,DBDUX,DBDUXX,NPDE)
      IMPLICIT DOUBLE PRECISION (A-H,O-Z)
      DIMENSION U(*),UX(*),UXX(*),DBDU(NPDE,*),DBDUX(NPDE,*),
     +  DBDUXX(NPDE,*)
      RETURN
      END
```

APPENDIX B

FORTRAN 77 CODE FOR SIMULATION OF THE INTEGRATED DEVICE WITH A COATED ZONE

The program for simulating the loading step of the integrated membrane filtration-cum-chromatography device with a coated zone is listed in this appendix.

```
C        PROGRAM USING PDECOL to simulate the loading step of the
integrated membrane filtration-cum-chromatography with a coated zone.
C        Equilibrium dispersion model.
C        Binary mixture tube side feed. Tube side flow rate and conc.
profile using analytical solution.
C        Linear isotherm Csi=Ki*Ci
C        Output is the conc. profile along the module at the end of the
loading.
C        Unit: cm/g/s system.
C        created on 08/16/2003   MODIFIED 11/08/2003
C-----------------------------------------------------------------
         IMPLICIT DOUBLE PRECISION (A-H,O-Z)
         PARAMETER (NPDE=2,NINT=100,NPTS = NINT+1,KORD=4,NCC=2,MF=22,
     +    NCPTS=KORD*NINT-NCC*(NINT-1),IQUAD=0,
     +    ML=NPDE*(KORD+IQUAD-1)-1,MAXDER=5,LIWORK=NCPTS*(NPDE+1),
     +    LWORK=KORD+4*NPDE+9*NPDE*NPDE+NCPTS*(3*KORD+2)+NPDE*NCPTS*
     +           (3*ML+MAXDER+7))
         DOUBLE PRECISION U(NPDE,NPTS),XBKPT(NPTS),SCTCH(NINT)
         DOUBLE PRECISION WORK(LWORK)
         INTEGER          IWORK(LIWORK)
         DOUBLE PRECISION USOL(NPDE,NPTS), CS(2,NPTS),WS(2)
//USOL: conc. in mobile phasel; CS: conc in stationary phase. WS: total
protein loaded
         DOUBLE PRECISION WK(2),C0(2),R(2)
C         DOUBLE PRECISION SUM1(2),SUM2(2),SUM3(2)
         COMMON /ENUPT/XLEFT,XRIGHT
         COMMON /GEARO/DTUSED,NC,NSTEPS,NF,NJ
         COMMON /ISOTHERM/WK
         COMMON /COL/COLLP
         COMMON /COF/CQ,CDL,CA,BETA,A1,A2,QF0,C0,R,EP,FAI,AS

C----------------------INPUT PROBLEM PARAMETERS-----------------------
         OPEN (UNIT=25,FILE='LOADINGC.DAT',STATUS='UNKNOWN')
C-----------------------------------------------------------------------
C     MEMBRANE MODULE PARAMETER
// A: membrane permeability.
         DATA SN0,DI,DO,DS/50.D0,0.1,0.16,1.524/
//SN0,total fiber number; DI,fiber inner diameter DO,fiber external
diameter; DS:shell inner diameter.
         DATA COLLEN,COLLP/24.5, 12.5/
// COLLEN: column length (cm); COLLP: Permeabale length (cm).
```

```
          DATA NINP/75/
// NINP: No. of grid in the permeable zone.
C     packing parameters.
          DATA DP, EP/90.D-4, 0.374 /
//DP: beads average diameter (cm); EP: bed void fraction,
          DATA A,B,R(1),R(2)/ 2.4D-9, 2.65D6, 0.52,0.88/
//Parameter A: permeability (cm/(dyn/cm2)/s=0.1 m/pa/s), B:
packing(dyn/cm2).s/ml=1.D5Pa.S/m3), R: REJECTION FACTOR
          DATA QF0,C0(1),C0(2)/3.333D0,0.505D0, 0.0467D0/
//QF0, feed flow rate (ml/s). C01: feed conc(mg/ml).
          DATA PF0,PPL/3.516D5,2.5D4/
//PF0: tube side inlet gauge pressure (dyne/cm2=0.1 Pa) PPL: shell side
outlet gauge pressure.
          DATA WK(1), WK(2)/43.4, 31099./
//Isotherm.
          DATA MIU,CDL/1.D-2, 7.83D-2/
//Viscosity (poise), DL Dispersion coefficient constance. (cm)
          FAI=(1.D0-EP)/EP
//EP: bed void fraction

C-----------------CALCULATION PARAMETERS-----------------------------

          write(*,*) 'liwork=',LIWORK, 'LWORK=',LWORK
          IWORK(1)=LWORK
          IWORK(2)=LIWORK
          INDEX=1
          TO=0.D0
          DT=1.D-10
          EPS=1.D-14
          DX1=COLLP/DBLE(NINP)
          DX2=(COLLEN-COLLP)/DBLE(NINT-NINP)
          DO 1 I=1,NINP+1
              XBKPT(I)=DX1*DBLE(I-1)
    1     CONTINUE
          DO 2 J=NINP+2, NPTS
              XBKPT(J)=COLLP+DX2*DBLE(J-NINP-1)
    2     CONTINUE
          XLEFT=XBKPT(1)
          XRIGHT=XBKPT(NPTS)

C-----------------------------------------------------------------------
          CM1=128.*MIU/DI**3
          AS=3.14159*(DS**2-SN0*DO**2)/4.
          CA=4.*DI*SN0/(DS**2-SN0*DO**2)
          CM2=QF0/SN0/3.14159/DI
C          B=150.*(1-EP)**2/DP**2/EP**3*MIU*CA
          BETA=DSQRT(A*(CM1+B))
          A2=-A*CM1*CM2/BETA
          A1=((PF0-PPL)*BETA**2+A*B*CM1*CM2*((COLLEN-COLLP)
A1 for tube-side loading in the coated module
     +       *DCOSH(BETA*COLLP)+DSINH(BETA*COLLP)/BETA-COLLEN))
     +       /(CM1+BETA*B*(COLLEN-COLLP)*DSINH(BETA*COLLP)
     +       +B*DCOSH(BETA*COLLP))

          CQ=SN0*3.14159*DI/BETA
C-----------------------------------------------------------------------
```

```
          DETAT=1.D0
          TOUT=0.0D0
          WRITE (6,241)
  241     FORMAT(//2X,'THE CALCULATION RESULTS ARE'//)

  51      TOUT=TOUT+DETAT
C-------------------CALL SUBROUTINE PDECOL----------------------------
          CALL PDECOL(TO,TOUT,DT,XBKPT,EPS,NINT,KORD,NCC,NPDE,MF,
     +    INDEX,WORK,IWORK)
          IF (INDEX .NE. 0) GOTO 105

C------------------CALL SUBROUTINE TO GENERATE VALUES-----------------
          CALL VALUES(XBKPT,USOL,SCTCH,NPDE,NPTS,NPTS,0,WORK)
          TTIME=TOUT
          IF ((TTIME.GE.3300.)) GOTO 105
//Compare to Loading end time.
          GOTO 51
  105     WRITE (6,205) INDEX
  205     FORMAT (10X,'INDEX=',I5)
C-------------protein concentrations in the stationary phase---------

          DO 90 I = 1,NPTS
//The concentrations at stationary phase.
             CS(1,I)=USOL(1,I)*WK(1)
             CS(2,I)=USOL(2,I)*WK(2)
   90     CONTINUE

C___________Total protein loaded_____________________________________
          WS(1)=0.0
          WS(2)=0.0
          DO 95 I=2,NINP+1
           WS(1)=WS(1)+(CS(1,I-1)+CS(1,I))/2.*AS*DX1*(1.-EP)
//In permeable zone
           WS(2)=WS(2)+(CS(2,I-1)+CS(2,I))/2.*AS*DX1*(1.-EP)
   95     CONTINUE
          DO 97 I=NINP+2, NPTS
           WS(1)=WS(1)+ (CS(1,I-1)+CS(1,I))/2.*AS*DX2*(1.-EP)
// In coated zone
           WS(2)=WS(2)+ (CS(2,I-1)+CS(2,I))/2.*AS*DX2*(1.-EP)
   97     CONTINUE
C------------Output-------------------------------------------------
          WRITE (6,151) TTIME
          WRITE (25,151)TTIME
  151     FORMAT (1X,'Loading time:', F10.4)
          WRITE (6, 153)
          WRITE (25,153)
  153     FORMAT (5X, 'X (cm)', 6X, 'C1 (mg/ml)',4X, 'C2(mg/ml)',5X,
     +            'CS1(mg/ml)',5X,'CS2(mg/ml)')
          DO 99 I=1,NPTS
           WRITE (6, 152)  XBKPT(I),USOL(1,I),USOL(2,I),CS(1,I),CS(2,I)
           WRITE (25, 152) XBKPT(I),USOL(1,I),USOL(2,I),CS(1,I),CS(2,I)
   99     CONTINUE
  152     FORMAT (1X, F10.4,4(4X, E10.4))
          WRITE(6,160)
          WRITE(25,160)
  160     FORMAT(1X, 'Total protein loaded (mg):')
          WRITE(6,161) WS(1), WS(2)
```

```
          WRITE(25,161) WS(1), WS(2)
  161     FORMAT(1X, 'WS1=', F10.4, 6X, 'WS2=',F10.4)

          STOP
          END
C
C
C------------SUBROUTINE FOR PDE AND ODE-------------------------------
          SUBROUTINE F(T,X,U,UX,UXX,FVAL,NPDE)
          IMPLICIT DOUBLE PRECISION (A-H,O-Z)
          DIMENSION U(2),UX(2),UXX(2),FVAL(2)
          DOUBLE PRECISION WK(2),C0(2),R(2)
          COMMON /COF/CQ,CDL,CA,BETA,A1,A2,QF0,C0,R,EP,FAI,AS
          COMMON /ISOTHERM/WK
          COMMON /COL/COLLP

          IF (X.LT.COLLP) THEN
              FJVZ=A1*DCOSH(BETA*X)+A2*DSINH(BETA*X)
// Permeable zone
              QPZ=CQ*(A1*DSINH(BETA*X)+A2*(DSINH(BETA*X)-1.))
          ELSE
              FJVZ=0.0
// Coated zone
              QPZ=CQ*(A1*DSINH(BETA*COLLP)+A2*(DSINH(BETA*COLLP)-1.))
          ENDIF
          UP=QPZ/AS
          QFZ=QF0-QPZ
          C1FZ=C0(1)*(QF0/QFZ)**R(1)
          C2FZ=C0(2)*(QF0/QFZ)**R(2)

          FVAL(1)=(CDL*UP*UXX(1)+(CDL*CA*FJVZ-UP/EP)*UX(1)
     +           +CA*FJVZ*(C1FZ*(1.-R(1))-U(1))/EP)/(1.D0+FAI*WK(1))
          FVAL(2)=(CDL*UP*UXX(2)+(CDL*CA*FJVZ-UP/EP)*UX(2)
     +           +CA*FJVZ*(C2FZ*(1.-R(2))-U(2))/EP)/(1.D0+FAI*WK(2))
          RETURN
          END
C------------ SUBROUTINE FOR BOUNDARY CONDITIONS-----------------------
          SUBROUTINE BNDRY(T,X,U,UX,DBDU,DBDUX,DZDT,NPDE)
          IMPLICIT DOUBLE PRECISION (A-H,O-Z)
          DIMENSION U(2),UX(2),DBDU(2,2)
          DIMENSION DBDUX(2,2),DZDT(2)
          COMMON /ENUPT/XLEFT,XRIGHT
          COMMON /GEARO/DTUSED,NC,NSTEPS,NF,NJ

          DO 10 I=1,NPDE
             DZDT(I)=0.0D0
          DO 10 J=1,NPDE
             DBDU(I,J) =0.0D0
             DBDUX(I,J)=0.0D0
10        CONTINUE
          DBDUX(1,1)=1.D0
          DBDUX(2,2)=1.D0

          RETURN
          END
C-------------SUBROUTINE FOR INITIAL CONDITIONS---------------------
          SUBROUTINE UINIT(X,U,NPDE)
```

```
          IMPLICIT DOUBLE PRECISION (A-H,O-Z)
          DIMENSION U(2)
              U(1)=0.0D0
              U(2)=0.0D0
C              U(3)=0.0D0
C              U(4)=0.0D0
          RETURN
          END
C------------------OPTION SUBROUTINE---------------------------------
          SUBROUTINE DERIVF(T,X,U,UX,UXX,DBDU,DBDUX,DBDUXX,NPDE)
          IMPLICIT DOUBLE PRECISION (A-H,O-Z)
          DIMENSION U(*),UX(*),UXX(*),DBDU(NPDE,*),DBDUX(NPDE,*),
     +    DBDUXX(NPDE,*)
          RETURN
          END
```

REFERENCES

Amersham Biosciences. 2000. Expanded Bed Adsorption Handbook: p. 9.

Amersham Pharmacia Biotech. 2000. "Instuctions for Fast Flow Media.".

Anderson, J. L. and J. A. Quinn 1974. "Restricted Transport in Small Pores: A Model for Steric Exclusion and Hindered Particle Motion." *Biophys. J.* **14**: 130.

Anspach, F. B., D. Curbelo, R. Hartmann, G. Garke and W.-D. Deckwer 1999. "Expanded-Bed Chromatography in Primary Protein Purification." *J. Chromatogr. A* **865**: 129-144.

Apelblat, A., A. Katzir-Katchalsky and A. Silberberg 1974. "A Mathematical Analysis of Capillary Tissue Fluid Exchange." *Biorheology* **11**: 1-49.

Bai, Y. and C. E. Glatz 2003. "Capture of a Recombinant Protein from Unclarified Canola Extract Using Streamline Expanded Bed Anion Exchange." *Biotechnology and Bioengineering* **81**(7): 855-864.

Beklaitis, G. V., A. Ravindran and K. M. Ragsdell 1983. *Engineering Optimization Methods and Applications*. New York, Wiley.

Bird, R. B., W. E. Stewart and E. N. Lightfoot 1960. *Transport Phenomena*. New York, John Wiley & Sons.

Bucak, S., D. A. Jones, P. E. Laibinis and T. A. Hatton 2003. "Protein Separations Using Colloidal Magnetic Nanoparticles." *Biotechnol. Prog.* **19**: 477-484.

Burns, D. B. and A. L. Zydney 1999. "Effect of Solution pH on Protein Transport through Ultrafiltration Membranes." *Biotechnol. Bioeng.* **64**(1): 27-37.

Byers, M. J., E. G. Jsacoff and J. O. Naples 1991. Separation or Purification of Biomaterials with Particulate Polymeric Adsorbents. Canada Patent: 1,292,952

Cadotte, J. E. 1981. Interfacially Synthesized Reverse Osmosis Membrane. US Patent: 4,277,344

Cadotte, J. E., R. S. King, R. J. Majerle and R. J. Petersen 1981. "Interfacial Synthesis in the Preparation of Reverse Osmosis Membrane." *J. Macromol. Sci-Chem.* **A15**: 727-755.

Chang, Y. K. and H. A. Chase 1996. "Ion Exchange Purification of G6pdh from Unclarified Yeast Cell Homogenates Using Expanded Bed Adsorption." *Biotechnolo. Bioeng.* **49**: 204-216.

Chase, H. A. 1994. "Purification of Proteins by Adsorption Chromatography in Expanded Beds." *Trends in Biotech.* **12**: 296-303.

Cheang, B. and A. L. Zydney 2003. "Separation of Alpha-Lactalbumin and Beta-Lactalglobulin Using Membrane Ultrafiltration." *Biotechnology and Bioengineering* **83**(2): 201-209.

Committee on Bioprocess Engineering, N. R. C. 1992. Putting Biotechnology to Work: Bioprocess Engineering. Washington, DC, Nat. Acad. Sci.: 2-22.

Dai, X.-P.2000. An Integrated Membrane-Based Chromatographic Process for Biomolecule Isolation and Purification. Doctoral Dissertation: 181. New Jersey Institute of Technology. Newark, NJ.

Dai, X.-P., R. G. Luo and K. K. Sirkar 1999. "An Integrated Process for Biomolecule Isolation and Purification." *Biotechnol. Prog.* **15**(6): 1095-1105.

Dai, X.-P., R. G. Luo and K. K. Sirkar 2000. "Pressure and Flux Profiles in Bead-Filled Ultrafiltration/Microfiltration Hollow Fiber Membrane Modules." *Biotechnol. Prog.* **16**(6): 1044-1054.

Dai, X.-P., S. Majumdar, R. G. Luo and K. K. Sirkar 2003. "Protein Loading, Elution, and Resolution Behavior in a Novel Device That Integrates Ultrafiltration and Chromatographic Separation." *Biotechnol. Bioeng.* **83**(2): 125-139.

Davis, J. C. 1990. Process for Selective Dialysis Using Polymeric Affinity Adsorbents and Size Selective Membranes. US Patent: 4,963,264

Deen, W. M. 1987. "Hindered Transport of Large Molecules in Liquid-Filled Pores." *AIChE J.* **33**: 1409.

Draeger, N. M. and H. A. Chase 1991. "Expanded Bed Adsorption of Proteins Using Ion Exchangers." *Bioseparations* **2**: 67.

Fernandez-Lahore, H. M., S. Geilenkirchen, K. Boldt, A. Nagel, M. R. Kula and J. Thommes 2000. "The Influence of Cell Adsorbent Interactions on Protein Adsorption in Expanded Beds." *Journal of Chromatography, A* **873**(2): 195-208.

Finette, G. M. S., B. Baharin, Q. M. Mao and M. T. W. Hearn 1998. "Optimization Considerations for the Purification of A1-Antitrypsin Using Silica-Based Ion-Exchange Adsorbents in Packed and Expanded Beds." *Biotechnol. Prog.* **14**: 286-293.

Gailliot, F. P., C. Gleason, J. J. Wilson and J. Zwarick 1990. "Fluidized Bed Adsorption for Whole Broth Extraction." *Biotechnol. Prog.* **6**: 370-375.

Ghosh, R. and Z.F. Cui, 2000. "Simulation Study of the Fractionation of Proteins Using Ultrafiltration." *J. Memb. Sci.* **180**: 29.

Harrison, R. G., Ed. 1994. *Protein Purification Process Engineering*. Bioprocess Technol. New York, Marcel Dekker.

Ho, W. S. W., K.K. Sirkar, Ed. 1992. *Membrane Handbook*. New York, Chapman & Hall.

Johansson, H. J., C. Jagerstern and J. Shiloach 1996. "Large Scale Recovery and Purification of Periplasmic Recombinant Protein from E. Coli Using Expended Bed Adsorption Chromatography Followed by New Ion Exchange Media." *J. Biotechnol.* **48**: 9-14.

Kalyanpur M. 2000. Downstream processing in the biotechnology industry, in M. Desai, (Ed.) *Downstream Processing of Proteins*, Totowa, NJ, Humana Press: 1-8.

Kang, W.1989. Hollow Fiber Membrane - Based Extractive Bioreactors and a Whole Cell Immobilization Technique. Doctoral Dissertation: pp20. Stevens Institute of Technology. Hoboken, NJ.

Kronman, M. J. and R. F. Andreotti 1964. "Inter- and Intramolecular Interactions of α-Lactalbumin. I. The Apparent Heterogeneity at Acid pH." *Biochemistry* **3**(8): 1145-1151.

Kulkarni, S. S., E. W. Funk and N. N. Li. 1992. Ultrafiltration. *Membrane Handbook*. W. S. W. Ho and K. K. Sirkar. New York, Chapman & Hall: 391-453.

Ladisch, M. R. 2001. *Bioseparations Engineering: Principles, Practice, and Economics*. New York, John Wiley & Sons, Inc.

LeVan, M. D., G. Carta and C. M. Yon. 1997. Adsorption and Ion Exchange. *Perry's Chemical Engineers' Handbook*. R. H. Perry, D. W. Green and J. O.Maloney. New York, McGraw-Hill: 16-1-16-66.

Lin, D.-Q., M.-R. Kula, A. Liten and J. Thommes 2003. "Stability of Expanded Beds During the Application of Crude Feedstock." *Biotechnology and Bioengineering* **81**(1): 21-26.

Longsworth, L. G. and C. F. Jacobsen 1949. "An Electrophoretic Study of the Binding of Salt Ion by β-Lactoglobulin and Bovine Serum Albumin." *J. Phys. Colloid Chem.* **53**: 126-135.

Madson, N. K. and R. F. Sincovec 1979. "PDECOL." *ACM Tans. Math. Software* **5**(3): 326-351.

Madson, N. K. and R. F. Sincovec 1992. "Remark on Algorithm 540, PDECOL." *ACM Tans. Math. Software* **18**(3): 343-344.

Michaels, A. S. 1968. "New Separation Technique for the CPI." *Chem. Eng. Prog.* **64**: 31.

Molinari, R., J. L. Torres, A. S. Michaels, P. K. Kilpatrick and R. G. Carbonell 1990. "Simultaneous Ultrafiltration and Affinity Sorptive Separation of Proteins in a Hollow Fiber Membrane Module." *Biotechnol. Bioeng.* **36**: 572-580.

Natarajan, V. and S. M. Cramer 2000. "Optimization of Ion-Exchange Displacement Separations: II. Comparison of Displacement Separations on Various Ion-Exchange Resins." *Journal of Chromatography A* **876**(1-2): 63-73.

Ohashi, R., J. M. Otero, A. Chwistek, I. Yamato and J.-F. P. Hamel 2002. "On-Line Purification of Monoclonal Antibodies Using an Integrated Stirred-Tank Reactor/Expanded-Bed Adsorption System." *Biotechnology Progress* **18**(6): 1292-1300.

Opong, W. S. and A. L. Zydney 1991. "Diffusive and Convective Protein Transport through Asymmetric Membranes." *AIChE J.* **37**(10): 1497-510.

Prouty, W. F. 1991. Production-Scale Purification Processes. *Drug Biotechnology Regulation.* Y.-Y. H. Chien and J. L. Gueriguian. New York, Marcel Dekker. **13:** 221-262.

Radola, B. J. 1973. "Isoelectric Focusing in Layers of Granulated Gels: I. Thin-Layer Isoelectric Focusing of Proteins." *Biochimica et Biophysica Acta* **295**: 412 -428.

Russotti, G. and K. E. Göklen 2001. Crossflow Membrane Filtration of Fermentation Broth. In: W. K. Wang, editor. *Membrane Separations in Biotechnology.* 2ed edition, New York: Marcel Dekker. pp. 85-160.

Saksena, S. and A. L. Zydney 1994. "Effect of Solution Ph and Ionic Strength on the Separation of Albumin from Immunoglobulins (IgG) by Selective Filtration." *Biotechnol. Bioeng.* **43**(10): 960-8.

Sirkar, K. K. and R. Prasad. 1986. Protein Ultrafiltration-Some Neglected Considerations. In: W. C. McGregor, editor. *Membrane Separations in Biotechnology.* 1st edition. New York, Marcel Dekker.

Sofer, G. and L. Hagel 1997. *Handbook of Process Chromatography: A Guide to Optimization, Scale up, and Validation.* New York, Academic Press.

Starling, E. H. 1896. "On the Adsorption of Fluid from the Connective Tissue Space." *J. Physiol.* **19**: 312-326.

Thommes, J., M. Halfar, S. Lenz and M. R. Kula 1995. "Purification of Monoclonal Antibodies from Whole Hybridoma Fermentation Broth by Fluidized Bed Adsorption." *Biotechnol. Bioeng.* **45**: 205-211.

Tunon, P. 2002. "Advances in Preparative Chromatography." *Genetic Engineering News* **22**: 16-18.

van Reis, R., E. M. Goodrich, C. L. Yson, L. N. Frautschy, R. Whiteley and A. L. Zydney 1997. "Constant C_{wall} Ultrafiltration Process Control." *J. Membr. Sci.* **130**(1-2): 123-140.

Wang, W. K. Ed 2001. *Membrane Separations in Biotechnology*. New York, Marcel Dekker.

Yamamoto, S., K. Nakanishi, R. Matsuno and T. Kamikubo 1983a. "Ion Exchange Chromatography of Protein - Prediction of Elution Curves and Operating Conditions. I. Experimental Verification." *Biotechnol. Bioeng.* **25**: 1373-1391.

Yamamoto, S., K. Nakanishi, R. Matsuno and T. Kamikubo 1983b. "Ion Exchange Chromatography of Protein - Prediction of Elution Curves and Operating Conditions. Ii. Theoretical Considerations." *Biotechnol. Bioeng.* **25**: 1465-1483.

Young, M. E., P. A. Carroad and R. L. Bell 1980. "Estimation of Diffusion Coefficients of Proteins." *Biotechnol. Bioeng.* **22**: 947.

Zeman, L. J. and A. L. Zydney 1996. *Microfiltration and Ultrafiltration*. New York, Marcel Dekker.

Zydney, A. L. and R. van Reis. 2001. High-Performance Tangential-Flow Filtration. *Membrane Separations in Biotechnology*. W. K. Wang. New York, Marcel Dekker: 277-298.